

Conditions Favouring Growth of Fresh Water Biofouling in Hydraulic Canals and the Impact of Biofouling on Pipe Flows

By

Xiao Lin Li BEng(Hons.)

Submitted in fulfilment of the requirements for the Degree of

Masters

University of Tasmania

October 2013

Declaration of Originality

This thesis contains no material which has been accepted for a degree or diploma by the University or any other institution, except by way of background information and duly acknowledged in the thesis, and to the best of candidates knowledge and belief no material previously published or written by another person except where due acknowledgement is made in the text of the thesis.

.....

Xiao Lin Li

Date: 12/10/2013

Statement Concerning Authority to Access

This thesis may be made available for loan and limited copying in accordance with the *Copyright Act 1968*.

.....

Xiao Lin Li

Date: 12/10/2013

Abstract

Biofouling increases frictional resistance and slows the water flow in fresh water canals and pipes. It results in up to 10% reduction in the flow carrying capacity in hydropower canals in Tasmania, Australia. This project investigated the effect of colour on the growth of biofouling in open channels and the impact of biofouling in pipes and penstocks.

The effect of substratum colour on the growth of biofouling was studied by submerging mild steel plates painted with four different coloured epoxy coatings in fresh water. The plates were placed in a concrete lined canal for a period of time to allow biofouling to grow. Results show that black was the favoured colour for the growth of biofouling whereas the white plates developed the least amount. The amount of biofouling increases progressively from white to grey to black at the settlement stage of biofouling. However, the effect of colour on the growth of biofouling became less significant when the biofouling was fully developed. It was found that the amount of light also affected the growth of biofouling. Under full sunlight and slow flow conditions (1 m/s), plates with lower total light intensity and lower UV light exhibited higher levels of biofouling.

In addition to open channels, biofouling also causes head losses in cooling water pipes and penstocks in hydroelectric power stations. The influence of water quality on the growth of biofouling was investigated by analysing water quality data of eight lakes used for hydroelectric power generation. It was found that power stations with fewer biofouling problems in their cooling pipes use water with a higher pH value and dissolved oxygen level, while having lower water conductivity, water turbidity, iron, manganese, aluminium and nutrients.

A new pipe rig was designed and built to investigate the impact of biofouling on pipe flows. Located in the hydraulics laboratory at the University of Tasmania, this consisted of a removable test section that was placed in a purpose built field test rig installed in a hydropower station canal. The pressure drop across the test section and velocity profiles under different flow rates were measured for both clean and fouled conditions. Results show that biofouling increased the head loss along the test section and changed the shape of the velocity profiles. This data did not fit the widely used Colebrook-White equation.

Acknowledgements

I am sincerely grateful to my supervisors, Dr Jessica M. Walker (nee Andrewartha) and Dr Alan Henderson, for their expert advice, clear guidance and invaluable support throughout the candidature. Special thanks are due to Dr Jane E. Sargison for her encouragement and assistance for this study.

I am also grateful to those who provided financial support for this project. My main scholarship was a UTAS Tasmanian Research Scholarship supplemented by a School Scholarship. The project was sponsored by the Australian Research Council and Hydro Tasmania.

During this research, I have been fortunate in having valuable support from many people from Hydro Tasmania. Thanks are due to Angus Swindon, Daryl Polzin, Norm Cribbin and Joshua Kline. The field experiments were conducted in the Tarraleah Power Scheme, owned by Hydro Tasmania. Thanks are due to Martin Doyle, Darren Nichols, Stephen Kelly and Brett Nichols for the arrangement of the site visits and support during the field inspection. I would like to thank Alison Howman, Chris Livingston, Wayne Soutter and Jurgen Surendorff for supplying the water quality data. Thanks are given to Carolyn Maxwell for providing detailed comments and suggestions on the water data analysis results.

I am indebted to all technical staff in the school for their assistance in performing the experiments. Thanks are due to Andrew Bylett, James Lamont and Peter Seward for building up the new pipe rigs in the hydraulics laboratory and on site. Thanks are given to David Morley and Brodie Coad for their assistance in the Engineering workshop. I am grateful to Justin Courtney and Max Fang for providing the IT support. Thanks are also due to Calverly Gerard, Sam Perkins and Dean Giosio for providing assistance in data acquisition and the setup of the new pipe rig. Thanks are given to other staff members in the school, especially Mary Dixon, who has provided assistance since the beginning of my candidature. I am grateful to Dr. Simon Wotherspoon for his assistance during the water data analysis.

To my husband, Hui, thank you for your assistance and support of my study. I owe a lot to my children, Deborah and Frank. Thank you for your patience and understanding during my study.

Table of Contents

Abstract..	iii
Acknowledgements ..	iv
Nomenclature ..	ix
Chapter 1 Introduction ..	1
Chapter 2 Literature Review ..	3
2.1 Biofouling in Fresh Water ..	3
2.1.1 The Character of Biofouling ..	4
2.1.2 Skin Friction caused by Biofouling ..	6
2.1.3 Biofouling in Tasmanian Hydropower Schemes ..	7
2.1.4 Methods of Biofouling Control ..	9
2.1.4.1 Chemical Methods ..	9
2.1.4.2 Physical Methods ..	10
2.1.4.3 Coatings ..	12
2.2 Effect of Substratum Colour and Ambient Light Conditions on Biofouling ..	13
2.2.1 Substratum Colour Effect ..	14
2.2.2 Light Effect on Biofouling ..	15
2.3 Effects of Water Quality and Physical Factors on Biofouling ..	16
2.3.1 Effect of Water Quality on Biofouling ..	16
2.3.2 Impact of Physical Conditions on Biofouling ..	20
2.4 Turbulent Flow in Pipes ..	22
2.4.1 Turbulent Flow in Pipes ..	22
2.4.1.1 Turbulent Flow in Smooth Pipes ..	24
2.4.1.2 Turbulent Flow in Biofouled Pipes ..	25
2.4.2 Turbulent Flow Measurement Techniques ..	30
2.5 Chapter Summary ..	33

Chapter 3	Effect of Substratum Colour and Ambient Light Conditions on Biofouling	34
3.1	Colour Effect on Biofouling	36
3.1.1	Methodology	36
3.1.1.1	Test Panels	36
3.1.1.2	Site Trials Locations	37
3.1.1.3	Sampling Position and Area	40
3.1.1.4	Colour Performance Grading	41
3.1.2	Site Trial in Transition No. 4	43
3.1.3	Site Trial in Pond No.1	45
3.2	Light and Temperature Effect on Biofouling	48
3.2.1	Temperature and Light Data Logger	48
3.2.2	UV Light Measurement	50
3.2.3	Light Data of Site Trial	51
3.2.3.1	Site Trial in Transition 4	52
3.2.3.2	Site Trial in Pond No.1	54
3.2.3.3	Total Light Summary of Two Locations	57
3.3	Chapter Summary	59
Chapter 4	Biofouling and Water Quality in Tasmanian Hydropower Schemes	61
4.1	Biofouling in Tasmanian Hydropower Conduits	61
4.2	Effect of Water Quality on Biofouling	66
4.2.1	Data Analysis Program R	67
4.2.2	Water Chemical Factors	67
4.2.2.1	Relationship between some Parameters and Depth	68
4.2.2.2	Boxplot Parameters	70
4.3	Chapter Summary	83

Chapter 5	Design and Instrumentation of the Pipe Rig.....	85
5.1	Lab Pipe Rig	85
5.1.1	Design of the Lab Pipe Rig	88
5.1.1.1	Design Calculations	89
5.1.1.2	Setup of the Lab Pipe Rig	94
5.1.2	Instrumentation of the Lab Pipe Rig.....	98
5.1.2.1	Water Pressure Measurement	98
5.1.2.2	Flow Rate Measurement.....	98
5.1.2.3	Velocity Profile	100
5.1.3	Calibration of Instruments	102
5.2	Site Pipe Rig	105
5.2.1	Site Pipe Rig Design	105
5.2.2	Flow Velocity of Site Pipe Rig	107
5.3	Chapter Summary	109
Chapter 6	Measurement of Velocity Profiles and Head Loss	110
6.1	Measurement of Equipment and Methods.....	110
6.2	Head loss of Biofouled and Clean Reference Pipes	114
6.2.1	Flow Rate Measurement	115
6.2.2	Head Loss Measurement	115
6.2.3	Moody Diagram	116
6.2.4	Roughness Height of Biofilms in Biofouled Pipe.....	118
6.3	Velocity Profiles of the Biofouled Pipe	121
6.3.1	Velocity Profiles of Biofouled Pipe	122
6.3.2	Non-Dimensional Analysis	126
6.3.3	Modification of the Colebrook-White Equation.....	128
6.4	Chapter Summary	130

Chapter 7	Conclusions and Recommendations	131
7.1	Effect of Substratum Colour and Ambient Light Conditions on Biofouling	131
7.2	Biofouling and Water Quality in Tasmanian Hydropower Schemes	132
7.3	The Impact of Biofouling in Pipes	134
7.3.1	New Pipe Rig Design and Calibration	134
7.3.2	Biofouling of the Test Section	134
7.4	Recommendations	136
7.4.1	Effect of Substratum Colour and Ambient Light conditions on Biofouling.....	136
7.4.2	Biofouling and Water Quality in Tasmanian Hydropower Schemes	136
7.4.3	The Impact of Biofouling in Pipes.....	137
References.....		138
Appendices.....		144
A	Water Level and Water Temperature Data for Chapter 3	144
A.1	Water Level of Pond No.1 and Transition 4	144
A.2	Water Temperature of Pond No.1 and Transition 4	145
B	Biofouling Data and R Program for Chapter 4	147
B.1	Biofouling Chemical Analysis	147
B.2	R Program for Water Data Analysis	148
C	Design of the New Pipe Rig	157
C.1	Dimension of the Lab Pipe Rig.....	157
C.2	Data of Penstock on Site.....	161
C.3	Buckingham Pi Theorem.....	162
C.4	Southern Cross Centrifugal Pump Performance in Lab.....	164
C.5	Validyne DP15 Pressure Range Chart.....	165
C.6	Performance of the Submersible Pump of the Rig on Site	166

Nomenclature

Symbols

A	Cross-sectional area of pipe
D	Diameter of pipe
f	Darcy-Weisbach friction factor of pipe
g	Gravity of fluid
H_D	Dynamic head
H_L	Total head loss
H_f	Major head loss
H_m	Minor head loss
κ	Von Karmon constant
k_s	Equivalent sand grain roughness
L	Length of pipe
ρ	Density of fluid
P	Static pressure
P_{stag}	Stagnation pressure
Q	Flow rate
Re	Reynolds number of pipe
τ_w	Shear stress at the pipe wall
U	Mean flow velocity of water in pipe
U_{max}	Maximum velocity at the centreline of pipe
u	Point velocity at a distance y from the pipe wall
u_*	Shear velocity
μ	Dynamic viscosity of fluid
ν	Kinematic viscosity of fluid
V	Velocity of point measured by the Pitot tube
y	Distance of point from the pipe wall

Chapter 1 Introduction

Hydropower is the largest source of renewable energy in the world (International Hydropower Association, 2012). Many hydropower schemes require the transportation of water over long distances from storage dams to power stations via canals and pipelines. These conduits are subject to the influence of freshwater biofouling, such as bacteria and algae. Biofouling adheres at the liquid-solid interface, reducing the water flow capacity and increasing the head loss.

A great proportion of electricity in Tasmania is generated by hydropower. Hydro Tasmania operates 30 power stations and a network of over 50 large dams, 170 km of open channels, as shown in Figure 1.1, and 60 km of pipelines and penstocks, as shown in Figure 1.2. These open channels and pipelines are experiencing increased friction and reduction in carrying capacity due to surface deterioration and biofouling.



Figure 1.1 Tarraleah No.1 Canal.



Figure 1.2 Poatina Penstock (looking downhill).

A reduction of 10% in flow carrying capacity of a hydropower canal was found to be the result of the growth of the biofouling diatom *Gomphonema tarraleahae* (Andrewartha et al., 2007). The increased friction at the liquid-solid interface results in energy loss in the water transport system, which can be improved by removing biofouling from pipes. For example, Barton et al. (2008) showed that the Tarraleah Hilltop pipeline significantly reduced the head loss with a net gain of 2 m from the station output, representing a 25% improvement over the fouled pipe conditions.

This study builds on previous studies on biofouling in hydropower systems by Barton (2007a), Andrewartha (2010b) and Perkins (2010a).

The primary objectives of this study were to investigate the effect of colour and light on the growth of biofouling in fresh water; to analyse the effect of water quality and flow mechanics on the growth of biofouling; and to examine the influence of biofouling on the head loss and the shape of the velocity profile in pipes.

Following an introduction and a literature review, Chapter 3 describes an experimental study of the effect of colour and light on the growth of biofouling. It focused on two diatom species, *Gomphonema tarraleahae* and *Tabellaria flocculosa*, which were found in the Tarraleah Power Scheme in central Tasmania, Australia (Perkins et al., 2010b).

Chapter 4 contains details on the water data analysis of eight lakes and one hydropower canal in Tasmania, Australia. The professional data analysis program R and boxplot method were used for analysing the impact of water parameters on biofouling. These parameters include water temperature, pH value, conductivity, turbidity, nutrient level, metal contents, oxygen level and organic material of water.

Chapter 5 introduces a new pipe rig which was designed and constructed to conduct head loss and velocity profile measurements of clean and biofouled pipes.

Chapter 6 describes the velocity distribution and head loss of fully developed turbulent flow in biofouled pipes at Reynolds numbers from 9.1×10^4 to 3.9×10^5 (was measured). Velocity profiles were obtained by using a Pitot tube and ring type static wall tappings. The results were examined by using Nikuradse's (1933) formula for artificial rough pipes and the Colebrook – White equation.

Finally, Chapter 7 summarises the main findings and presents recommendations for future work.

Chapter 2 Literature Review

This chapter reviews previous studies of biofouling in water. It includes the effect of substratum colour and water quality on biofouling. Literature on the structure of turbulent flow in pipes and the techniques available to measure turbulence in fluids is also reviewed.

2.1 Biofouling in Fresh Water

Biofouling is the unwanted growth of biological matter, and includes bacteria, algae and fungi organisms at liquid-solid, solid-air and liquid-air interfaces. It slows the flow in water conveyance structures, increases the drag on ships, reduces the efficiency of heat exchange systems, causes substantial corrosion problems and increases energy demand for air-conditioning in hot countries (Andrewartha et al., 2010; Flemming, 2002; Melo et al., 1997; Picologlou et al., 1980; Teng et al., 2008).

The effect of colour on marine biofouling has been investigated in the last few decades (Dahlem et al., 1984; Hodson et al., 2000; Su et al., 2007). However, the effect of substratum colour on freshwater biofilms has not been well studied. Chapter 3 aims to investigate the effect of substratum colour on known freshwater biofouling species in the Tarraleah canals, owned by Hydro Tasmania.

It is believed that the growth of biofouling is also dependent on water quality, but only some water parameters have been studied (Lee et al., 1998; Minkus, 1954; Terry, 2007; Tyler, 1968). Thus, possible links between biofouling and water quality in Tasmanian Hydropower Schemes are investigated in Chapter 4.

The effect of biofouling on skin friction has been established over the last century, with research conducted in many industries such as hydropower generation, shipping, heat exchange systems and bulk water supply systems (Andrewartha et al., 2010; Barton et al., 2008; Melo et al., 1997). However, the mechanisms causing skin friction due to biofouling in pipes are not well understood and are investigated in Chapter 6.

2.1.1 The Character of Biofouling

Biofilms tend to reside on a surface in an aqueous environment rather than “free floating”, because they can obtain enough nutrients and oxygen from the adsorbed surface (Melo et al., 1997). Nearly all micro-organisms are capable of forming a biofilm, due to the life feature of micro-organisms. Biofilms excrete extracellular polymer substances (EPS), which fill the space between the cells and form the internal structure of the biofilm. EPS represents the “house of the biofilm cells” (Flemming et al., 2007). Life embedded in the EPS matrix offers important advantages for biofilm organisms. They can maintain stable arrangements of micro-organisms of different species, and the matrix can simultaneously catch enough nutrients from the environment for the growth of biofilms. Biofilms are the most successful form of life on Earth and can tolerate high amounts of biocides (Flemming, 2002).

In open recirculation systems, abundant opportunities exist for water to “pick up” nutrients and light. Algal biofilms will form on any moist, illuminated surface, while bacterial biofilms can form in both illuminated and dark conditions. A common fouling species in freshwater open conduits and other illuminated locations is the diatom (Andrewartha, 2010b; Perkins et al., 2010b), but in cold freshwater pipelines the fouling is dominated by thin bacterial slimes (Barton, 2007a; Callow, 1993; McFie, 1976).

according to Callow (1993), diatoms produce EPS in the form of stalks, tubes, apical pads, adhering films and cell coating. Diatom slimes are not prerequisite for the growth of micro-organisms, and the growth in a succession depends on a variety of factors, including nutrient status, substrate, grazing, temperature and turbulence.

Pollard et al. (1959), Tyler (1968) and Barton (2007a) found that the deposits were mainly dominated by iron and manganese bacteria. Upon drying, these tended to become friable and easily broken into small flakes (Barton, 2007a). Iron bacteria belong to the group of aerobic bacteria which appeared to utilise the oxidation of ferrous and/or manganous ions as an essential component in their metabolic functioning. These aerobic bacteria could grow under low-nutrient conditions (Ghiorse, 1984).

Pollard et al.(1959) examined some specimens from the closed pressure conduit of Santeetlah Hydroelectric USA. It was found that the first layer of the deposit was black, 0.6 mm in

thickness; the second layer was red, 0.5 mm in thickness, and consisted predominantly of iron; the third layer was black, 0.9 mm in thickness, of the same character as the first and later deposit; the fourth was red, 1.0 mm in thickness, and was the thickest and most well defined of the layers. Pollard et al. (1959) believed that the total eighteen layers on the walls of the conduit corresponded to yearly accumulations.

They also found that the colour of a fresh deposit in a closed pressure conduit was light brown. For the later black deposit under the fresh deposit, his explanation was “the selective adsorption of manganese and desorption of iron”.

Minkus (1954) and Tyler (1968) proposed that the deposit layers depended on the variations of the iron and manganese concentrations. Minkus (1954) plotted some water parameters, including water temperature, pH, alkalinity, carbon dioxide, iron and manganese. Carbon dioxide appeared to have the same cycle as iron and manganese. However, he was unable to conclude that carbon dioxide was the sole cause of the pipe deposits.

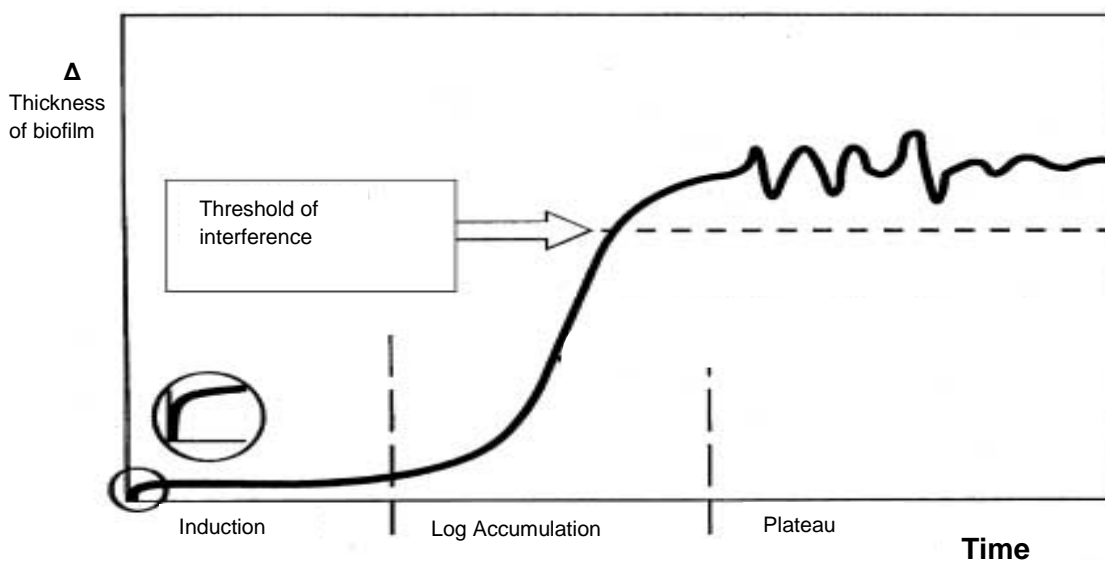


Figure 2.1 Schematic depiction of biofilm development (Flemming, 2002). The dotted line indicates an arbitrary threshold of interference.

Flemming (2002) used a similar schematic curve of the biofilm development to Melo (1997), as shown in Figure 2.1. From the figure, it can be seen that there is a "delay" before the biofilm begins to develop. After the conditioning and initiating of biofilm growth, there is a rapid

development in the thickness of biofilm, and after a further period, this becomes stabilized around a mean value. The growth speed of biofouling depends on a number of factors, including water flow velocity, water quality, light and orientation.

2.1.2 Skin Friction caused by Biofouling

Biofilms increase frictional resistance and reduce hydraulic capacity. The energy losses due to biofilms are of major concern to industries, including hydroelectric power generators, water supply industries and ship owners (Andrewartha, 2010b; Lambert et al., 2008; Pryogle et al., 1997; Schultz et al., 1999).

Pollard et al. (1959) discovered that the head loss in a closed conduit (3.3m in diameter and 7.35 km in length) increased from 12.4 m to 16.8 m at a flow rate of 25.5 m³ in 17 years (35% increase). A rough black fouling deposit was found on the concrete lined walls. The average thickness of biofouling was 12 mm and the maximum depth up to 16 mm. The reduction in tunnel diameter of 25 mm by the fouling deposit would account for only 0.25 m additional head loss leaving a 4.15 m increase caused by the interaction of the flow with the deposit.

Melo (1997) reported that fouling in a cooling water heat exchanger was dominated by bacteria. This fouling increased back pressure for a given flow rate and reduced heat transfer for a given temperature difference in heat exchangers.

Minkus (1954) described the problem of a very smooth thin coat of dark-coloured slime which occurred in a 42 inch (1m) cast iron pipeline lined with 1/4 inch (6 mm) cement. It was found that the flow capacity was reduced from 50 million gallons per day to 44 million gallons (12 % loss) in 2 years. The cement lining was in good mechanical condition, but a very thin - about 1/32 to 1/16 of an inch (0.8 mm – 1.6 mm) deposit was found attached to the wall.

Picologlou (1980) conducted experiments on the pressure drop in tubular fouling reactors and concluded that the increase in friction corresponded to the increase of biofilm thickness or biofilm mass. The constriction of the tube due to biofilm production accounted for only approximately 10% of the frictional resistance. The biofilms caused more pressure drop across a tubular flow cell than a rigid film of the same thickness. He hypothesized that the increased pressure drop was due to the viscoelasticity of the biofilms.

Table 2.1 shows the design flow capacity reduction and head loss caused by biofouling in hydraulic pipes.

Reduction in design flow capacity	Duration	Biofilm thickness (mm)	Conduit diameter (cm)	Conduit length (km)	Conduit surface	Reference
12%	2 years	0.8	105	13	cement	(Minkus, 1954)
23%	----	1.6	90	13	concrete	(Minkus, 1954)
16%	3 weeks	3.0	90	41	steel	(Picologlou et al., 1980)
55%	3 years	0.635	60	93	steel	(Picologlou et al., 1980)
3.50%	1 year	----	36	2.5	steel	(Picologlou et al., 1980)
35% head loss	17 years	12.0	330	7350	concrete & steel	(Pollard et al., 1959)
29% head loss	9	--	258-293	1.725	steel	(Brett, 1980)
25% head loss	--	0.02-0.3	250	---	steel	(Barton, 2007a)

Table 2.1 Data of flow capacity reduction and head loss caused by biofouling in pipes.

2.1.3 Biofouling in Tasmanian Hydropower Schemes

About 60% of renewable energy has been generated by Hydro Tasmania in Australia since April 2006. Hydro Tasmania has been connected to the National Energy Grid (NEG) through Basslink (Perkins, 2010a). The Tarraleah Hydropower Scheme is located in the central highlands of Tasmania, and is a major generation scheme of Hydro Tasmania.

It was found that in Tarraleah, a common fouling species in open conduits and other illuminated locations is the diatom, but in cold freshwater pipelines the fouling mainly consists of thin bacterial slimes (Andrewartha, 2010b; McFie, 1973; McFie, 1976; Perkins et al., 2010b).

Brett (1980) reported that the headloss in Hydropower freshwater conduits was due to the amount of slime growth. The effective roughness caused by the slime was considerably larger than the absolute thickness of the layer measured in dewatered conduits. For example, the head loss test of a steel penstock 1,725 metres long and the internal diameter ranging from

2.93 m to 2.58 m in the Poatina Power Scheme increased from 6.50 m to 8.41 m at the flow rate 28.3 m³/s due to bacterial biofilms over a nine year period.

Brett (1980) also found that manganese bacterial slimes existed in the closed conduits and aquatic mosses and algae in the concrete canals of Hydro Tasmania's freshwater conveyance systems. Most of Hydro Tasmania freshwater steel penstocks were coated with coal-tar enamel, and the deposited bacteria biofilm causes this coating to crack after several decades of service, causing increased frictional resistance and reducing the protection against corrosion (Barton, 2007a; McFie, 1976).

Studies by former Hydro Tasmania and University of Tasmania research groups have shown that the accumulated biofilms in freshwater pipelines cause an increased head loss, and hence reduced generating efficiency for hydroelectric schemes. Cleaning of three main penstocks, including Wilmot penstock (2m ID), Poatina penstock (3m ID) and Tarraleah Hilltop No.1 pipeline (2.5m ID) was commenced between 2003 and 2005 by Hydro Tasmania (Barton, 2007a).

Head loss tests before and after cleaning with an unmanned high pressure water jet revealed a reduction in headloss of approximately 1.5 m at full machine load for the Wilmot penstock. At the same time, the equivalent sand grain roughness value k_s was improved from 0.21 mm to 0.04 mm (Barton, 2003). The Tarraleah Hilltop No.1 pipeline also showed a significant reduction in head loss, with a net gain of 2 m from the station output; a 25% improvement over the fouled pipe conditions. The equivalent sand grain roughness value k_s improved from 0.30 mm to 0.02 mm (Barton, 2005). However, the Poatina penstock showed no improvement in power station output. The friction factor f only changed from 0.0150 to 0.0147, mainly due to the deteriorated lining being having been exposed after the fouling layer was removed (Barton, 2004). This penstock was subsequently refurbished in 2011 to improve the internal surface condition.

The effect of biofilms on freshwater canal systems has also been documented by the University of Tasmania research group. A water tunnel was used for drag testing of rough and smooth test plates (Sargison et al., 2009). Andrewartha (2010) and Barton (2007) conducted a series of tests on freshwater biofilms grown on both smooth and rough test plates placed on site at Tarraleah. These plates were brought back to the UTAS for hydraulic testing and photogrammetric roughness characterisation; the results conclusively showing that both low-form gelatinous biofilms and filamentous biofilms grown on smooth or rough surfaces caused

significantly greater drag than the equivalent clean surface. It was also found that rough surfaces accumulated the most biofilms.

Three main different types of biofilms have been identified in Hydro Tasmania's freshwater conduit, including soft gelatinous slime (Barton, 2007a; Brett, 1980), hard deposits (Barton, 2007a; McFie, 1973), and filamentous algae (Andrewartha et al., 2007; McFie, 1976; Perkins, 2010a). Algal biofilm and soft bacteria slime photos are shown in Figure 2.2.

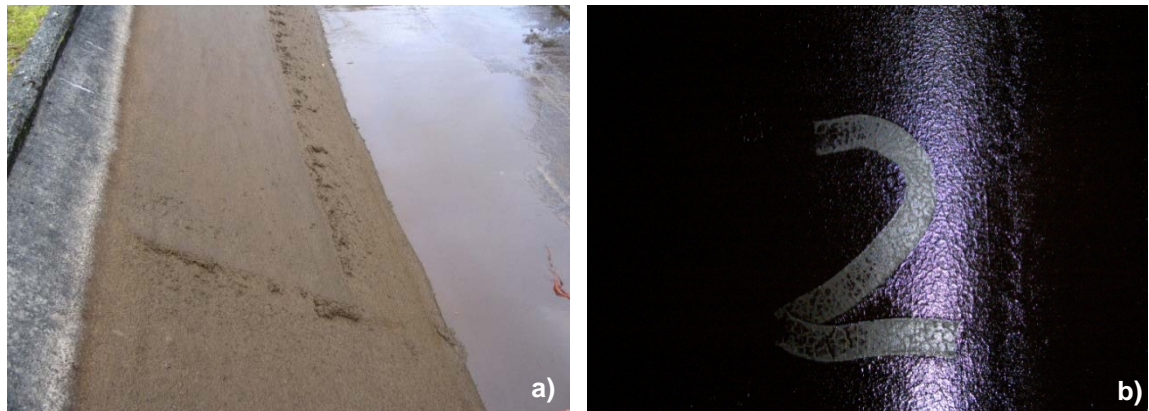


Figure 2.2 Different types of biofouling: (a) heavy algal biofouling of a hydropower canal in Tarraleah (Perkins, 2010a); (b) bacteria slime in a penstock at Poatina.

2.1.4 Methods of Biofouling Control

Methods such as chemical, physical, combined chemical and physical and surface coating have been used for fouling control (Bott, 2009). Volk (1999) suggested that biofilm problems could be limited by simultaneously addressing the three issues of nutrient levels, corrosion, and disinfection.

2.1.4.1 Chemical Methods

Since the 1950s, chlorine dosing in fresh water systems or directly spraying chlorine on fouling had been widely used for biofouling mitigation (Characklis, 1973; McFie, 1973; McFie, 1976; Minkus, 1954). However, new Environment Protection Agency regulations now restrict the use of chlorine disinfection in biofouling mitigation; chlorination can no longer be used, despite being the most efficient method for fouling removal. In industrial cooling water systems, some biocides with low environment impact are still used because of ease of use and efficiency. Lee et al.

(1998) found that chemical additives killed over 90% of biofouling, especially in the low velocity condition.

It is well known that calcium ions have a hardening effect on gelatinous biofouling. Pollard et al. (1959) used calcium ions to clean the closed pressure conduit. Here a concentration of 20 ppm calcium hydroxide was used to feed the conduit, and an impressive amount of the deposit was washed out.

LeChevallier (1991) found that when the biofouling was caused by living organisms, biocide would be useful for the cleaning of biofouling. However, when the deposit was caused by dead organic matter, biocide treatment was useless. Indeed, some biocides could increase the nutrient content by oxidising recalcitrant organics, making them more bio-available. Sommerfeld (1999) concluded that more oxidant dosages increased the residuals of iron and manganese.

Forward (1994) found the performance of many pumps in the Woolpunda Salt Interception Scheme in South Australia to be seriously degraded by up to 45% in 50 days due to iron bacteria fouling. Iron bacteria in the saline ground water pumping scheme was controlled by employing in situ generation of chlorine through electrolysis, which electrolysis provided effective control of iron deposition for the saline groundwater.

Schwartz et al. (2003) investigated the respiratory activities of the micro-organisms under UV disinfection (254 nm; 400 J/m²) and chlorine dioxide disinfection (0.12-0.16 mg/l) in drinking water. The results showed that *enterococci* were able to pass the UV disinfection barrier and persist in biofilms of the distribution system, but not after chlorine dioxide disinfection. The bacteria in drinking water were also able to regenerate more effectively after UVC irradiation than after chlorine dioxide disinfection.

2.1.4.2 Physical Methods

Generally, physical methods of biofouling control are short-term solutions (Colman, 2005). Underlying surfaces can be damaged by certain mechanical cleaning methods, including high-pressure water jet sprays, compressed air and steel brooms. The damaged substrates would then increase surface roughness and provide a preferred environment for colonisation of biofilm (Andrewartha, 2010b; Barton, 2007a). Methods such as ultra violet light, thermal, ultrasonic and filtration are other physical means of controlling the growth of biofouling.

Compressed water or air

Some mechanical cleaning methods such as steel broom and high-pressure water jet sprays are still widely used for cleaning canals and penstocks of freshwater conveyance facilities (Andrewartha, 2010b; Barton et al., 2008). Compressed air may be used to clean fouling in pipes (Lehtola et al., 2004). The main concern with these methods is that the cleaning process may damage the underlying surfaces and increasing the surface roughness of the substrate.

Ultraviolet treatment

The effect of UV irradiation on biofouling has been studied by some researchers. Panchal et al. (1995) carried out a laboratory experiment, which showed that UV irradiation could not completely eliminate biofouling. However, this method reduced the total use of chemical dosing.

Two experiments were conducted by Munshi et al. (2005) to investigate the UV effect on biofouling. Biofouling with and without UV treatment were compared. Results showed that bacteria were significantly reduced with only 0.85% remaining after UV radiation treatment.

UV light irradiation is being increasingly applied as a primary process for water disinfection, effective for inactivation of suspended cells. Lakretz et al. (2010) concluded that wavelengths between 254 nm and 270 nm were optimal for inactivation. The effect of UV on biofouling growth is examined in Chapter 3.

Ultrasonic treatment

It is possible to achieve chemical free microbial control in industry cooling water systems using ultrasonic treatment (Broekman et al., 2010). A combination of shear, micro-bubbles, high frequency (1.5-2.0 MHz), and low power (10 W/cm²) ultrasonic treatment was used by Broekman et al. (2010) in industry cooling systems, and the treatment showed excellent results in controlling bacteria and algae.

Thermal

Thermal treatment was successfully used by Callow (1993) to control young and adult mussels. Temperatures of 31.5 °C for 5 hours and 35 -38 °C for 1 – 2 hours were used. However, Perkins (2010a) found that a Jetwave pressure blasting unit spraying water at 60 °C and 2000psi pressure could not slow the re-growth rate of diatom fouling in a freshwater hydropower canal.

Filtration

Filter media for biofouling could be sand, filter coal, and manganese greensand in situ. It was a suitable method for pipes with low water flow rate (Flemming, 2002). Sommerfeld (1999) used a patented “High Rate Adsorption Iron & Manganese Removal Process” to remove high levels of iron bacteria, organic carbons, hydrogen sulfide and ammonia for low water flow pipes. Arsenic was also reduced to very low levels after this process. The result showed the filter media removed almost all the iron and manganese using the same filter vessel.

Physical plug

A method of maintenance for power station condenser heat transfer efficiency is the circulation of sponge rubber balls with the cooling water (Melo et al., 1997). However, these may block cooling pipes.

2.1.4.3 Coatings

It is well known that surface coatings can create a very smooth surface. The smooth surface decreases the surface roughness of the substrate, prevents biofilm colonisation and reduces the adhesion strength of biofilm (Andrewartha et al., 2009; Hodson et al., 2000). It also protects the substrate from corrosion and damage, and reduces the need for maintenance (Andrewartha, 2010b; Barton, 2007a; Pelletier et al., 2009). The ideal method of fouling prevention using protective surface coatings is a non-polluting one which produces no toxic component and does not affect the surrounding ecosystem.

Two-component epoxy paint is a type of convertible coating which dries by chemical curing. DTM 985 epoxy paint was used in the Colour Effect on Biofouling Trials in this thesis, and will be discussed in Chapter 3.

The internal surfaces of some steel penstocks in Hydro Tasmania were painted with coal-tar enamel in their internal surfaces (Barton et al., 2008). However, this is no longer used owing to environmental concerns.

Barton (2007a) conducted an experiment to investigate the performance of different types of paints on the growth of biofouling. Twenty types of paints were used on mild steel plates. Painted plates were submerged in freshwater canal and pond at three locations of the Tarraleah

Power Scheme in Hydro Tasmania. It was found that five paints were better performing than the others.

Andrewartha et al. (2009) examined the performance of plates with smooth, coated surfaces and those with rough surfaces (with or without coating). Two types of coating (Sikagard 680s and Jotamastic 87) were applied on smooth and rough plates. Plates were then submerged in fresh water over seven months at Pond No. 1 and Canal No. 1, which are both lined with concrete at the Tarraleah Power Scheme Hydro Tasmania, Australia. It was found that smooth plates with surface coating performed best and rough plates without coating performed worst in resisting the growth of biofouling.

Silicone coatings are also a type of antifouling coating (Candries et al., 2000b; Hodson et al., 2000). It was found that a plate with a silicone coating had 1.4% lower fouling than one coated with a Tributyltin-free Self-Polishing Co-polymer (Candries et al., 2000b). Less fouling weight also occurred on white silicone coated netting (1.9 kg/m^2) compared to uncoated white netting (7.8 kg/m^2) after 163 days of immersion (Hodson et al., 2000).

2.2 Effect of Substratum Colour and Ambient Light Conditions on Biofouling

It is well known that a large number of factors may influence biofouling community development. Characklis (1981) suggested that the formation of biofouling was due to two major mechanisms: (1) settlement of microorganisms from suspension in fluid onto the surface and (2) growth and reproduction of microorganisms within the biofilm.

The settlement of biofilms on a surface is affected by many factors, including surface colour, surface texture, surface orientation, position and the light that the surface receives (Dahlem et al., 1984; Hodson et al., 2000; Swain et al., 2006). Guenther et al. (2009) found that colour affected not only the settlement but also the adhesion strength of biofouling. The settlement of fouling is a main factor influencing the growth rate of biofouling (Su et al., 2007).

2.2.1 Substratum Colour Effect

Colour is believed to have a short-term effect on the settling of a biofouling community. The long-term colour effect on biofouling may be reduced as biofilms develop and obscure the primary colour effect from the surface. However, the delayed settlement of biofouling means fouling will take a longer time to fully develop. Su et al. (2007) studied smooth and rough plates with or without biofilms, and it was found that rough plate without biofilm had less fouling than smooth plate with biofilm after four days.

The effect of colour on marine biofouling has been investigated during last few decades. Generally, deep colour substrates (black) attracted far more fouling than light colour (white) substrates under light conditions (Dahlem et al., 1984; Shine et al., 2010; Su et al., 2007). Some results of these experiments are shown in Table 2.2.

Colours & materials	Duration	Fouling Results	Reference
light & black clear PVC panels	—	Black and horizontal surfaces collected most fouling, Light coloured and horizontal panels collected the most number of species	(Dahlem et al., 1984)
white silicone-coated; uncoated white & uncoated black nets	163 days	White silicone-coated net: 1.9 kg/m ² ; uncoated white net: 7.8 kg/m ² ; uncoated black: 8.5 kg/m ²	(Guenther et al., 2009)
white, banded & black turtle-headed sea snakes	5 years	Black snakes had most heavily algae-covered	(Shine et al., 2010)
white, banded & black banded plastic snake models	29 days	Black snakes had most heavily algae-covered	(Shine et al., 2010)
red, green, blue, white & yellow	5 months	Red and blue coloured surfaces collected more fouling	(Satheesh et al., 2010)
black, red, blue, yellow & white Perspex plates	—	Red and black surfaces collected more fouling	(Yule et al., 1984)
red, blue, green & yellow	4 days	Red and blue coloured surfaces collected more larvae	(Su et al., 2007)
white, black & clear acrylic plates	14 days	Acrylic with white colour background had less fouling than those with black colour background	(Swain et al., 2006)

Table 2.2 Effect of substratum colour on biofouling

The effect of colour on freshwater biofouling was investigated by Swain et al. (2006). It was found that acrylic plates with a white colour background had less fouling than those with a black background.

2.2.2 Light Effect on Biofouling

It is known that visible light has a wavelength ranging from approximately 380-760nm, and Ultraviolet (UV) light is in the range 10 nm to 400 nm. The sun emits ultraviolet radiation in the UVA (320 - 400 nm), UVB (290 - 320 nm), and UVC (220 – 290 nm) bands. About 98.7% of the ultraviolet radiation reaching the Earth's surface is UVA.

While ordinary window glass passes about 90% of the light above 350 nm, it blocks over 90% of the light below 300 nm. Transmittance of light in water decreases with increasing depth, water turbidity and dissolved salts. Former researchers found that shaded surfaces are better collector of fouling organisms than well-illuminated substrates (Andrewartha, 2010b; Barton, 2007a). Callow et al. (2000) and Prendergast et al. (2009) also found the settlement of some biofouling species showed negative phototaxis; in other words, the biofouling species moved away from light.

Swain et al. (2006) suspended six sandwich-like test sections 40 cm under the water surface in different orientations, including north, south, east and west. The test section that faced west was the most fouled. However, the effect of light on biofouling was not investigated in their site experiment.

Dobretsov et al. (2010; 2005) studied the effects of ambient solar ultraviolet radiation (UVR) and photosynthetically active radiation (PAR) on the growth of biofouling at depths of 4 cm and 15 to 20 cm. The results concluded that UVR and PAR controlled the fouling composition of early succession, settlement and development of biofouling communities in tropical waters.

Hung et al. (2005) investigated effects of UV radiation on larval attachment. Results showed that both UVA and UVB caused a decrease in the percentage of respiring bacterial cells in microbial films, and this effect increased with UV energy. UVB caused a greater decrease in respiring bacterial cells than UVA at the same UV energy.

The impact of ultraviolet light on bacterial adhesion to glass and metal oxide-coated surfaces (TiO_2 & SiO_2) was studied by Li et al. (2005). UV light irradiation reduced the adhesion of bacteria on both glass and metal oxide-coated surfaces. UVA light reduced the bacterial adhesion to the TiO_2 surface by 20–50%. UVC light reduced bacterial adhesion to both TiO_2 and SnO_2 surfaces by 20–68%.

Perkins (2010a) examined fouling samples which were taken from a hydropower canal. Maximum quantum yield and minimum saturating irradiance measurement method were used in the study. It was found that fouling on the less-exposed wall had adapted to lower light and was healthier. Perkins (2010a) thought less healthy biofouling might be due to light exposure, nutrient depletion, or both.

2.3 Effects of Water Quality and Physical Factors on Biofouling

The effects of colour and light on biofouling have been reviewed in Section 2.2. The following section details the effects of water quality and physical factors such as water flow velocity and surface texture on the growth of biofouling.

Field experience shows that a variety of parameters influence biofilm growth. Volk et al. (1999) found that factors such as water temperature, disinfectant type and residual, selection of pipe material, corrosion control, and hydraulic conditions might be more influential than the levels of organic matter in regulating the biological activity of biofilms.

2.3.1 Effect of Water Quality on Biofouling

It has been reported that the growth rate of biofouling is affected by many factors such as temperature, pH value, metals, nutrients, oxygen, organics, velocity and turbulence, surface condition and types of bacteria (Bott et al., 1977; Cullimore et al., 1978; Melo et al., 1997). A change in nutrient concentration, shear forces, temperature or other factors can cause either biomass production or the sloughing of biofilms.

Effect of temperature

Bott et al. (1977) explained that thickness of a biofilm increased by 70% in slime mass by raising the temperature from 30 °C to 35 °C, as shown in Figure 2.3. Lee et al. (1998) also found that the biofouling at 35 °C was about 1.75 times thicker than at 45 °C in cooling water pipes.

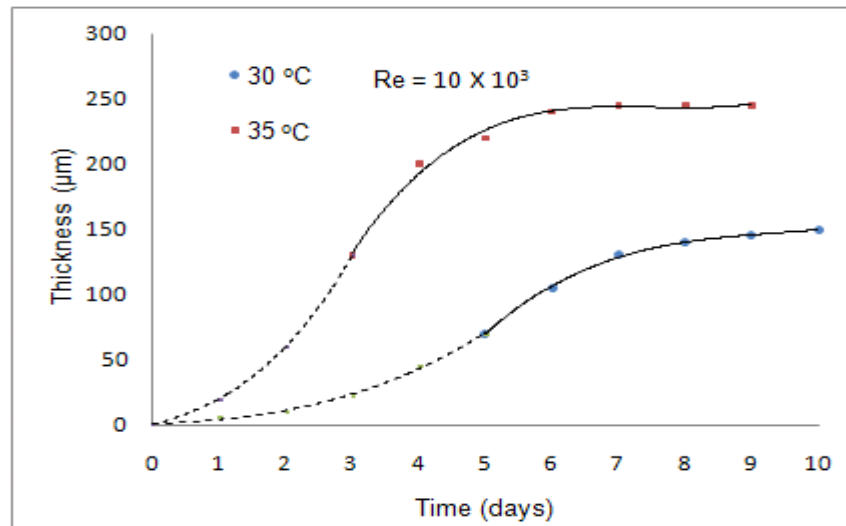


Figure 2.3 Effect of temperature on slime formation (Bott et al., 1977).

Hallam et al. (2001) studied biofilm activity and found that most of biofilm activity fell with lower water temperatures, suggesting that biofilm activity was approximately 50% lower at a temperature of 7 °C than at 17 °C.

For many types of bacteria found in cooling water systems, the optimum temperature for maximum growth is about 40 °C (Melo et al., 1997), the temperature likely to be encountered in industrial water coolers. The cooling water of Tungatinah Power Station operated by Hydro Tasmania reaches a temperature of 27 °C with flow rate 2.33 cubic metres per minute. At this temperature, small changes in temperature are likely to produce substantial changes in biofilm growth, since microbial activity is highly sensitive to temperature.

pH value

pH value is one of the factors that affect the growth speed of biofouling (Cullimore et al., 1978). Pinheiro et al.(1988) found that some iron bacteria grow faster with pH values of 7 rather than more alkaline values of pH = 9.

Iron and Manganese

As suggested by the name “iron bacteria”, iron can play a key role in controlling the growth of the organisms. However, manganese is a major component of “iron bacteria” in penstocks (Barton, 2007a; Minkus, 1954; Pollard et al., 1959; Tyler, 1968). The rate of reduction of dissolved manganese may be affected by the concentration of iron present. Iron and manganese are two main factors that commonly affect the growth of bacteria biofouling in pipes (Barton, 2007a; Minkus, 1954; Pollard et al., 1959; Tyler, 1968).

Minkus (1973) dried bacterial slime from a pipeline and found the iron content ranged between 8% -- 20%, the remainder consisting of silica, calcium and magnesium. He took two water samples from the intake of Phelps Brook Dam, New England and the discharge end of the supply mains on the same day. The chemical analysis showed that the manganese level was 0.008 ppm and 0.004 ppm at the intake and the discharge respectively. The 50% reduction indicated that some manganese was left behind in the pipeline.

Cullimore et al. (1978) found that the growth of iron bacteria occurred in static water at between 1.6 and 12 mg/L iron. In flowing water, such as a pumping well, growth of iron bacteria could occur if the iron concentration exceeded 0.2 - 0.5 mg/L because of the continuous flow of nutrients.

Tyler (1968) conducted an experiment to investigate the effect of manganese on biofouling using lake freshwater from Hydro Tasmania, Australia. Three recirculatory apparatus were used in the experiment. Manganese sulphate was put into the lake water of one apparatus and nothing into the other two. A heavy deposit was observed in the apparatus containing the added manganese sulphate, but only a slight trace was found in the other two apparatus after five days. Tyler (1968) concluded the level of available manganese plays an important role in biofilm formation.

Stalk bacteria was found in fouled wells by Stuetz et al. (2004), who concluded the concentration of dissolved iron in the aquifer to be the key factor that determined whether a well was fouled. It was also found that dissolved oxygen in all wells was adequate to support bacterial growth and did not appear to be a controlling factor in whether these wells fouled.

Nutrients

Cullimore et al. (1978) found that high levels of nutrients appeared to produce an "open" structure in the biofilm. The growth speed of bacteria was controlled by the amount of nutrients in the water, such as organic carbon. Organic carbon exists in a variety of types, such as citrate, glucose and even lettuce and willow leaves. Sommerfeld (1999) found that levels over 2 mg/L total organic carbon can result in elevated iron and manganese residuals. Melo et al. (1997) conducted an experiment at a given velocity of 1.2 m/s through a tube, and it was found that raising the nutrient level (based on glucose) from 4 mg/L to 10 mg/L increased biofilm thickness by more than 400%. Lee et al. (1998) also found the growth rate of biofouling increased proportionally to the concentration of microbial suspended solids and displayed linearly with time.

Pryfogle et al. (1997) found that the algae growth speed was affected by other nutrients, including nitrate, nitrite, orthophosphate and ammonia. Volk et al. (1999) also found that lower nutrient levels with biological filtration led to lower biofilm densities. However, the effect of nutrient reduction on biofilm concentrations was not immediate.

Lambert et al. (2009) investigated the growth of biofilms from different initial inoculums and the results showed that growth patterns and strengths of biofilms under different initial inoculums were different.

Dissolved organic carbon:

Lambert et al. (2008; 2009) found that dissolved organic carbon (DOC) worked as a nutrition factor that increased the growth of biofouling. Lambert et al. (2008) studied two different concentrations of DOC to investigate the growth of biofilm, finding that the growth of biofilm increased when the DOC level increased. Pabich et al. (2001) found that the concentrations of DOC decreased with increasing depth below the water table.

Turbidity and particles:

Turbidity is a physical characteristic of water, which depends on the concentration of the fine particles in the water. Bacteria growth may affect the turbidity, taste, odour and colour of water. Lehtola et al. (2004) found that the turbidity of water was increased by increased microbial numbers in water due to biofouling.

Attraction between negatively-charged bacteria and the electro-positive surfaces of the particles could occur, depending on the pH value of water. The adsorption of molecules on the surface of clay particles may have an important effect on the activity of the bacteria, leading to an increase in biomass formation. Vieira et al. (1995) found that when kaolin particles were used in the experiment, these particles increased the accumulation of biomass. However, abrasive particles such as sand may have a scouring effect on biofouling (Melo et al., 1997).

2.3.2 Impact of Physical Conditions on Biofouling

The physical characteristics of the solid-water interface are among the controlling factors that may influence the growth of biofouling. Barton (2007a) found that pipe characteristics and conditions were determining factors in bacterial re-growth. An increase in wall shear stress could cause significant changes in the morphology and thickness of the biofilm (Bott et al., 1977; Lee et al., 1998).

Velocity

Velocity is one of the factors that affect the growth of biofouling. Lambert et al. (2009) studied the impact of velocity on growth of biofilms, finding to be the dominant factor in determining the roughness of biofilms and their resistance to fluid shear. It was found that the thickness of biofilm decreased with an increase in velocity (Bott et al., 1977; Cloete et al., 2003; Lauchlan et al., 2007; Lee et al., 1998). However, the cohesive strength of biofilm which was the maximum shear strength the biofilm could afford when water flowed was higher in the case of the biofilm formed at higher shear stress (Lambert et al., 2009; Vieira et al., 1993).

Bott et al., (1977) explained the effect of fluid velocity on the thickness of slime, which is shown in Figure 2.4. It can be seen that an increase in Reynolds number by a factor of 2.5 (from 6.3×10^3 to 15.3×10^3) promoted a decrease in slime thickness by nearly the same factor (245 μm to 100 μm). However, the decrease in slime thickness was not necessarily a decrease in the slime mass (an increase in slime density).

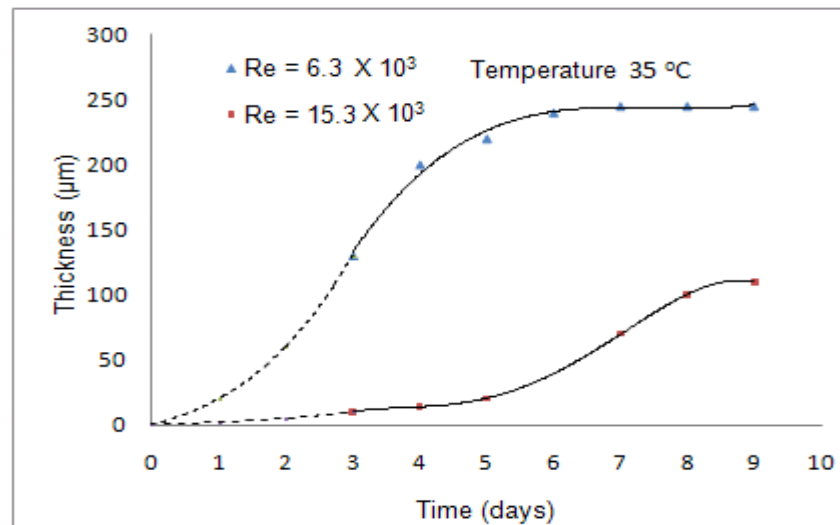


Figure 2.4 Effect of Reynolds number (velocity) on slime formation (Bott et al., 1977).

Melo (1997) stated that at the fixed conditions of nutrient concentration for a velocity of 0.54 m/s, the biofilm thickness after 15 days was ten times as thick as that developed under a 2 m/s water flow. Velocity also affects the density of the biofilm. Experiments with *Pseudomonas fluorescens* showed that as the velocity increased from 0.13 m/s to 0.43 m/s, the density of the dry biofilm increased from 26 kg/m³ to 61 kg/m³ for an aluminium cylindrical duct at pH = 7 (Pinheiro et al., 1988).

Bott et al. (1983) conducted an experiment in aluminium tubes with no added nutrient to investigate the effect of velocity on biofouling in cooling water pipes. It was found that an increase in velocity up to 1.0 m/s resulted in an increase in biofilm weight, due to the increased deposit rate. Lee et al. (1998) also found that the growth rate of biofouling at a velocity 0.15 m/s was four times higher than at a velocity of 0.3 m/s in a cooling water system.

Two sets of experiments were conducted by Pujo et al. (1991) to investigate fouling in cooling water systems at different fluid velocities with a constant Reynolds number, and also at different Reynolds numbers with constant fluid velocity. It was found that the maximum biofilm growth occurred at a velocity of around 0.5 m/s under a low Reynolds number (12,000). At a Reynolds number of 16,800 (water velocity of 1 m/s at 25 °C and 15 mm tube diameter) with a different velocity, biofilm development was very low, even at a velocity of 0.46 m/s. The effect of a Reynolds number at the constant velocity of 0.9 m/s showed that biofilm development was suppressed at a Reynolds number of 16,800. The results of the experiment suggested that a

velocity over 1 m/s should be used in industrial cooling water systems to minimise fouling growth.

Surface roughness

Surface roughness is known to influence the settlement of biofouling species and communities. Texture can influence the nature of the flow over the surface; hence rougher surfaces are more prone to microbial colonisation than smooth ones (Andrewartha, 2010b; Barton et al., 2010). Barton et al. (2007b) used two plates with fine grit (0.5 - 4 mm particles) and coarse grit surfaces (2 - 4 mm particles) to investigate the difference in growth of biofilms. Results demonstrated that biofilms colonised faster on the plate with the coarser grit surface.

Verran et al. (1991) investigated the effect of surface roughness on biofouling by using polished, clear acrylic sheets which had been abraded by emery paper of different grit size. It was found that the adhesive numbers of biofilms on the roughened acrylic sheet were significantly higher than those on the smooth acrylic sheet, and that the maximal adhesion was achieved on acrylic sheet roughened with medium grit size emery paper.

Coletti et al. (2010) studied the effect of surface roughness on growth of biofouling in industrial cooling pipes. The results demonstrated that the growth rate of biofouling in rougher pipes was faster than that in smoother pipes.

2.4 Turbulent Flow in Pipes

This section introduces the concept of turbulent flow, the impact of biofouling on skin friction and velocity distribution in biofouled pipes.

2.4.1 Turbulent Flow in Pipes

Velocity profiles of laminar and turbulent flow in smooth and rough pipes are given in Figure 2.5.

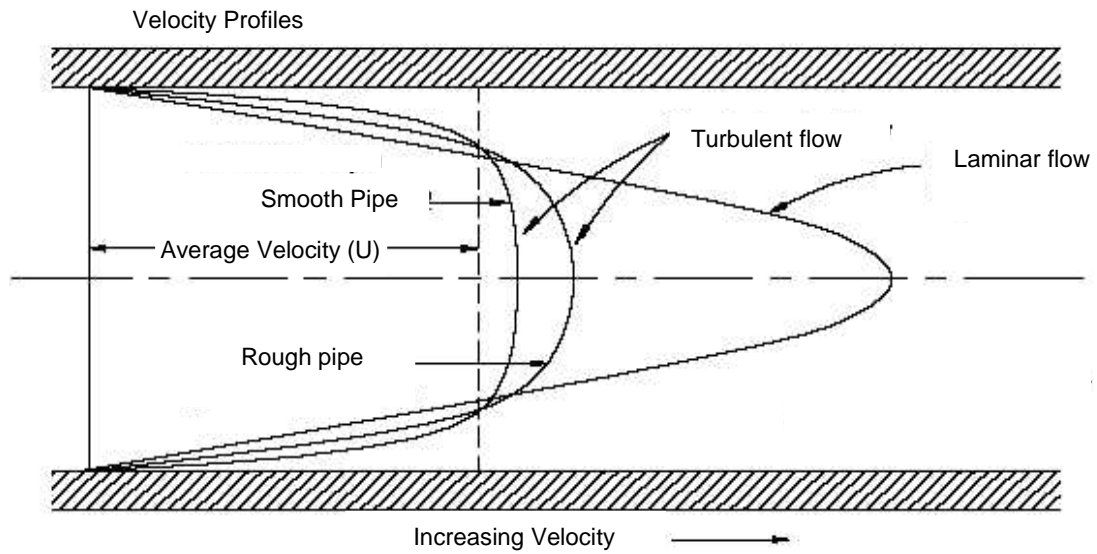


Figure 2.5 Laminar flow and turbulent flow in smooth and rough pipes (Cengel et al., 2006).

As flow enters into a pipe, the boundary layer is initially in a laminar form, and will change depending on the ratio of inertial and viscous forces, called Reynolds number (Re , Equation 2.1).

$$\text{Reynolds number} = \frac{\text{Intertial forces}}{\text{Viscous forces}} = \frac{\rho U D}{\mu} \quad (\text{Equation 2.1})$$

The flow is said to be fully developed once the boundary layer has reached the centre of the pipe and the velocity profile no longer changes with distance. The entry lengths of a pipe for fully developed flow, laminar and turbulent flow are different, with entry lengths of 115 times and 10 times the diameter of pipe for laminar flow and turbulent flow respectively (Cengel et al., 2006).

Turbulent flow is a flow regime in which the movement of fluid particles is eddying and unsteady. It produces high levels of mixing and has a more uniform velocity profile than a laminar flow profile. Normally, turbulent flow occurs in pipes when the Reynolds number $Re \geq 4,000$. Most flows of practical engineering interest, including flows in hydropower pipelines and canals are turbulent.

It is difficult to establish mathematical models for turbulent flow due to its complex nature. However, over the years researchers have proposed many equations for shear stress and head loss in turbulent flow. Empirical information has been used successfully and extensively in turbulent flow design. Empirical equations including the Darcy-Weisbach equation, Colebrook-White equation (Colebrook, 1939) and Moody diagram (Moody, 1944) are commonly used.

Darcy-Weisbach equation

$$H_f = f \frac{L U^2}{D 2g} \quad (\text{Equation 2.2})$$

Colebrook-White equation

$$\frac{1}{\sqrt{f}} = -2.0 \log_{10} \left(\frac{k_s}{3.7D} + \frac{2.51}{\text{Re} \sqrt{f}} \right) \quad (\text{Equation 2.3})$$

2.4.1.1 Turbulent Flow in Smooth Pipes

Friction in pipe flows is governed by the relative roughness of the pipe wall and the Reynolds number. The velocity distribution and skin friction for both smooth and fouled rough pipes under high Reynolds numbers have been investigated by Lambert et al. (2009).

Lambert et al. (2009) used the following logarithmic law equation from Cengel et al. (2006) (Equation 2.4) to calculate the velocity distribution in hydraulically smooth pipes.

$$\frac{u}{u_*} = \frac{1}{\kappa} \ln \frac{y u_*}{\nu} + A \quad (\text{Equation 2.4})$$

where $\kappa = 0.40$ is Von Karman constant; A was chosen as 5.5 by Nikuradse (1933) for smooth pipes. The friction velocity u_* is described in the following equations:

$$u_* = \sqrt{\frac{\tau_w}{\rho}} \quad (\text{Equation 2.5})$$

$$\tau_w = f \rho \frac{U^2}{8} \quad (\text{Equation 2.6})$$

Lambert et al. (2009) plotted the theoretical velocity profiles and the measured velocity profiles of smooth pipes using Equation 2.4 as shown in Figure 2.6. It can be seen that good agreement between the theoretical and measured velocity profiles was achieved.

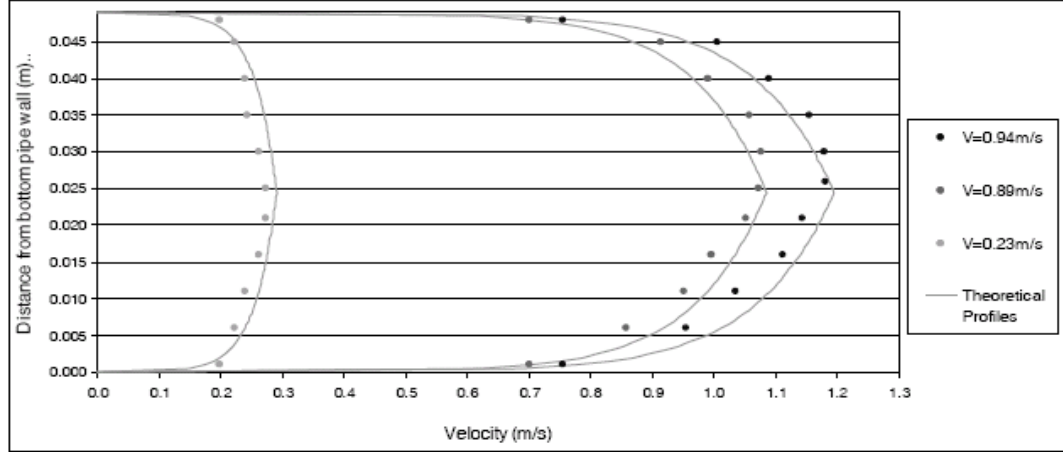


Figure 2.6 Theoretical and measured velocity profiles in smooth pipes (Lambert et al., 2009).

2.4.1.2 Turbulent Flow in Biofouled Pipes

The effect of biofouling on skin friction of pipes has been investigated over the last century. The friction depends on the smoothness (absolute roughness) of the surface in pipes. Relatively small projections and irregularities have a significant effect on these friction losses, particularly at high velocities, due to the boundary layer effect. It was recognised that fouling caused additional energy dissipation due to the viscoelastic and filamentous structure of biofouling (Andrewartha et al., 2010; Picologlou et al., 1980).

Colebrook-White Equation in biofouled pipes

For fully developed steady flow in circular fouled pipes, two important formulas have been used to calculate and evaluate the friction factor f . Equation 2.7 was used to find the friction factor f in the circular pipes after the head loss was obtained (Barton et al., 2008; Lambert et al., 2009) and the Colebrook-White equation (Equation 2.3) was used to evaluate the friction factor by Lambert et al. (2009) in the Moody diagram (Moody, 1944).

$$f = H_f \frac{D}{L} \frac{2g}{U^2} \quad (\text{Equation 2.7})$$

Head loss between two test points in Equation 2.7 can be obtained through the Energy Equation (Equation 2.8) for steady, incompressible water flow.

$$\frac{P_1}{\rho g} + \frac{U_1^2}{2g} + z_1 = \frac{P_2}{\rho g} + \frac{U_2^2}{2g} + z_2 + H_l \quad (\text{Equation 2.8})$$

Barton et al. (2008) studied the hydraulic performance of pipelines at three different Hydro Tasmania sites in Tasmania, Australia. It was found that when the data (f , k_s/D , Re) of fouled pipelines were plotted in a Moody diagram (Moody, 1944), they did not follow the Colebrook-White friction type relationship in the smooth-rough transition regime. Results of Barton et al. (2008) for the Wilmot Penstock and the Tarraleah No.1 Hilltop Pipeline are shown in Figures 2.7 & 2.8.

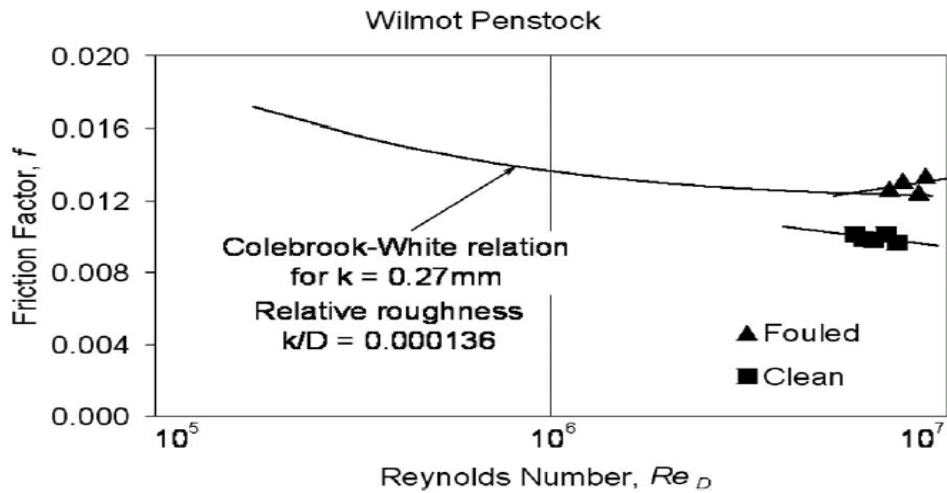


Figure 2.7 Moody diagram for Wilmot penstock (Barton et al., 2008).

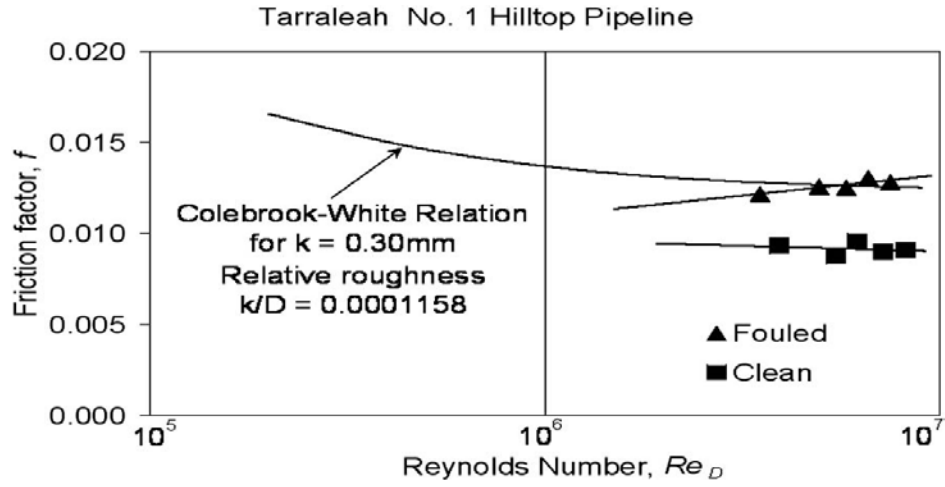


Figure 2.8 Moody diagram for Tarraleah hilltop pipelines (Barton et al., 2008).

Lambert et al. (2009) found that the Von Karman constant was lower in biofouled pipes than the generally accepted value of 0.4 for rough pipes. They also found that the Colebrook–White equation (Equation 2.3) for rough pipes was not suitable for fouled pipes. There was a trend of decreasing κ with the decrease of the velocity.

A modified Colebrook–White equation (Equation 2.9) was suggested by Lambert et al. (2009) for fouled pipes. This is shown to have better agreement than the standard correlation for rough pipes (Figure 2.9).

$$\frac{1}{\sqrt{f}} = -\frac{1}{\sqrt{8\kappa}} \ln \left[\frac{k_s}{0.85D} + \frac{2.51}{Re_c \sqrt{f}} \right]$$

(Equation 2.9)

where κ is the Von Karman constant of biofouled pipe.

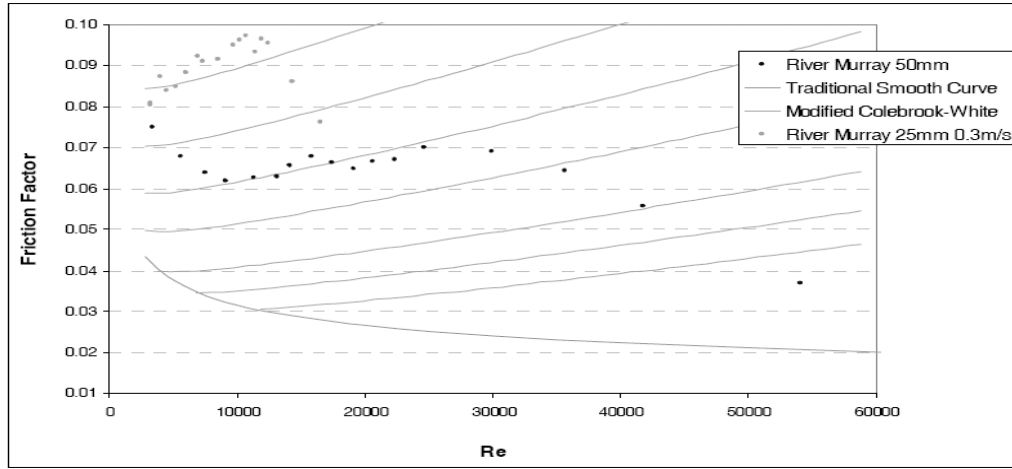


Figure 2.9 Modified Colebrook-White curves with observed data (Lambert et al., 2009).

Velocity distribution in biofouled pipes

The velocity profiles in biofouled pipes were also investigated by Lambert et al. (2009). The theoretical velocity profiles were plotted by using Nikuradse (1933) formula (Equation 2.10) for artificial rough pipes:

$$\frac{u}{u_*} = \frac{1}{\kappa} \ln \frac{y}{k_s} + B \quad (\text{Equation 2.10})$$

where $\kappa = 0.4$ is the Von Karman constant and $B = 8.48$ for artificial rough pipes.

Both theoretical velocity profiles from calculation (Equation 2.10) and data from the biofouled pipes experiment are given in Figure 2.10 from Lambert et al. (2009). It was found that the expected velocity profile was lower near the centre of pipes than the velocity distribution tested in biofouled pipes. Lambert et al. (2009) made some modifications to the Von Karman constant κ and B for Equation 2.10, as shown in Table 2.3.

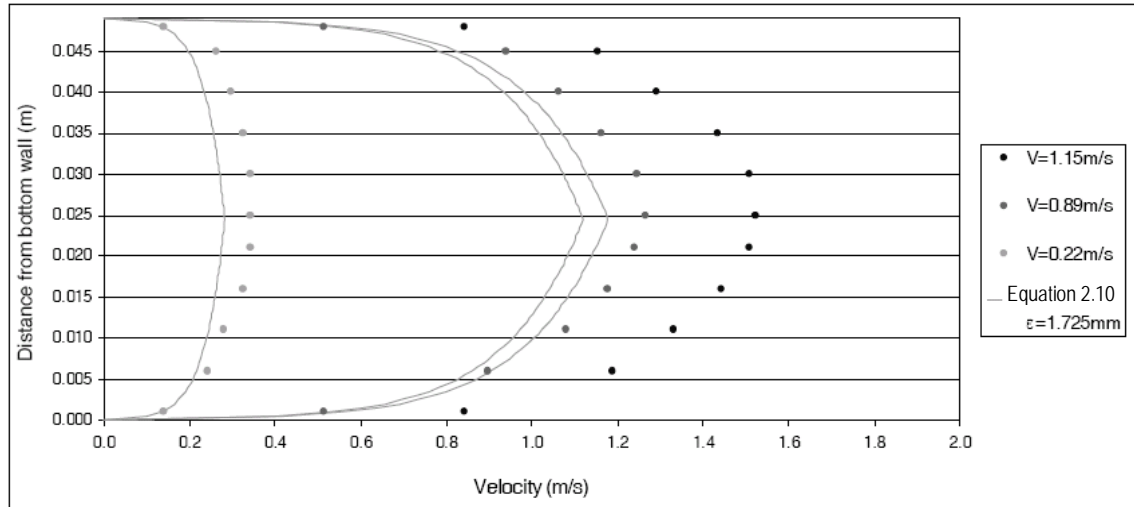


Figure 2.10 Expected velocity profiles $k_s = 1.725 \text{ mm}$ ($k_s/D = 0.034$) (Lambert et al., 2009).

Velocity profiles (m/s)	κ	B
1.15	0.3569	12.25
0.89	0.3106	8.85
0.22	0.2821	9.60

Table 2.3 Variable constant B and Von Karman constant κ in fouled pipes (Lambert et al., 2009).

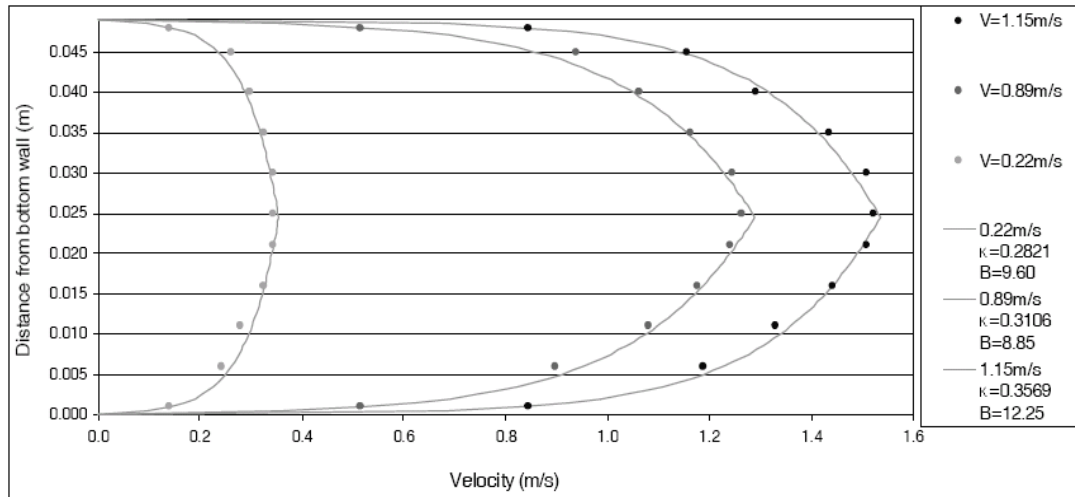


Figure 2.11 Observed and expected velocity profiles using modified variable κ and B of Table 2.3 in Equation 2.10 (Lambert et al., 2009).

The velocity profiles were obtained using the above modified Von Karman constant κ and constant B in Table 2.3 and Equation 2.10. The modified velocity and tested velocity profiles were well matched, as shown in Figure 2.11.

Greater B values and a smaller Von Karman constant κ were used by Lambert et al. (2009), as listed in Table 2.3 as compared to a Von Karman constant $\kappa = 0.4$ and $B = 8.48$ adopted by Nikuradse (1933) for artificial rough pipes. The increased B and decreased κ values in Equation 2.10 resulted in an increased value of u/u_* . Therefore, the velocity profiles in the centre streamline of biofouled pipe were faster than that of artificial roughed pipe at the same equivalent sand grain roughness, in order to keep the same average flow velocity in pipes (Figure 2.11).

2.4.2 Turbulent Flow Measurement Techniques

There are several well known techniques for measuring velocity profiles of turbulent flow in pipes, such as Pitot-Static Probe, Laser Doppler Velocimetry (LDV) and Ultrasound Doppler Velocimetry (UDV). These measuring instruments were evaluated against the requirements in this project to ascertain the suitability for the pipe rig in the laboratory of the School of Engineering at UTAS.

Pitot tube and static wall tapping

The Pitot tube is a simple, inexpensive, highly reliable device because it has no moving parts. It was invented in the eighteenth century and is still widely used for velocity profile and flow rate measurements (Allen et al., 2007; Lambert et al., 2009).

The Pitot tube uses the theory of the Bernoulli equation (Equation 2.11) to measure the velocity of turbulent flow (Cengel et al., 2006).

$$P + \rho \frac{V^2}{2} + \rho g z = \text{constant (along streamline)} \quad (\text{Equation 2.11})$$

where P is the static pressure, $\rho V^2/2$ is the dynamic pressure and $\rho g z$ is the hydrostatic pressure.

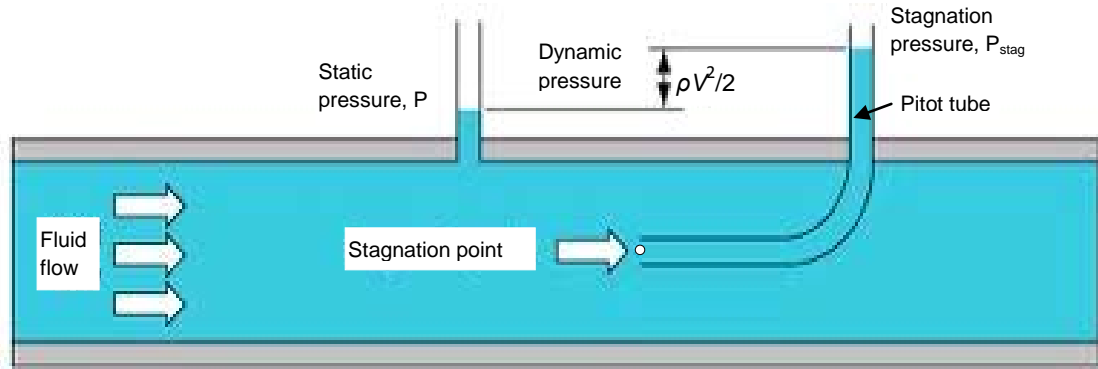


Figure 2.12 Static, dynamic, and stagnation pressures.

The sum of the static and dynamic pressures is called the stagnation pressure, which is expressed in Equation 2.12. Stagnation pressure is measured by a Pitot tube; static pressure is measured by static wall tapping at a specified position, and the velocity at that point can be calculated by Equation 2.13.

$$P_{stag} = P + \rho \frac{V^2}{2} \quad (\text{Equation 2.12})$$

$$V = \sqrt{\frac{2(P_{stag} - P)}{\rho}} \quad (\text{Equation 2.13})$$

The disadvantage of the Pitot tube is that the streamline is affected by the tube in turbulent pipe flow (Zagarola et al., 1997) and the measured results need to be corrected to maintain the measurement accuracy for velocity in the fully developed turbulent pipe (McKeon et al., 2003).

Laser Doppler Velocimetry (LDV)

The Laser Doppler Velocity Profiler is a popular instrument used in laboratory research due to its high accuracy and high frequency response. It is widely used for turbulent boundary layer studies (Andrewartha et al., 2010; Candries et al., 2005; Schultz, 2004; Schultz, 2000).

LDV uses two beams of laser light obtained by splitting a single beam to ensure the coherency between the two beams. The point measurement is made through two laser beams crossing. LDV was used to investigate the velocity distribution in turbulent flow pipes made of Perspex and acrylic polymer (Den Toonder et al., 1997; Sato et al., 2002). Den Toonder et al. (1997)

found that it was difficult to measure the velocity at locations close to the pipe wall with LDV, due to the refraction of the laser beam by the curved pipe wall. A special test section was made to eliminate this problem.

Ultrasound Doppler Velocimetry (UDV)

UDV uses pulsed ultrasound echo to detect the Doppler shift of the ultrasound wave reflected from moving particles in the fluid. Detailed working principles and methods of UDV were described by Takeda (1995). It was found that the UDV technique had three major advantages:

- (1) It obtained spatio-temporal information about the flow field.
- (2) It was applicable to no-transparent liquids.
- (3) It was a line measurement and the flow mapping was practicable.

UDV was used to measure the velocity profile in both transparent and non-transparent liquids in plastic and copper pipes (Brito et al., 2001; Zidouh, 2009), and performed well in both experiments.

Summary

In summary, a suitable method in the current study for measuring velocity profiles is the Pitot tube. UDV is suitable for velocity measurement of the non-metal and metal pipes with its wall cut at an angle (Brito et al., 2001). LDV is not particularly well-suited for velocity measurement of metal pipes since it requires a flat transparent window to enable a laser beam to travel across the window to the measurement volume.

2.5 Chapter Summary

This chapter has reviewed previous research on the effect of substratum colour and ambient light on the growth of biofouling in fresh water, the effect of water quality on the growth of biofouling and the velocity profile measurement in fouled pipes.

The effects of substratum colour and UV light on the growth of biofouling in open channels were also reviewed. This study will focus on the effects of colour and UV light on two diatom species, *Gomphonema tarraleahae* and *Tabellaria flocculosa*, which were found in Tarraleah Canal No.1 and Pond No. 1 in central Tasmania, Australia.

This chapter also reviewed literature and research on biofouling in pipes. It has revealed that pipes that are subject to biofouling may not follow the widely used Colebrook-White equation and Moody diagram, which has significant implications. The velocity distribution and skin friction of fully developed turbulent flow in biofouled pipes will be investigated in detail in this study over a wide range of Reynolds numbers. Velocity profiles will be obtained by using a Pitot tube and static wall tapping in the laboratory. The results will be examined using Nikuradse's (1933) formula for typical rough pipes and the Colebrook-White equation.

The effects of chemical elements in fresh water and of flow mechanics on the growth of biofouling have been reviewed. This study will investigate the links between biofouling and different water parameters in nine lakes of Hydro Tasmania, Australia.

Several techniques for measuring the velocity distributions in the pipe flows have also been reviewed.

Chapter 3 Effect of Substratum Colour and Ambient Light Conditions on Biofouling

It has been reported that the settlement of biofilms on a surface is affected by factors such as surface colour, surface texture, surface orientation, position and the light that the surface receives (Dahlem et al., 1984; Hodson et al., 2000; Swain et al., 2006).

Colour is regarded as having a short-term effect on the settling of a biofouling community. Delayed settlement of biofouling will increase the amount of time it takes for the fouling to become fully developed (Dahlem et al., 1984; Hodson et al., 2000; Swain et al., 2006). It is believed that colour affects not only the settlement but also the adhesion strength of biofouling (Guenther et al., 2009).

In this chapter, the effects of colour, position and light on the growth of biofouling were investigated. Site experiments were conducted in Tarraleah No.1 Canal and Pond No.1 of the



Figure 3.1 Locations of Tarraleah Power Scheme in Hydro Tasmania, Australia.



Tarraleah Power Scheme in the Derwent Catchments, Tasmania, Australia. This study will provide a reference for the Hydro power industry for selecting an appropriate coloured surface coating for the maintenance of the canals, with the aim of minimising the growth of biofouling. The location of the Tarraleah Power Scheme in central Tasmania is shown in Figure 3.1.

This chapter is divided into two parts. The first part discusses the effect of four different colours on the growth of biofouling, while the second part discusses the effect of light on the growth of biofouling.

3.1 Colour Effect on Biofouling

To investigate the effect of colour on biofouling settlement and development, four different colours (white, lightbox grey, blue grey and black) were painted onto 600 X 300 mm² steel plates. These plates were placed in normal flow conditions at two different sites in the Tarraleah Power Scheme over several months and regularly inspected to assess the settlement and development of biofouling on the different coloured plates.

3.1.1 Methodology

3.1.1.1 Test Panels

The test plates were made of mild steel and were previously used to investigate biofouling in fresh water in Hydro Tasmania canals by Barton (2007a) and Andrewartha (2010b). The dimensions of each plate were 600 mm X 300 mm X 6 mm. Each test plate was divided into 300 X 300 mm² panels, as shown in Figure 3.3 and 3.4, and coated with two different coloured coatings of EPINAMEL[®] DTM985.

DTM985 is widely used for recoating Hydro Tasmania gates and valves because it has excellent recoat ability under cold temperatures. According to the data sheet of DTM985, it is direct high build to metal, suitable for immersion in fresh water, has excellent abrasion resistance and cures at a temperature as low as 5 °C.

The test plates were first cleaned by sand blasting, and then two coats of DTM985 were applied by spray painting. The same coating smoothness was achieved on each of the four different colours.

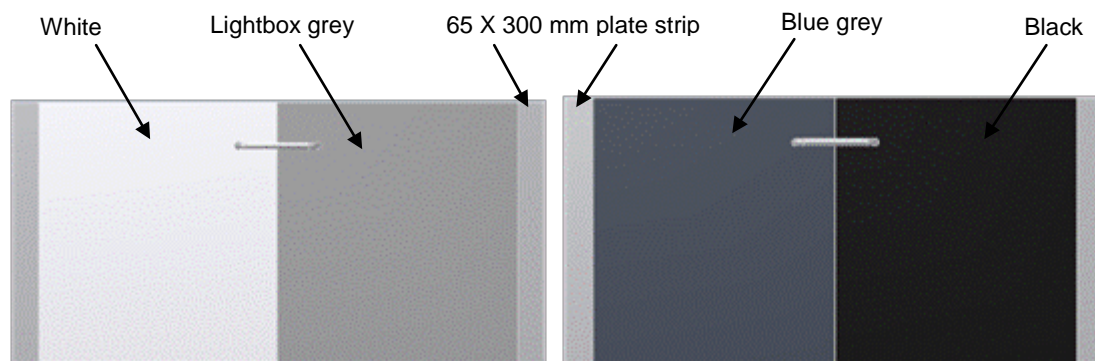


Figure 3.3 White and lightbox grey coating.

Figure 3.4 Blue grey and black coating.

Four different colours were chosen for the experiment: white (colour code: N14), lightbox grey (colour code: N33), blue grey (colour code: N53) and black (colour code: N61) (Colour Chart, 1996) Colours were painted as 300 X 300 mm² on the test panels as shown in Figures 3.3 and 3.4.

3.1.1.2 Site Trials Locations

Two locations, Transition No. 4 and Pond No. 1 in the Tarraleah Power Scheme were selected to conduct the colour and light effect on biofouling trials. The water level of Transition 4 and Pond No.1 during the period of the experiments are plotted in Appendix A.1.

Transition No. 4

Transition No. 4 is fully concrete lined, located in the lower section of Tarraleah Canal No. 1 and is close to Pond No.1 (Figure 3.2). Frames at Transition No. 4 were installed just downstream of the transition from the above ground flume section (rectangle cross section) to the in-ground canal (trapezoidal cross section). The test plates were inserted into frames bolted to the walls of the concrete canal. Figure 3.5 shows the detailed design of the frame and plates. The secondary currents are clearly apparent, and large eddies were observed around frames which located at Transition No. 4, as shown in Figure 3.6.

The average velocity in Transition No. 4 is approximately 2 m/s when the canal is full and carrying a flow rate of 24 m³/s. The biofilms which grow here are high flow conditioned biofilms. The angle between the inclined concrete wall and water surface is 40 degrees at Transition No. 4.

Plates were placed under the water at a depth of approximately 0.2 m for the upper edge of the top plate and 0.4 m for that of the bottom plate.

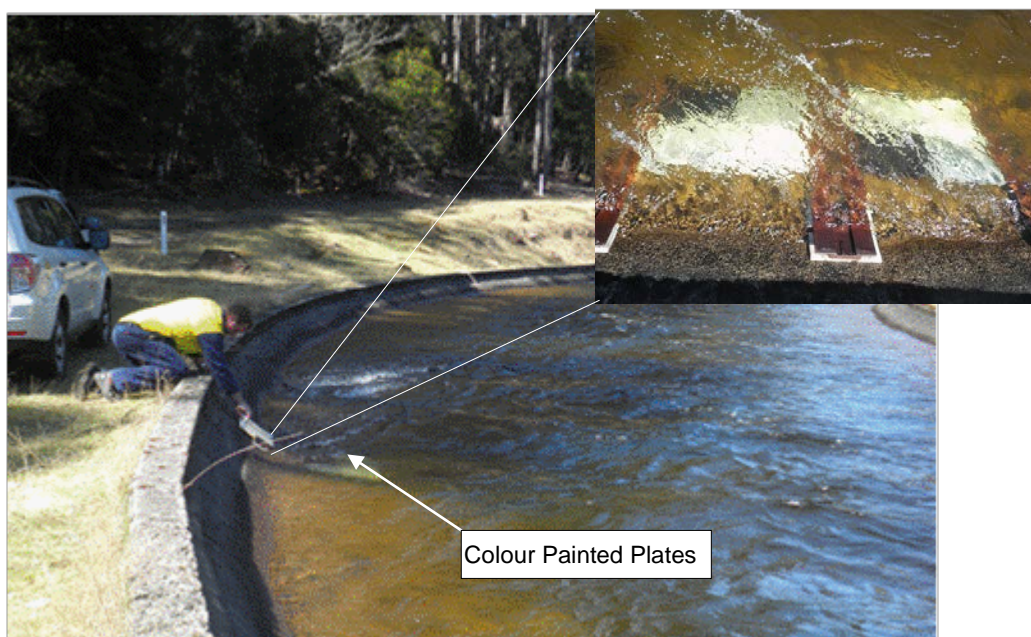


Figure 3.6 Plates with different colours were located on the concrete wall at Transition 4.

Pond No. 1

Pond No. 1 is located at the downstream end of Tarraleah Canal 1. Water flows from Tarraleah Canals 1 and Canal 2 to Pond No.1, then from Pond No.1 to the Hilltop Pipelines (Figures 3.2 and 3.7). The majority of Pond No.1 is earth lined, containing considerable of freshwater vegetation.

The average flow velocity in Pond No.1 is approximately 1 m/s; hence the biofilms which grow in Pond No.1 are conditioned to a lower flow speed than in Transition 4. The angle between the inclined concrete wall and the water surface at Pond No.1 is 30 degrees. Plates were placed

under the water at a depth of approximately 0.15 m for the upper edge of the top plate and 0.3 m for that of the bottom plate.

Two frames were installed on the concrete wall to hold test plates, close to the skimmer gate which controls the flow rate to the Hilltop Pipelines (Figure 3.7).

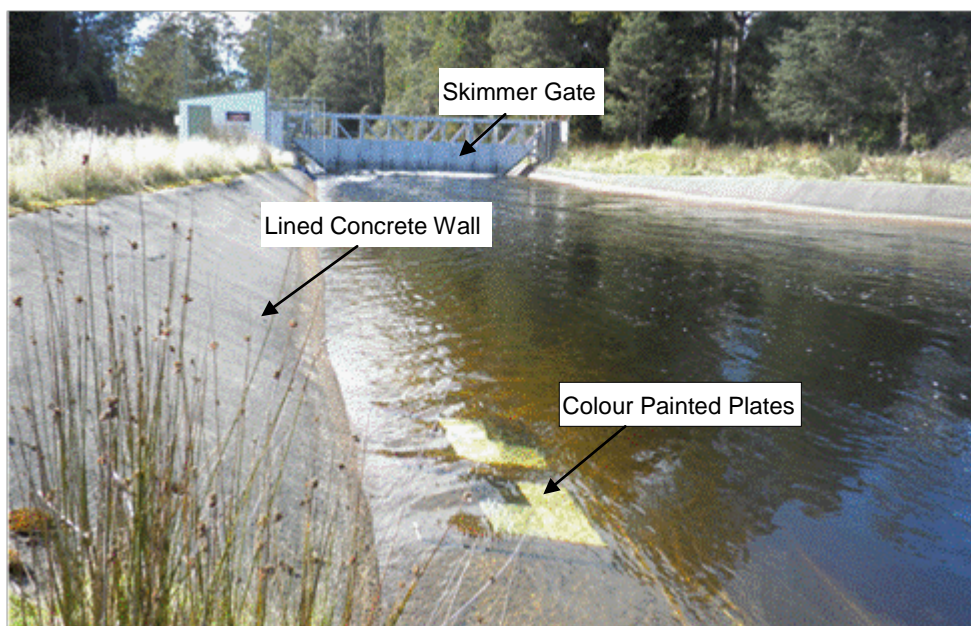


Figure 3.7 Plates with different colours were located on the concrete wall at Pond No. 1.

The mounting frames were designed to keep test plates as close to the concrete wall as possible to replicate the wall shear velocity (Andrewartha, 2010b; Barton, 2007a). These plates were installed approximately 20 mm above the concrete wall. Two frames were mounted onto the inclined concrete wall at each location. Four painted test plates were slid into two frames with the bottom plates first followed by the top plates, as shown in Figures 3.6 and 3.7, to allow flow-conditioned biofilms to grow.

3.1.1.3 Sampling Position and Area

Biofouling samples were taken at different times during the trial. Only part of the biofouling on each coloured panel on each test plate was taken as a sample. The following factors were considered when taking samples from plates.

Firstly, samples were taken in the central area away from the edges of the plate due to the fact that the flow may separate in this region, with quite strong turbulent fluctuations as the flow reattached to the plate surface. Secondly, the samples were not taken near the junction of the two different colours. The plate surface near the junction was not very smooth, and it was found to have more fouling at the junction line between different colours (Figure 3.10). Thirdly, there were two screws on one plate which was located at Transition 4, as shown in Figure 3.9. Lastly, the handle position of one plate installed in Pond No.1 was lower than others, as shown in Figure 3.11 c). Thus, the position of sampling for biofouling is described in Figure 3.8. Samples were taken from the middle of the plate, with a dimension of 150 mm X 200 mm.

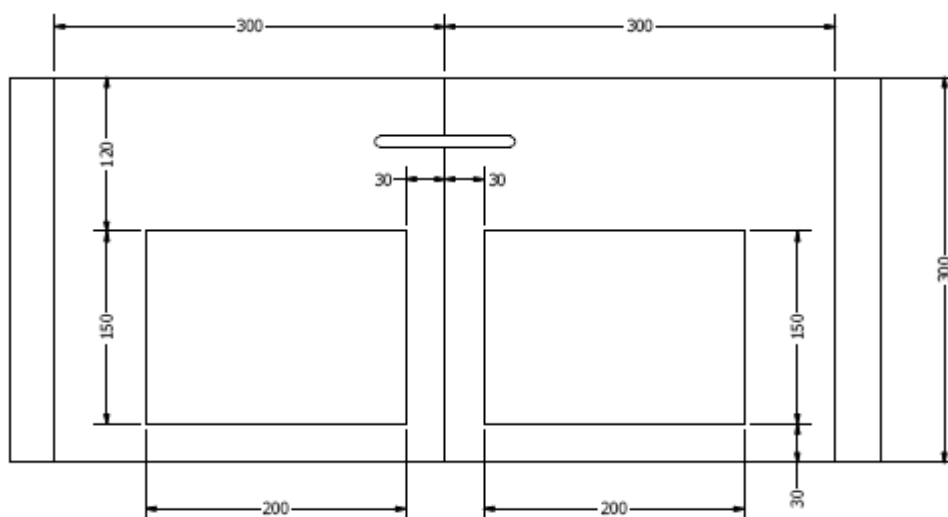


Figure 3.8 Area and position of sampling for biofouling.

A transparent plastic paper was cut to a dimension of 150 mm X 200 mm for biofouling sampling. The sampling position was decided by putting the cut transparent paper on each coloured panel according to Figure 3.8. A plastic spatula was used to scrape biofouling from each panel. The collected samples were put into glass containers and returned to the laboratory for further analysis.

3.1.1.4 Colour Performance Grading

A grading system was used to assess the performance of the four colours on the settlement and development of biofouling. This grading system was previously used (Andrewartha, 2010b; Barton et al., 2004). Table 3.1 shows the standard of the grading system.

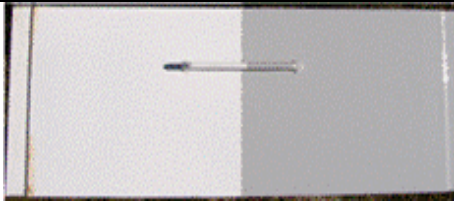

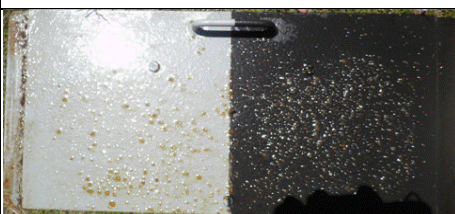

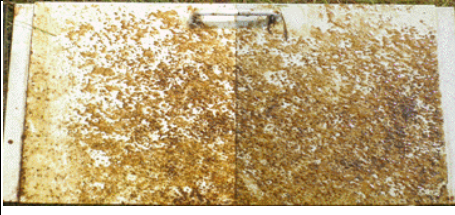

Grading	Description (Andrewartha, 2010b; Barton et al., 2004)	Photograph
A	A clean plate, with no biofilm present.	
B	A very lightly fouled plate, with the biofilm found to be present by wiping a finger across the surface and looking at the residue. It may not cover the entire plate.	
C	A lightly fouled plate, with the biofilm less than a few millimetres thick. The biofilm consists of only a thin layer with no clumps of algae present. It may not cover the entire plate.	
D	A moderately fouled plate, with the biofilm typically a few millimetres thick. The biofilm consists of a thin layer with some clumps of gelatinous algae formations. It may not cover the entire plate and may appear as patches.	
E	A very fouled plate, with biofilm thickness in the order of several millimetres. The biofilm consists of large, numerous clumps of gelatinous algae formations, but does not cover the entire plate and may appear as patches.	
F	A fully-fouled plate, with biofilm thickness in the order of several millimetres. The biofilm consists of large, numerous clumps of gelatinous algae formations, with coverage over the entire plate.	

Table 3.1 The grading system of biofouling.

3.1.2 Site Trial in Transition No. 4

Only one site trial was conducted at Transition 4 due to the fast average velocity and resultant slow development of biofouling. The biofilms which grew in Transition 4 were conditioned to higher average velocities of up to 2 m/s. This site trial was conducted over a 9 month period from March 2011 to December 2011.

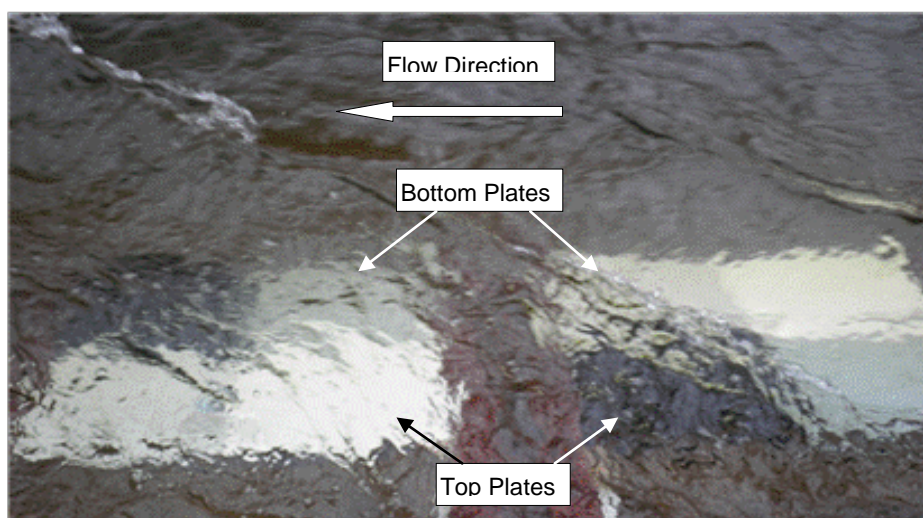


Figure 3.9 Plates painted in four different colours located at Transition 4.

The colour order of the top plates differed from that of the bottom plates at Transition 4, as shown in Figure 3.9. Photos of the biofouled plates were taken on 21/12/2011, as shown in Figure 3.10. It was found that the white panels had the least biofouling and the black panels had the most for both top and bottom plates.

The grading of biofouling samples taken from areas of different colours was assessed according to Table 3.1 at Transition 4. The panels at the shallower depth (designated as the ‘top plates’) were assessed as B, C, C, C for white, lightbox grey, blue grey and black, respectively. The bottom plates were assessed as B, B, B, C for white, lightbox grey, blue grey and black, respectively.

The water level during the period of the experiment was plotted, as shown in Appendix A.1. The plates were submerged in water during the testing period.

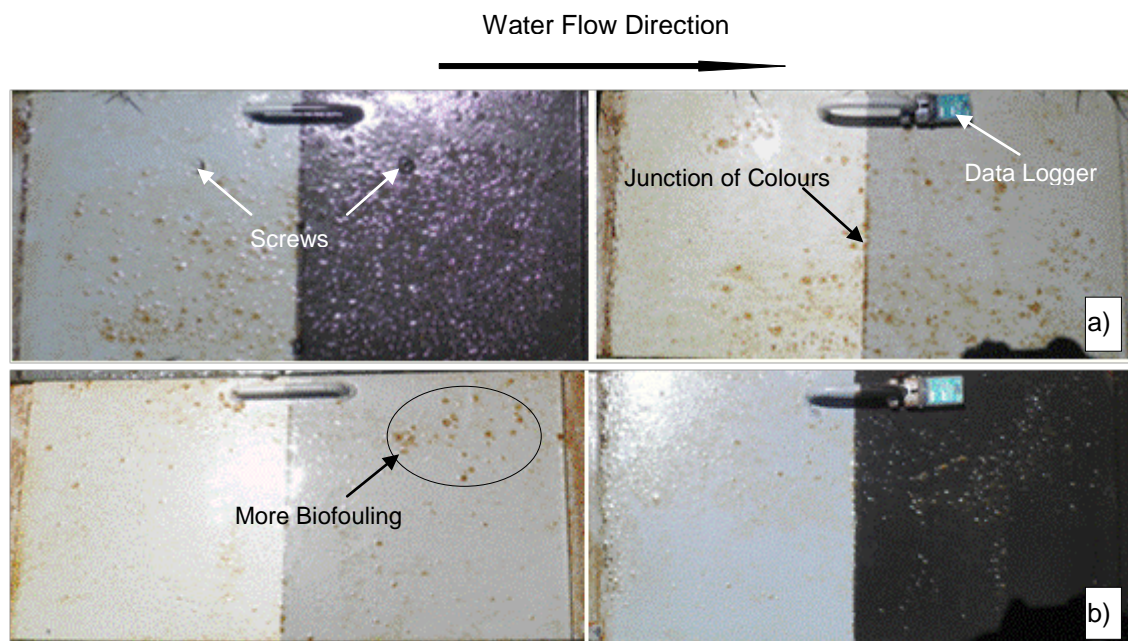


Figure 3.10 Biofouling grew on plates with different colours: a) Top layer plates, b) Bottom layer plates.

It was found that the bottom lightbox grey panel had more fouling on the top right area than other areas of the same colour, as shown in Figure 3.10 b). This was due to the fact that part of the coating was scratched away. However, since it was located outside of the area from which a sample was taken (as shown in Figure 3.8), the effect of paint missing was ignored.

The biofouling samples, collected as described in Section 3.1.1.3, were returned to the laboratory at the University of Tasmania and weighed in both wet and dry state by using a scale with ± 0.001 g accuracy.

Firstly, wet biofouling and the glass containers were weighed and recorded, then placed in an oven and dried at 87°C for 7 hours. The dried biofouling and glass container were weighed after the temperature had dropped to room temperature over a one hour period. After the above measurements, all glass containers were cleaned, dried and weighed. Hence, the weights of wet and dry biofouling were obtained. A comparison was made for biofouling collected on the top and the bottom layer plates, as shown in Tables 3.2 and 3.3.

	Weight (g)		Area (m ²)	Coverage (g/m ²)	
	Wet	Dried		Wet	Dried
White	2.593	0.035	0.030	86.43	1.17
Lightbox grey	3.311	0.068	0.030	110.37	2.27
Blue grey	3.947	0.089	0.030	131.57	2.97
Black	5.585	0.125	0.030	186.17	4.17

Table 3.2 Weight and coverage of biofouling of top plates.

	Weight (g)		Area (m ²)	Coverage (g/m ²)	
	Wet	Dried		Wet	Dried
White	0.196	0.005	0.030	6.53	0.17
Lightbox grey	0.360	0.012	0.030	12.00	0.40
Blue grey	0.849	0.019	0.030	28.30	0.63
Black	1.945	0.038	0.030	64.83	1.27

Table 3.3 Weight and coverage of biofouling of bottom plates.

It can be seen from Table 3.2 and 3.3 that the weight and the coverage of the wet and dried biofouling samples decreased progressively from dark to light colours, i.e. from black and blue grey to lightbox grey and white. The white panels had the least biofouling and the black had the most.

3.1.3 Site Trial in Pond No.1

The average velocity at Pond No.1 was approximately 1 m/s, thus the biofilms grown here were conditioned to lower velocities than at Transition 4. Biofouling also developed faster at Pond No.1.

This site trial was conducted in summer over a four month period from 13/09/2011 to 11/01/2012. The plate arrangement during the experiment is shown in Figure 3.11. The water level during the period of the experiment was plotted, as shown in Appendix A.1. The test plates were fully submerged for the duration of the testing period.

It can be seen that the leading edge of the blue grey coloured top panel subjected to higher shear stress than any of the other panels due to the frame being 20 mm higher than the concrete wall, as shown in Figure 3.12 a).

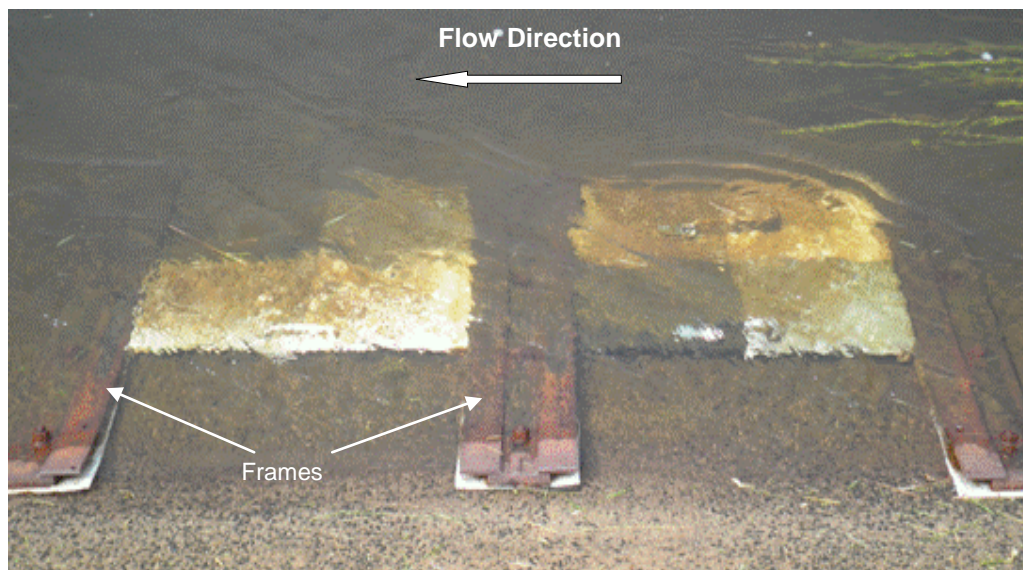


Figure 3.11 Plates painted by four different colours located at Pond No. 1 on 11/01/2012.

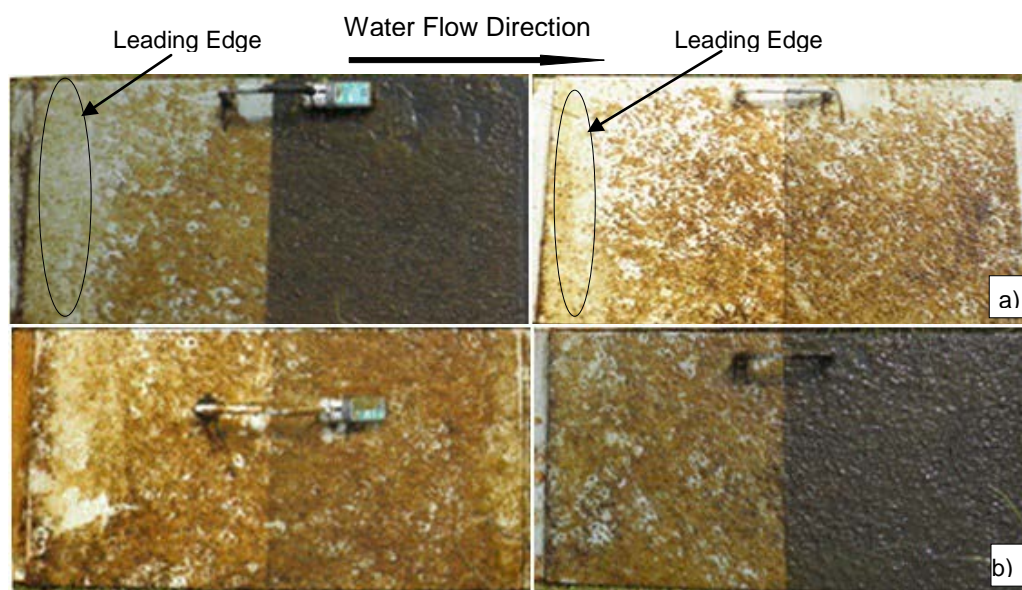


Figure 3.12 Biofouling of Pond No. 1: a) Top layer plates, b) Bottom layer plates.

The grading of biofouling samples taken from areas of the different panels was assessed according to Table 3.1, as grade A-F. The biofouling of the top panels was assessed as developing biofouling: D, E, E, E for the white, lightbox grey, blue grey and black panels respectively. The biofouling on the bottom panels was assessed as being fully-developed and all four colours were given a rating of F.

The biofouling on each panel was sampled as described in Section 3.1.1.3, and samples were transferred to the UTAS laboratory, weighed and then dried at 89 °C for 17 hours.

The weight and coverage of the samples on top panels are shown in Table 3.4. It was observed from this data that the white panel attracted the least amount of biofouling, while the black panel had the most. However, due to the influence of the shear stress of the water flow on plates, the lightbox grey panel had a higher fouling coverage than that on the blue grey panel, even though the latter appeared darker.

	Weight (g)		Area (m ²)	Coverage (g/m ²)	
	Wet	Dried		Wet	Dried
White	22.216	0.653	0.030	740.53	21.77
Lightbox Grey	26.194	0.674	0.030	873.13	22.47
Blue Grey	23.594	0.663	0.030	786.47	22.10
Black	29.726	0.784	0.030	990.87	26.13

Table 3.4 Weights and density of wet and dried biofouling on top plates.

Weight and density data for the bottom panels are shown in Table 3.5. It was found that the dried biofouling coverage increased progressively from light colour to dark colour, i.e. from white and lightbox grey to blue grey and black.

	Weight (g)		Area (m ²)	Coverage (g/m ²)	
	Wet	Dried		Wet	Dried
White	33.043	0.906	0.030	1101.43	30.20
Lightbox Grey	35.871	0.929	0.030	1195.70	30.97
Blue Grey	30.962	0.983	0.031	998.77	31.71
Black	25.398	1.076	0.030	846.60	35.87

Table 3.5 Weights and density of wet and dried biofouling on bottom plates.

For panels with fully developed biofouling, the black panel attracted the most. However, the average data was not significantly different for biofouling on white, lightbox grey and blue grey panels when biofouling was fully developed, as shown in Table 3.5.

It was observed that the biofouling which grew on the bottom black panel had a composition differing from that on the other bottom panels. It appeared drier and had the least wet weight; however, it had the highest biofouling coverage when dried.

3.2 Light and Temperature Effect on Biofouling

It was reported that shaded surfaces are better collectors of fouling organisms than well-illuminated substrates (Andrewartha, 2010b; Perkins, 2010a; Su et al., 2007). Callow et al. (2000) and Prendergast et al., (2000) also found that the settlement of some biofouling species showed negative phototaxis; ie. the biofouling species moved away from the light.

To investigate the effect of total light and temperature on biofouling, the temperature and light intensity were measured for the duration of the deployment time using a 64k temperature/light data logger. The UV was measured during an inspection using UV light metre PMA 2100 and waterproof UVA+UVB PMA2107 detector.

3.2.1 Temperature and Light Data Logger

The HOBO Pedant 64K, model UA-002 temperature and light data logger is a waterproof; two-channel logger which can measure combined temperature and light readings up to 64K in memory. The performance of this data logger is shown in Figure 3.13. It uses a coupler and optical base station with USB interface for launching and data transfer to a computer (Figure 3.14). The total light data were recorded once per hour by the data logger.

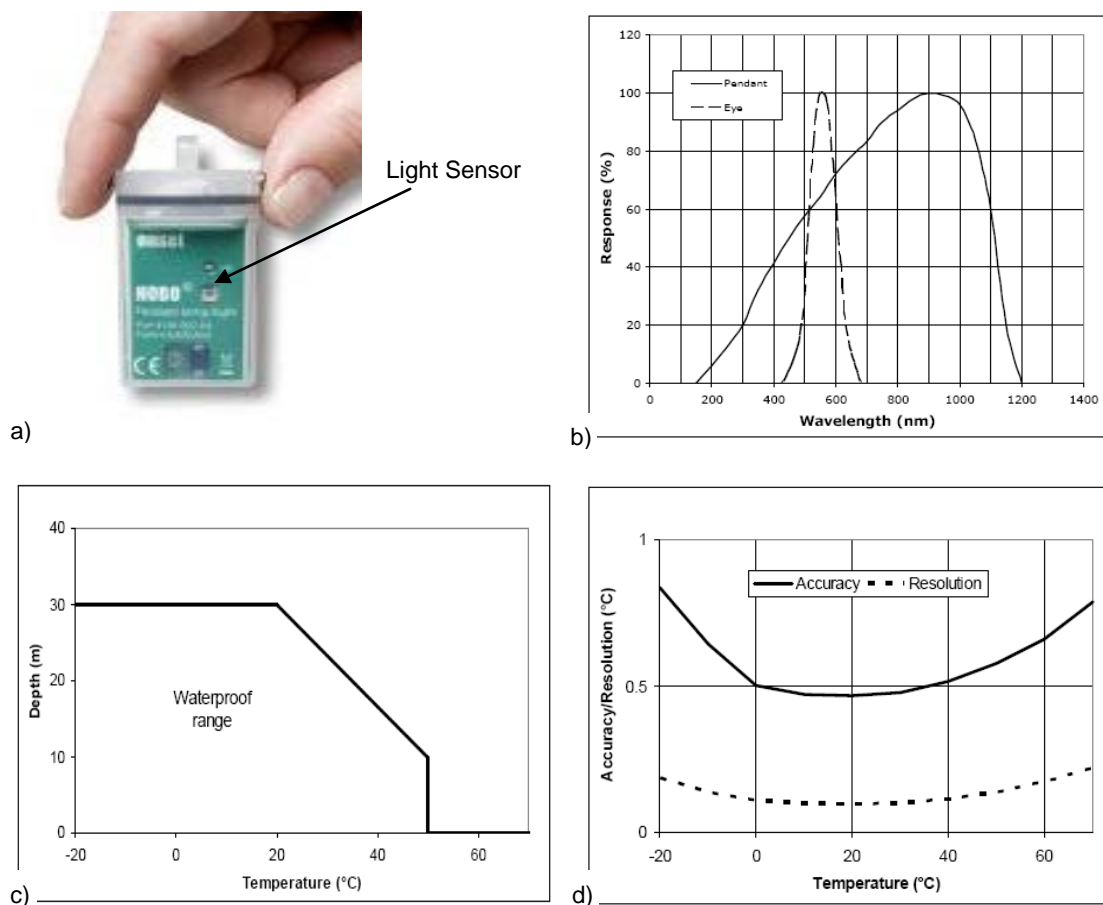


Figure 3.13 Image and performance of HOBO UA-002: a) Image of HOBO Pedant Temperature/Light data logger. b) Spectral response of data logger. c) Waterproof ability of data logger. d) Response accuracy of data logger.

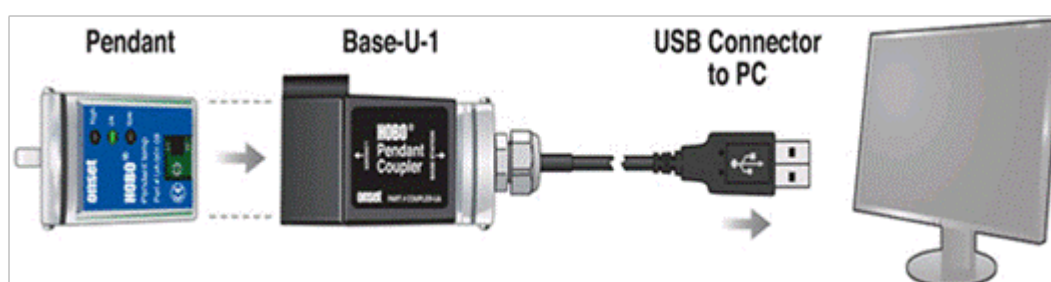


Figure 3.14 Launching of HOBO UA-002 and data readout.

Lux was used as the light intensity measurement unit in this study. The data logger detects light further into the ultraviolet and infrared wavelengths than the response of the human eye, as shown in Figure 3.13 b).

3.2.2 UV Light Measurement

Datalogging radiometer PMA2100 can be used with over 35 different detectors measuring UVA, UVB, UVC, Visible, and IR light. It has two channels to allow dual input with two detectors recording up to 1024 data points. A PMA2107 UVA+UVB detector together with a PMA 2100 were used in this study to investigate the impact of UV light on the growth of biofouling.

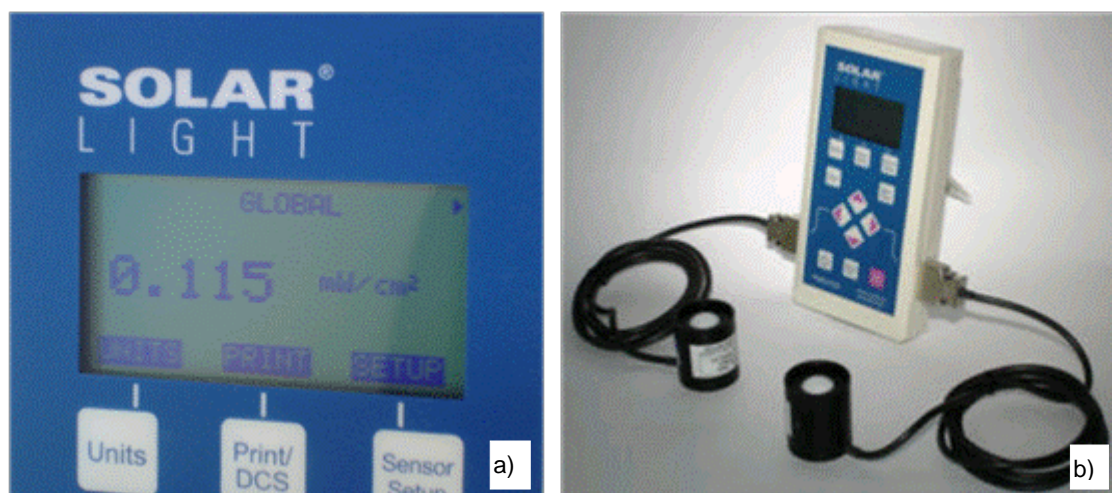


Figure 3.15 Data logger radiometer PMA2100. a) Front panel of PMA2100. b) PMA2100 with two detectors.

Figure 3.15 shows the front panel of PMA2100 and PAM2100 with two detectors. The UVA+UVB detector, PMA2107, shown in Figure 3.15 b) is waterproof and gives an accurate measurement of the non-weighted UVA+UVB ultraviolet radiation from sunlight. The spectral response of the PMA2107 sensors is shown in Figure 3.16.

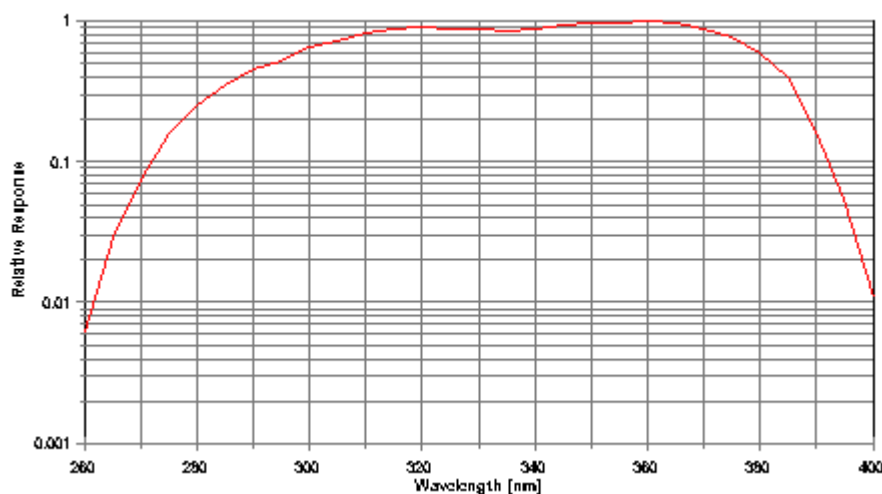


Figure 3.16 PMA2107 spectral responses.

3.2.3 Light Data of Site Trial

Total light data obtained from the total light sensor (see section 3.2.1) for the top and bottom plates were analysed to investigate the effect of total light on the growth of biofouling. The UV sensor (see section 3.2.2) was used to investigate the effect of UV light on the growth of biofouling. The temperature obtained from the total light sensor was plotted for both top and bottom layer plates in Appendix A.

The HOBO data logger was tied to the handle of the test plate using cable ties at the beginning of the study. However, it was found that the cable ties were not rigid enough to hold the logger, and the light reading varied significantly when the sensor in the HOBO data logger was rotated a few degrees.

Aluminium data logger holders were made and installed on site to keep all data loggers in the same direction on 13/10/2011 for both sites in this study. Thus, data collection from 13/10/2011 to the end of the experiment was used to investigate the impact of light and temperature on the growth of biofouling.

The intensity of total light and temperatures obtained from the HOBO data logger were plotted by HOBOWare Lite software.

3.2.3.1 Site Trial in Transition 4

Transition No. 4 is exposed to sunlight for a shorter period each day than Pond No. 1 due to surrounding trees providing increased shade in the early morning and late afternoon.

Total light was recorded hourly by the data logger. After the installation of improved holders as mentioned above, data from 70 days were obtained for the top and bottom plates between 13/10/2011 and 21/12/2011 for the nine month trial period at Transition 4, giving a total of 1657 readings. Total light data were analysed and plotted as follows.

The total light data obtained at Transition 4 for the top and bottom plates is plotted in Figure 3.17. It should be noted that the recording time of the bottom plate data logger occurred one minute earlier than the top plate data logger during the experiment. This was caused during the setup of the data logger. It can be seen that the overall light received by top plates exceeds that received by bottom plates. Some black spikes in Figure 3.17 were due to the change of weather during data logging.

Details of the light data are shown in Table 3.6. It was found that the top plate received over 30% more light than the bottom one. The mean light values recorded for top and bottom plates were 12506 Lux and 9059 Lux during the same period. Both the median light value and the maximum light value the top plate received also exceeded that of the bottom plate.

It was found that 641 data points recorded zero lux for the bottom plate (during night time) and 621 data points for the top plate. This means that the top plate received a longer period of light than the bottom plate, as shown in Table 3.6.

	Mean (Lux)	Max (Lux)	Min (Lux)	No. of readings as 0
Top plate	12506	209424	0	621
Bottom plate	9059	170846	0	641

Table 3.6 Light intensity of top and bottom plates located at Transition 4.

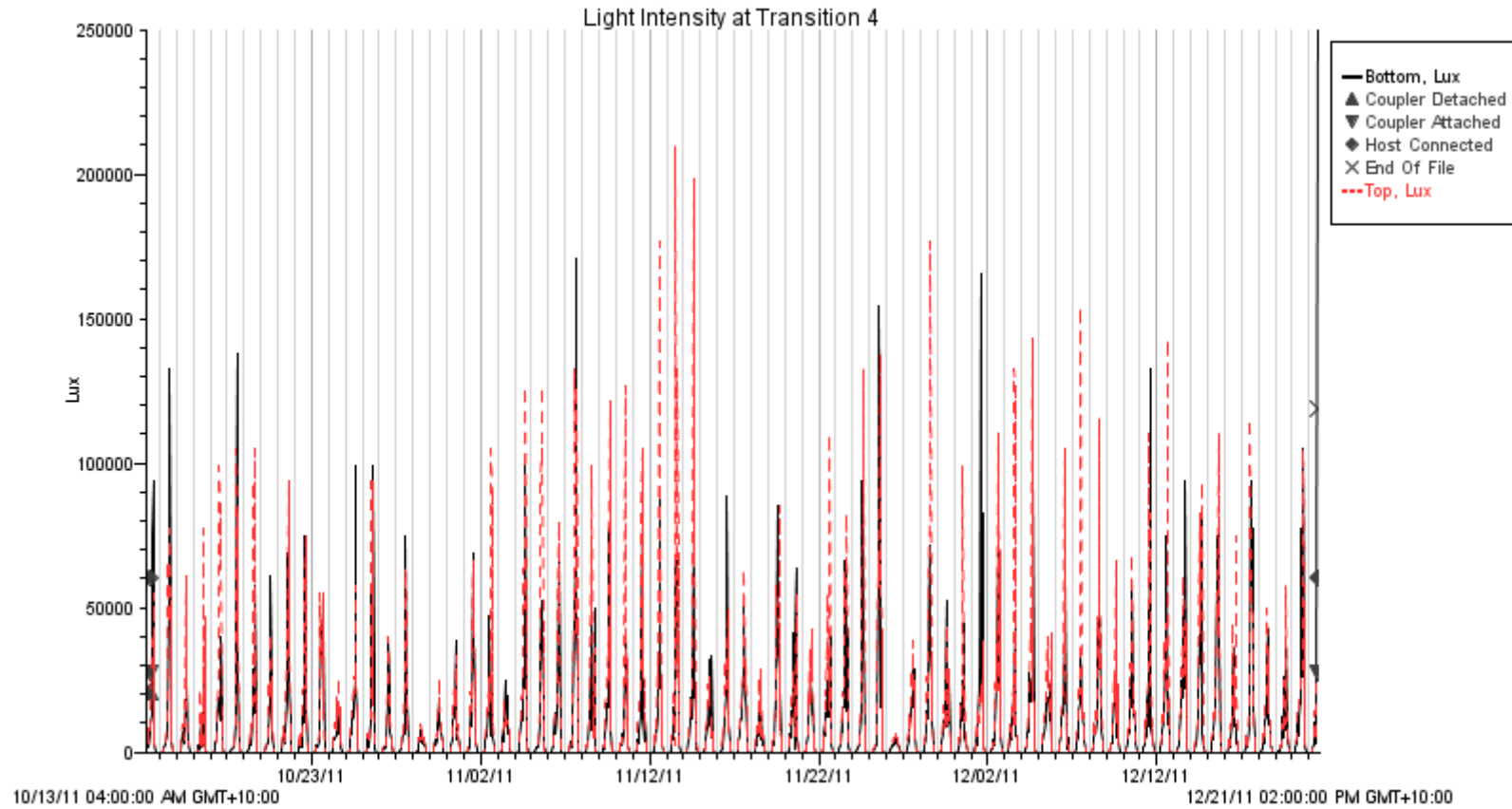


Figure 3.17 Total light data obtained by HOBO data logger for Transition 4 (USA date format, M/D/YY).

The water temperature data during the experiment are shown in Table 3.7. The difference in temperature was only 0.1 °C between the top and bottom plates. Hence, the difference of temperature between these plates was ignored.

	Mean (°C)	Max (°C)	Min (°C)
Top plate	11.05	16.14	7.68
Bottom plate	10.92	15.28	7.58

Table 3.7 Temperature of top and bottom plates located at Transition 4.

3.2.3.2 Site Trial in Pond No.1

Both the total light intensity and UV light were measured at Pond No.1.

The total light intensity at Pond No.1 was measured by another pair of HOBO data loggers. The light intensities on the top and the bottom plates at Pond No.1 are plotted in Figure 3.18.

A total of 91 days of data between 13/10/2011 and 11/01/2012, with a total of 2160 total light intensity data points were recorded for the four month trial period at Pond No.1.

The total light data are plotted in Figure 3.18. It can be seen that the top plate received more total light than that received by the bottom plate. Details of total light, water temperature and logger voltage are shown in Tables 3.8 and 3.9.

	Mean (Lux)	Max (Lux)	Min (Lux)	No. of readings as 0
Top plate	17125	330669	0	790
Bottom plate	10238	159823	0	804

Table 3.8 Light intensity of top and bottom plates located at Pond No.1.

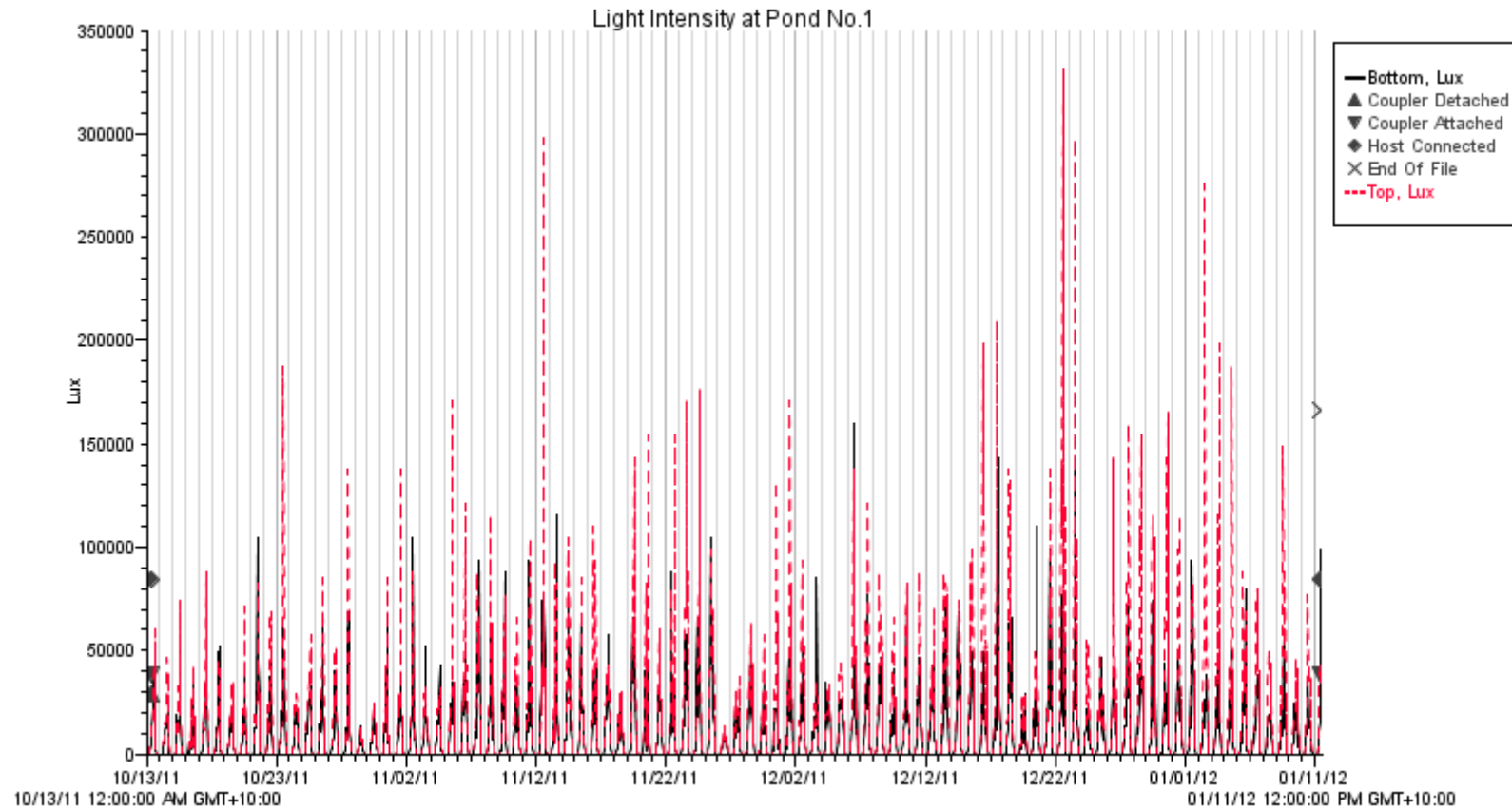


Figure 3.18 Total light data obtained by HOBO data logger for Pond No.1.

	Mean (°C)	Max (°C)	Min (°C)
Top plate	13.71	20.33	6.37
Bottom plate	13.66	19.95	6.37

Table 3.9 Temperature of top and bottom plates located at Pond No. 1.

It can be seen from Table 3.9 that the top plate received longer and higher intensity light than the bottom plate. The difference of temperature between top and bottom plates was minor and it can be ignored.

UV light at Pond No.1

Irradiance penetration of UV light in fresh water has been studied by previous researchers. It was found that the attenuation of UVA+UVB light depended on water quality, such as the concentration of dissolved organic carbon (Huovinen et al., 2003; Hurtubise et al., 1998; Sommaruga et al., 1997). Huovinen et al. (2003) conducted a field measurement and found that 99% of the UV radiation was attenuated to 0.5 m depth for UVB and to 1 m depth for UVA in a very clear lake. UVB measurements were also conducted by Hurtubise et al. (1998) in a pond, where it was found that 10% of the irradiance penetrated to 30 cm depth and 1% to 57 cm depth.

UV light was measured by data logging radiometer PMA2100 and UVA+UVB detector PMA 2107 in the current study. As described in section 3.2.2, only one UV detector was used to measure UV light in the current study. To investigate the difference in the UV light received by the top and bottom plates at Pond No.1, a HOBO data logger was used together with the UV detector to measure total light during the UV measurement.

The UV light measurement was conducted on 11th January, 2012. A HOBO data logger was installed on the handle of the bottom plate during the entire process to record the total light intensity every minute. The UV detector was installed on a plate and inserted into another frame at the bottom position. UV light was measured separately for both top and bottom positions of the frame.

The UV data was recorded at one minute intervals over a 30 minute period. Total light on the top and bottom plates was recorded simultaneously during the test period.

The mean and median values of total light and UV light are shown in Table 3.10. The mean and median values between positions could not be compared directly because the weather was not consistent during the measurement of different positions of the frame.

	Total light (Lux)		UV light (W/m ²)	
	Mean	Median	Mean	Median
Top position	48980	46845	8.30	9.56
Bottom position	35095	31000	3.10	3.18

Table 3.10 Mean and median values of total and UV light for top and bottom plates located at Pond No. 1.

It was found that the total light mean value at the bottom position of the frame increased 1.3 times over the period of measurement. However, the UV light mean value increased 2.6 times from the bottom to the top plate during the same period. Increased mean and median proportions in this measurement are shown in Table 3.11.

Mean		Median	
Total light	UV light	Total light	UV light
1.4	2.7	1.5	3.0

Table 3.11 Increased proportion of mean and median values for total and UV light at Pond No. 1.

The above results show that the top plate received higher UV light than the bottom plate during the measurement period.

3.2.3.3 Total Light Summary of Two Locations

Total light data obtained at Transition 4 and Pond No.1 is summarised in Tables 3.12 and 3.13. There were 1657 data points used for the calculation during the same period from 13/10/2011 10:15 am to 21/12/2011 8:16 am. Data were compared in groups for the top and bottom plates respectively.

It was found that plates located at Pond No.1 received a longer period of light with higher intensity than those located at Transition 4. It was also found that the top plates received higher light intensity and UV readings than the bottom plates.

Chapter 3 – Effect of Substratum Colour and Ambient Light Conditions on Biofouling

	Mean (Lux)	Median (Lux)	No. of readings of 0 (Lux)
Pond No.1	15229.2	2927.8	619
Transition 4	12515.5	1894.5	624

Table 3.12 Total light of top plates located at Pond No.1 and Transition 4.

	Mean (Lux)	Median (Lux)	No. of readings of 0 (Lux)
Pond No.1	10056.1	1894.5	628
Transition 4	9062.2	1377.8	644

Table 3.13 Total light of bottom plates located at Pond No.1 and Transition 4.

3.3 Chapter Summary

The effect of substratum colour on the growth of biofouling was investigated by installing different coloured panels at two locations in a hydropower canal. EPINAMEL[®] DTM985 paints were used as coating on the mild steel plates.

Two site trials under different flow conditions at different locations were conducted. The water temperature, total light and UV light were measured for slow flow (1 m/s) under full sunlight conditions. The water temperature and total light were measured for fast (2 m/s) flow under partial sunlight conditions.

Biofouling samples were weighed at wet and dried conditions, and samples from different locations were compared.

The following conclusions regarding the effects of substratum colour and light received on biofouling were drawn based on the measurements in this study:

- Black substrates attracted earlier settlement and faster growth rates of biofouling than grey or white substrates. The amount of biofouling increased progressively from the colour of white, lightbox grey, blue grey to black at the settlement stage of biofouling. However, the effect of colour on the growth of biofouling became less significant when biofouling became fully developed.
- Plates located at Pond No.1 received earlier and higher total light than those at Transition 4, since Transition 4 is partly shaded by trees, and plates were located in deeper water.
- The amount of biofouling increased with depth under slow flow (1 m/s) and full sunlight conditions (Pond No.1), as demonstrated by the bottom panels (0.3 m under water) attracting more fouling than the top ones (0.15 m under water). It was also found that the light intensity was higher at shallower depths, as the top plate received higher intensity and longer total light than the bottom plate.

- At Pond No.1, the top plate received more UV light than the bottom plate, and the top plate attracted less biofouling than that the bottom plate.
- In contrast, the amount of biofouling decreased with the increase in water depth under fast flow (2 m/s) and partially shaded conditions (Transition 4), as the bottom panels had less biofouling. The top plate received higher intensity and longer total light than the bottom plate. This may be due to the light intensity being too low for the growth of biofouling on the bottom plate. More tests are needed to further investigate.

Chapter 4 Biofouling and Water Quality in Tasmanian Hydropower Schemes

This chapter describes the possible impact of water quality parameters in Tasmanian lakes on biofouling of power station cooling pipes and penstocks. Water quality data of lakes including water temperature, pH value, conductivity, turbidity, nutrient concentrations, metal content, oxygen concentrations and organic material of water are discussed in this analysis. The chemical composition and morphology of biofouling in penstocks and cooling pipes of power stations is also discussed.

4.1 Biofouling in Tasmanian Hydropower Conduits

A survey was undertaken in July 2010 of Hydro Tasmania power station operators to find out the extent of the problem of biofouling in cooling pipes. Detailed results are shown in Table 4.1 (Polzin, 2010).

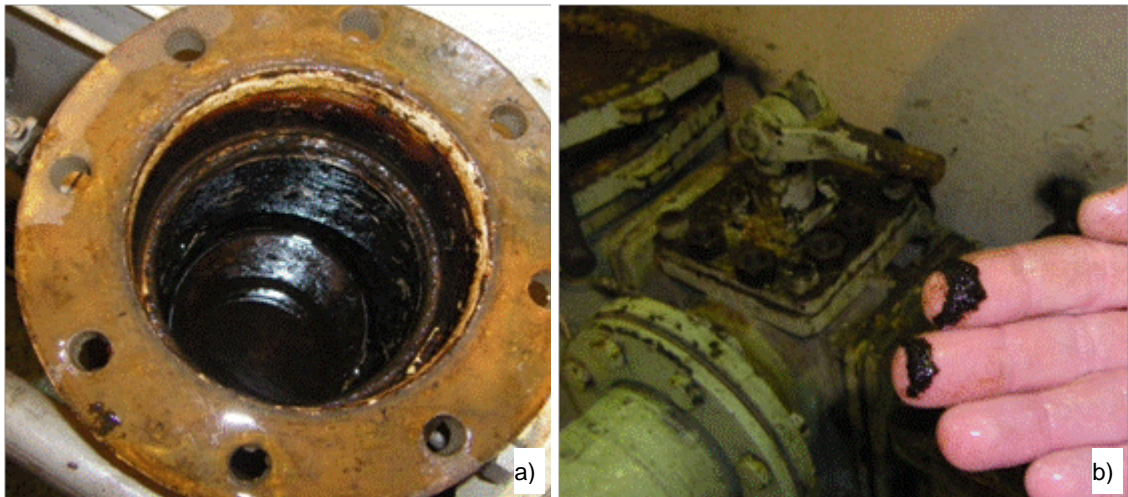


Figure 4.1 a) Biofouling in cooling pipe of Wilmot Power Station. b) Biofouling sample in cooling pipe of Wilmot Power Station.

While no biofouling problems have been reported in cooling pipes of power stations and penstocks in the Great Lake-South Esk and Derwent Catchments, such problems in cooling systems of power stations in the Pieman-Anthony, Mersey-Forth and King-Yolande Catchments

were reported by Hydro Tasmania. An extremely thin layer of soft slime biofouling with a black-brown colour and smooth surface was found in the cooling pipes of the Wilmot Power Station (Mersey-Forth Catchment), as shown in Figure 4.1. Biofouling found in the cooling pipes of the Wilmot Power Station was similar to that found in the biofouled test section, described in Chapter 5.

Station	With Biofouling problem (Yes/No)	
	Cooling pipes	Penstock
Poatina	No issues	Light
Trevallyn	No issues with algal but dirty water does create problems	Light
Tods Corner	No issues	The flume has problems with algal growth
Mackintosh	Yes	
Bastyan	Yes	
Reece	Yes	Yes
John Butters	Yes	
Tribute	Yes	
Rowallan	Yes	
Fisher	Yes	
Lemonthyme	Yes	
Wilmot	Yes	Yes - decreases efficiency
Cethana	Yes	
Devils Gate	Yes	
Paloona	Yes	

Table 4.1 Biofouling problem status in cooling pipes of power stations and penstocks.

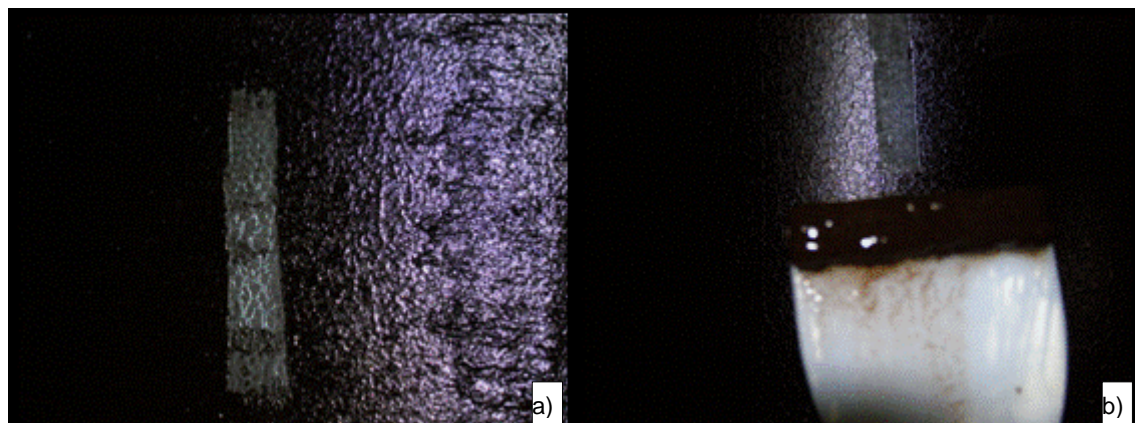


Figure 4.2 a) Biofouling in Poatina penstock. b) Bacterial sample in Poatina penstock

Minkus (1954) proposed that the deposit layers depended on variations in iron and manganese concentrations. The bacterial deposits on the wall of closed conduits appear to be a dense layer of soot. Pollard et al. (1959), Tyler (1968) and Barton (2007a) found such deposits were mainly dominated by iron and manganese bacteria. Upon drying, it tended to become friable and was easily broken into small flakes.

Different surface patterns of biofouling were observed in cooling pipes and penstocks. While smooth biofouling was found in cooling pipes as shown in Figure 4.1 a), ripple patterned (ridges and folds) dark black-brown coloured slime biofouling of 1mm thickness was observed in the Poatina penstock, as shown in Figure 4.2. A similar observation of biofouling in penstock was also reported by Tyler (1968) and Barton (2007a). This difference in the surface pattern of biofouling may be due to the slow flow velocity and lower wall shear in cooling pipes (Bott et al., 1983).

Biofouling samples taken from the Poatina penstock and Fisher and Wilmot Power Stations' cooling pipes (Mersey-Forth Catchment) were chemically analysed. The results show that manganese, iron and aluminium are the three main chemical elements composing the biofouling. Analysis results are shown in Appendix B.1.

Table 4.2 compares the main elemental composition (as percentages) for several biofouling samples. Further details are provided in Appendix B.1, with the biofouling results of previous researchers.

Date	Catchment	Location		Fe	Mn	Al	Ca	Mg	S	Reference
Aug-10	Mersey-Forth	Wilmot cooling pipe	Dried	15.3	18	2.42	0.74	0.19	0.11	
			Wet	13.4	2.18	1.93	0.52	0.24	0.16	
Jul-10	Mersey-Forth	Fisher cooling pipe		4.29	25	5.2	0.79	0.11	0.27	
Jun-10	Great Lake	Poatina Penstock		2.33	18.2	2.15	1.63	2.78	0.47	
Aug-04	Great Lake	Poatina Penstock	Tunnel	16.9	23	NA	NA	NA	NA	(Barton, 2007a)
			IP4	1.57	9.75	1.81	0.94	1.64	0.4	
Sep-04	Derwent	Tarraleah Pipeline		2.26	14.5	3.06	1.34	0.35	0.41	(Barton, 2007a)
1967	Great Lake	Waddamana Shannon Pipeline		3.24	20.8	5.44	1.02	0.24	0.23	(Tyler, 1968)
1967	Derwent	Tarraleah Pipeline		6.8	37.4	0.8	3.4	0.1	NA	(Tyler, 1968)
1967	Derwent	Liapootah Pipeline		NA	31	NA	3.2	0.3	NA	(Tyler, 1968)
1967	Derwent	Wayatinah Pipeline		5.2	23.7	3.9	NA	NA	NA	(Tyler, 1968)
1967	Derwent	Catagunya Pipeline		NA	20	3.4	0.5	NA	NA	(Tyler, 1968)

Table 4.2 Percentage elemental compositions of biofouling samples collected in cooling pipes, penstocks and comparison with previous studies.

It was found that biofouling in Wilmot and Fisher cooling pipes contained large amounts of iron and manganese (around 30% of Fe and Mn). Barton (2007a) and Tyler (1968) reported similar results in penstocks (16% to 44% of Fe and Mn).



Figure 4.3 Locations of lakes and canal from which water quality data were obtained from Hydro Tasmania.

4.2 Effect of Water Quality on Biofouling

Eight power stations, Poatina, Mackintosh, Bastyan, Reece, John Butters, Lemonthyme, Wilmot and Gordon were selected, and the water quality data from upstream lakes of the above power stations were extracted from the TimeStudio database by Entura (former Hydro Tasmania Consulting), including Great Lake, Lake Mackintosh, Lake Rosebery, Lake Pieman, Lake Burbury, Lake Parangana, Lake Gairdner and Lake Gordon. The locations of these lakes are shown in Figure 4.3.

No biofouling problems were reported in the cooling pipes in Poatina (Great Lake) and Gordon (Lake Gordon). However the “Cooling Water Design Standard of Hydro Tasmania” (Kruger, 2009) mentioned that some chemical dosing was used in the cooling pipes of Gordon Power Station. Thus, Lake Gordon was considered to have biofouling problems in cooling pipes for the purpose of this report.

An attempt was made to compare the current water quality in lakes with that of previous studies. Tyler (1968) studied the water quality of Great Lake, Lake St. Clair, Lake King William and Arthur’s Lake. However, it was difficult to compare due to the lack of iron and manganese data in his study. Barton (2007a) studied the water quality data of Tarraleah No.1 Canal Bridge 3, and these data were selected as a reference only since the water was not taken from the upstream lake (Lake King William). No biofouling problem was reported in the cooling pipes of the Tarraleah Power Station. However extensive algal biofouling occurs in the canal and bacterial fouling has been found in the hilltop pipelines.

It has been reported by many researchers that the growth rate of biofouling is affected by many factors such as water temperature, pH value, metals, nutrients, oxygen, organics, types of bacteria, water-solid surface condition and flow velocity and turbulence (Bott et al., 1977; Cullimore et al., 1978; Melo et al., 1997).

In this analysis, parameters of water temperature, pH value, nutrients (such as dissolved organic carbon), metals (such as iron and manganese), oxygen and organics were analysed as below, including data from different power stations with or without biofouling problems in cooling pipes.

4.2.1 Data Analysis Program R

The Data Analysis Program 'R' is a high-level language that provides a programming environment for statistical data analysis and graphics. Languages C and C++ can also be linked and called at run time (Dalgaard, 2002).

In this study, 'R' was used to analyse biofouling related factors from the original water quality data of the selected lakes. Boxplot, xy plot, mean value of parameters and three quartiles (0.25, 0.5 and 0.75) methods were used in the data analysis.

4.2.2 Water Chemical Factors

The intake level of lakes varies for different lakes. However, water temperature, field pH value, water conductivity and water turbidity are only available at depths greater than 5 metres from the lake's surface. Moreover, dissolved oxygen is available at depths greater than 15 metres from the lake surface. Therefore, the data were analysed for water temperature, field pH value, water conductivity and water turbidity at depths greater than 5 metres and the dissolved oxygen data at depths greater than 15 metres. For those parameters for which data at depths greater than 5 metres were not available, such as metals, all data were used.

Some parameters of water quality data in cooling pipes are quite different from the parameters in lakes. For example, the temperature at intake level of Great Lake is around 7~15 °C in different seasons. However the temperature of industrial water coolers is different from the lake temperature at intake level. Melo et al. (1997) found the optimum temperature for maximum growth of many bacteria in cooling water systems is 40 °C, which is the temperature encountered in industrial water coolers. Although the water temperature in cooling system pipes was not available, it is very likely to be warmer than the water at the storage inlet.

Water quality parameters for eight different lakes are presented in the following sections. Great Lake was the only one with no report on biofouling problems in the downstream Poatina Power Station cooling systems.

4.2.2.1 Relationship between some Parameters and Depth

The relationships between temperature, pH, conductivity and turbidity with depth measured from lake surfaces in different years and seasons are shown in Figures 4.4 to 4.7.

In this study, water temperature data ranging from 1975 to 2010 were analysed in Figure 4.4. It shows that the water temperature decreases with the depth at different sites and seasons (red, pink, blue and green represent data obtained in winter, spring, autumn and summer, respectively). Variations in water temperature at the same depth were found from different sites in different seasons. However, water temperature was similar at the same depth and season from different lakes.

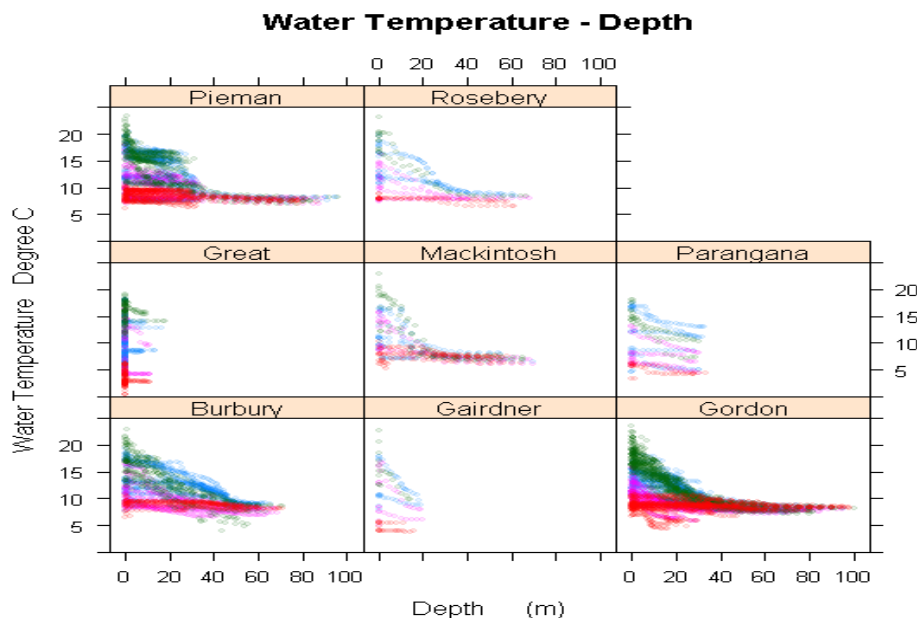


Figure 4.4 Relationship between water temperature-depth of lakes and canal.

Tyler (1968) reported a similar relationship between the water temperature and depth from the lake surfaces for Lake St. Clair and Lake King William in Hydro Tasmania.

Field pH value data from 1990 to 2010 were analysed in the current study. Field pH value decreases slightly with depth in each lake (Figure 4.5). Field pH variations at the same depth were found at different sites.

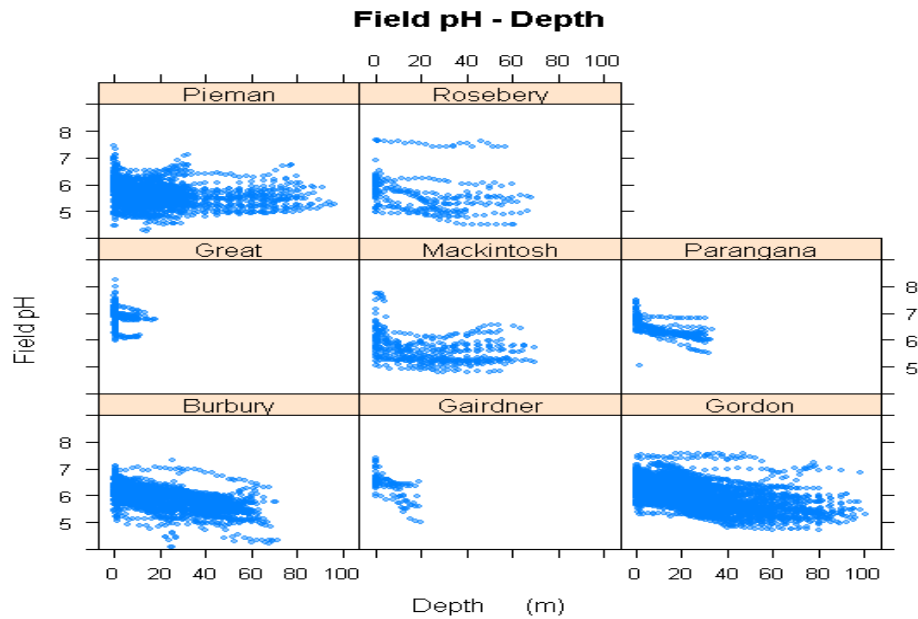


Figure 4.5 Relationship between pH field value-depth of lakes and canal.

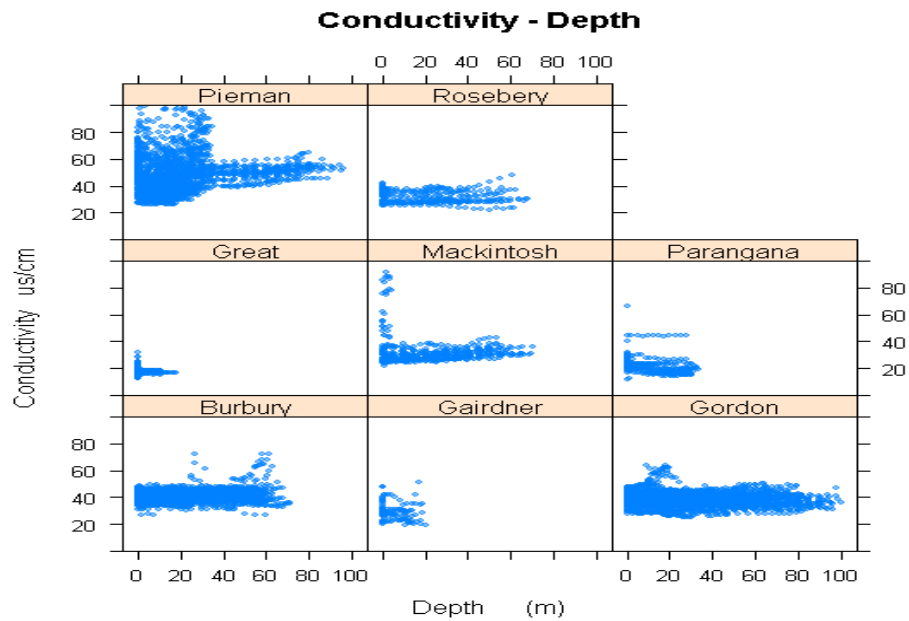


Figure 4.6 Relationship between conductivity-depth of lakes.

Water conductivity and turbidity from 1986 to 2010 were analysed in the study. It was found that water conductivity and turbidity are generally quite consistent with depth in lakes, as shown in Figures 4.6 & 4.7 respectively.

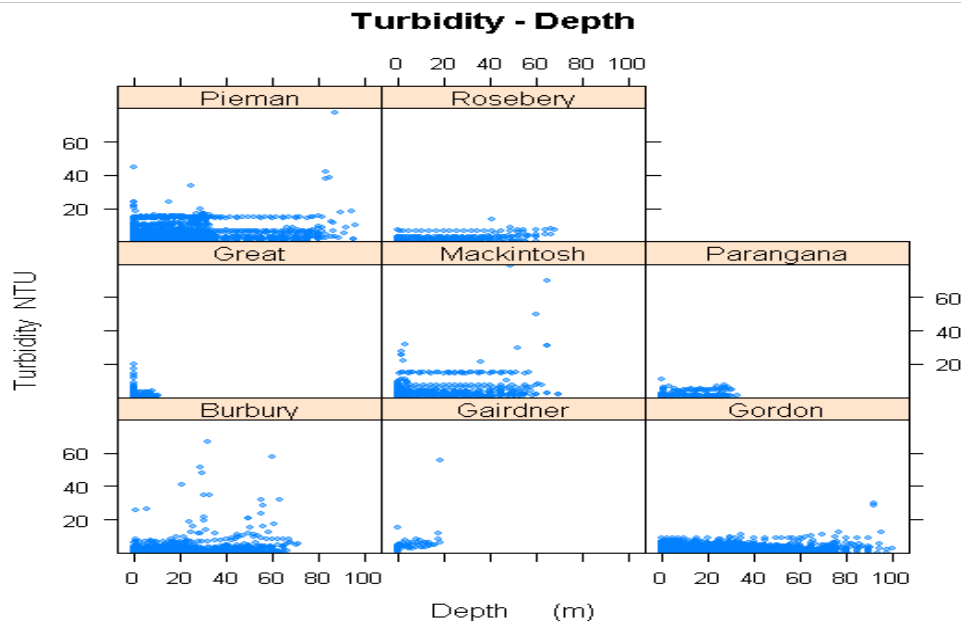


Figure 4.7 Relationship between water turbidity-depth of lakes.

4.2.2.2 Boxplot Parameters

A boxplot, which is also called “box and whiskers plot”, provides a graphical summary of distribution (Dalgaard, 2002). The dot or line in the middle of a box indicates the median value, which is the central value of the data distribution of the parameter. This allows future interpretation of the data not shown in the scatter graphs.

The bottom and top of the box show the 25th and 75th percentiles respectively. The location of the middle 50% of the data is called the upper and lower quartiles. The whiskers (vertical dash lines) show the largest and smallest observation that falls within a distance of 1.5 times the box size from the median (upper and lower whiskers). If any observations fall further away, the additional points are defined as outliers and are shown separately (Crawley, 2007). For a normalised data distribution, about 99% of the observations will fall between the whiskers (Braun et al., 2007). The construction of a boxplot is shown in Figure 4.8.

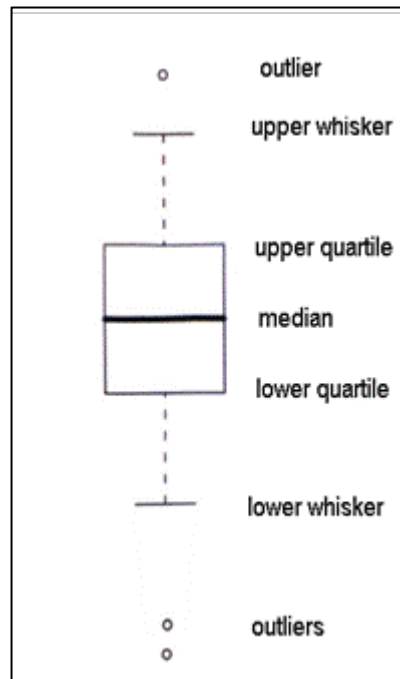


Figure 4.8 Construction of a boxplot.

Parameters including pH value, water turbidity, water conductivity and water temperature, with values at depths greater than 5 m, are shown in Figures 4.9 to 4.12. Values of dissolved oxygen at depths greater than 15 m are shown in Figure 4.13.

Cullimore et al. (1978) found that pH value was one of the factors that affect the growth rate of biofouling. Pinheiro et al. (1988) also found that some iron bacteria grow faster when the pH is neutral (pH = 7) rather than more alkaline (pH = 9). Median values and mean values of field pH are shown in Figure 4.9 and Table 4.3. The highest field pH median value was found in Great Lake (Figure 4.9), and the maximum mean field pH value was also found in Great Lake (6.73), as summarised in Table 4.3.

Chapter 4 – Biofouling and Water Quality in Tasmanian Hydropower Schemes

Lake	pH D>5m	Total Dissolved Oxygen (mg/L) D>15m	Turbidity (NTU) D>5m	Conductivity (TRef) D>5m	Dissolved Organic Carbon (mg/L)	Total Iron (mg/L)	Total Manganese (mg/L)	Total Kjeldahl Nitrogen	Total Aluminium (mg/L)	Total Nitrate as NO ₃ (mg/L)	Total Sulphate (mg/L)	Biofouling in Downstream Cooling Pipes
Burbury	5.8	32.53	2.426	42.475	4.785	0.282	0.023	0.166	0.139	0.012	2.512	Yes
Gairdner	6.1	32.47	7.184	30.814	4.600	0.302	0.022	0.171	0.185	0.019	0.507	Yes
Gordon	6.0	27.77	2.230	38.468	6.016	0.637	0.057	0.209	0.173	0.060	1.002	Yes
Great	6.8	46.56	0.936	17.200	2.683	0.085	0.009	0.119	0.055	0.005	0.527	No
Mackintosh	5.5	18.98	6.607	30.445	8.800	0.326	0.021	0.206	0.065	0.010	0.863	Yes
Parangana	6.3	42.82	2.353	20.913	2.470	0.066	0.007	0.099	0.265	0.023	0.578	Yes
Pieman	5.6	32.99	4.930	55.645	7.379	0.395	0.067	0.218	0.229	0.021	2.451	Yes
Rosebery	5.5	28.31	3.000	31.130	7.567	0.349	0.024	0.222	0.082	0.011	1.129	Yes

Table 4.3 Summary mean values of water data parameters.

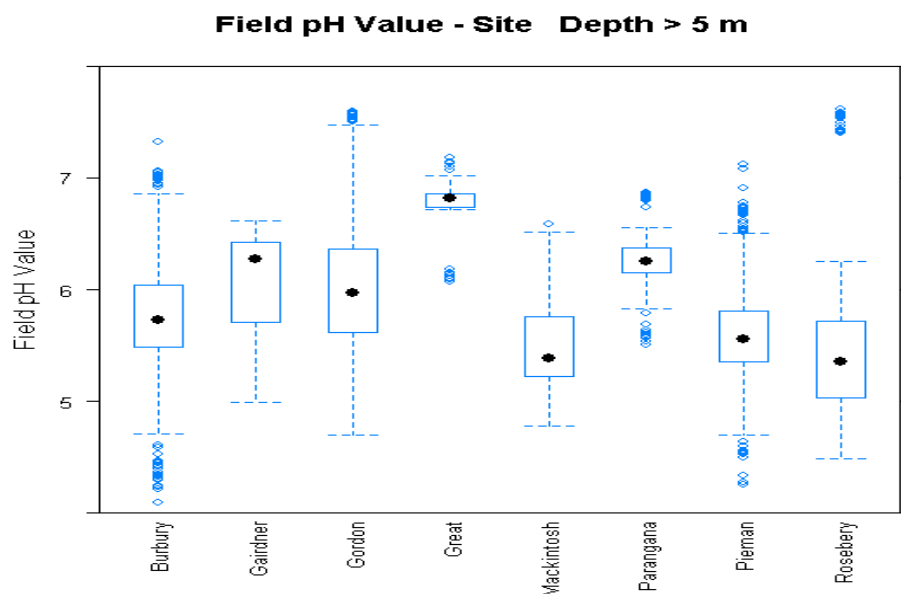


Figure 4.9 Field pH boxplots at depths greater than 5 m of lakes.

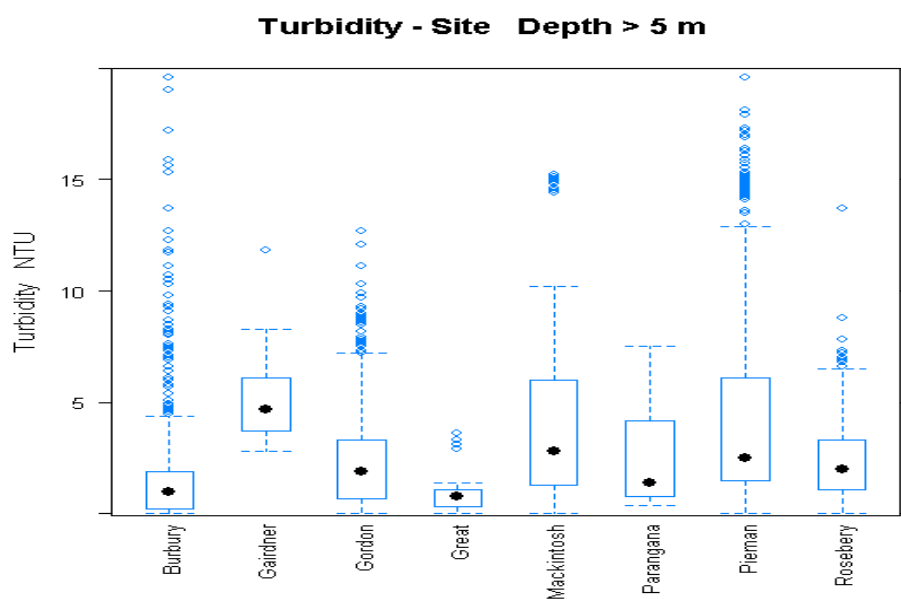


Figure 4.10 Turbidity boxplots at depths greater than 5 m of lakes.

Turbidity is a physical characteristic of water. It was found that the median and mean turbidity values of Great Lake were lower than those of other lakes (Figure 4.10 and Table 4.3).

The conductivity of water increases as the concentration of ions increases. It was found that the median and mean values of water conductivity of Great Lake were lower than those of other lakes, as shown in Figure 4.11 and Table 4.3.

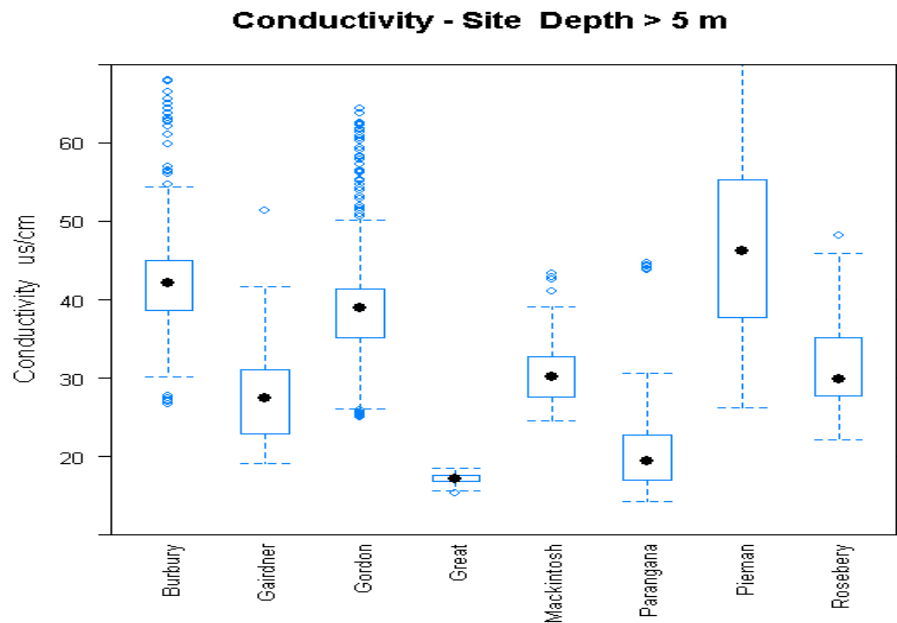


Figure 4.11 Conductivity boxplots at depths greater than 5 m of lakes.

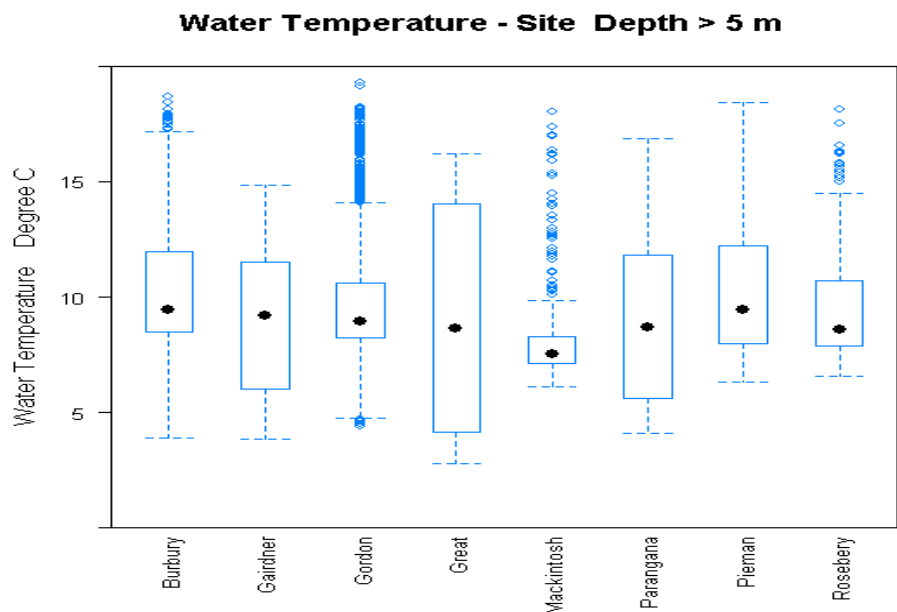


Figure 4.12 Water temperature boxplots at depths greater than 5 m of lakes.

Water temperatures are plotted in Figure 4.12. No difference was found in water temperature between Great Lake and others.

In Figure 4.13, there are no outliers; hence the top of the upper bar represents the maximum value of the response for the dissolved oxygen at depths greater than 15 m, the bottom of the lower bar representing the minimum value.

The highest median value for parameter dissolved oxygen was in Great Lake than (Figure 4.13), and the maximum mean value of dissolved oxygen was also found there, as shown in Table 4.3.

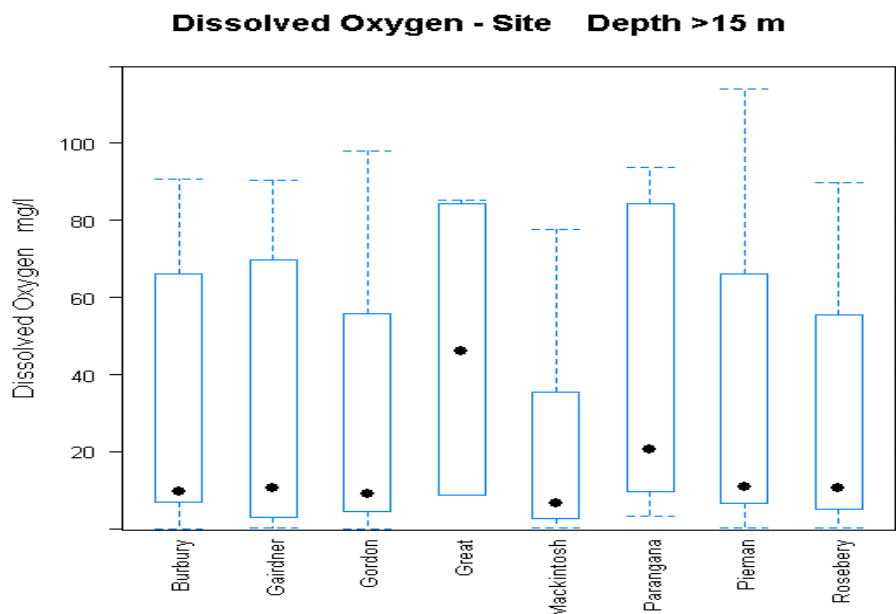


Figure 4.13 Dissolved oxygen boxplots at depths greater than 15 m of lakes.

All available data are analysed for parameters measured at depths less than 5 metres including metals, nutrients and salts, as shown in Figures 4.14 to 4.25 and Table 4.3.

It was found that iron and manganese are the two main factors affecting the growth of bacteria biofouling in pipes (Barton, 2007a; Minkus, 1954; Pollard et al., 1959). As described in Chapter 2, Tyler (1968) found that a higher concentration of manganese in water produced more biofouling. The median value of total iron and manganese in Great Lake, where there was no reported biofouling problem in the cooling pipes at the downstream power station, was also

found to be lower than most of the values in other lakes used in the study (Figure 4.14 and Figure 4.15).

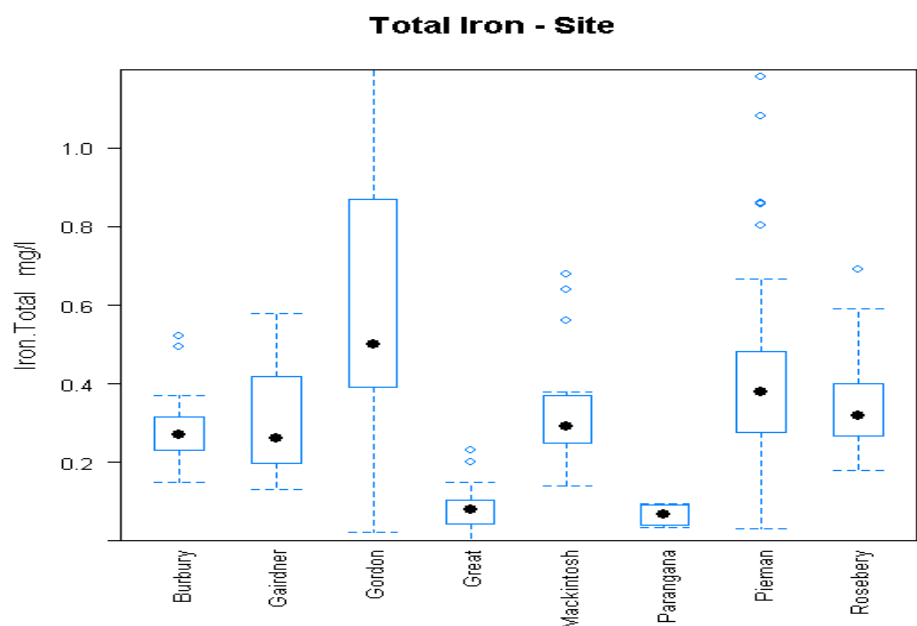


Figure 4.14 Total iron boxplots of lakes.

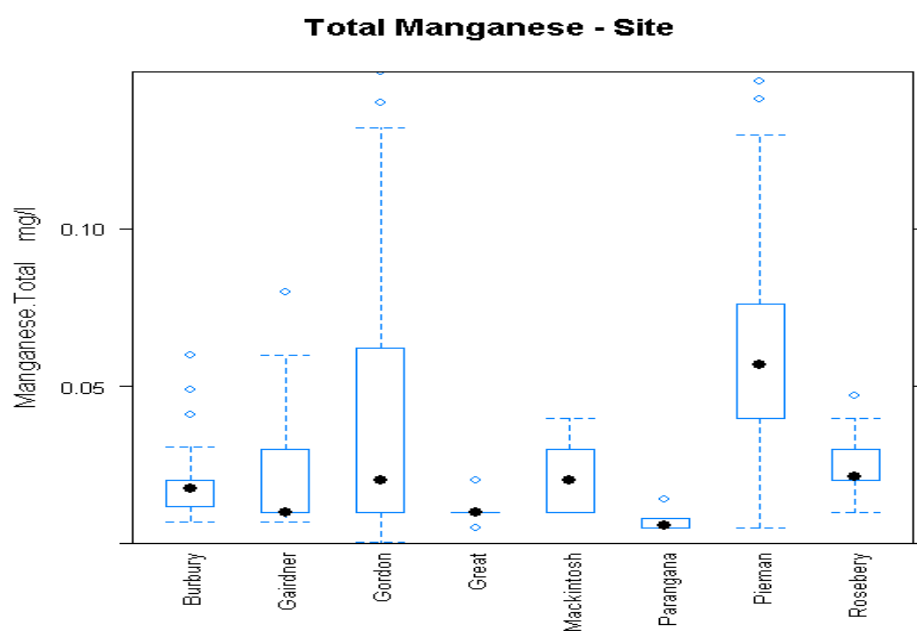


Figure 4.15 Total manganese boxplots of lakes.

It can be seen from Table 4.3 that Lake Parangana contains similar mean values of iron and manganese to those in Great Lake, and they are less than those in other lakes. The power station downstream of Lake Parangana, Lemonthyme Power Station, reported biofouling problems in the cooling pipes. However, it can be seen that the pH and the dissolved oxygen of Great Lake are higher than that of Lake Parangana; the turbidity and conductivity of Great Lake are lower than that of Lake Parangana (Figures 4.9 - 4.11 & 4.13 and Table 4.3).

Lower median values of total aluminium have been found in Great Lake than other lakes studied (Figure 4.16). The mean values of lakes have been calculated in Table 4.3. Unfortunately, the effect of aluminium on the growth of biofouling has not been well-studied by previous researchers. Thus, it is recommended that the effect of aluminium on biofouling be further investigated.

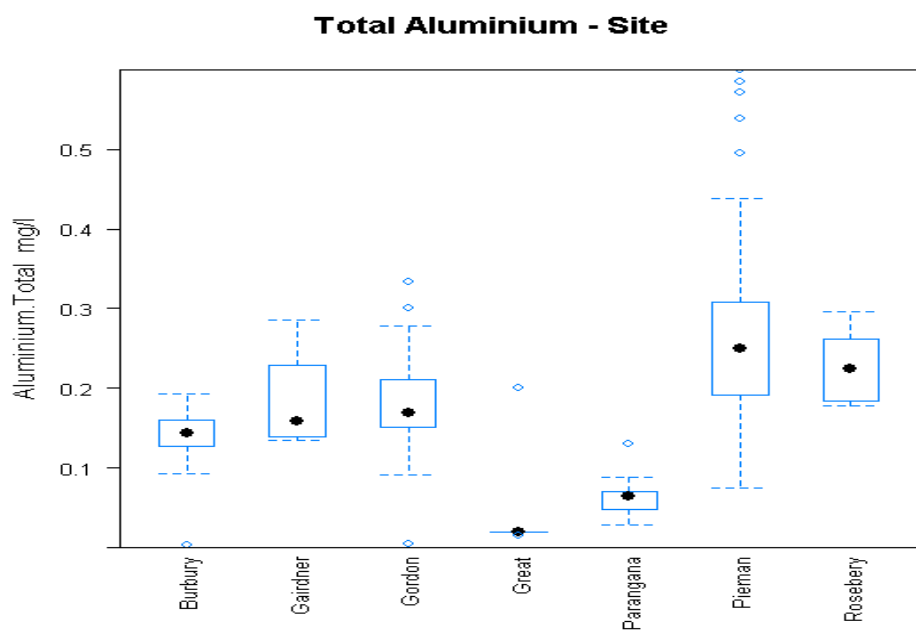


Figure 4.16 Total aluminium boxplots of lakes.

The amount of dissolved iron is thought to be one of the key factors that affect the growth rate of bacteria. Stuetz et al. (2004) found that the concentration of dissolved iron in the aquifer is the key factor in determining whether biofouling develops in a well. Data of dissolved iron are only available for lakes Burbury, Gordon, Parangana and Pieman, as plotted in Figure 4.17. Due to the limited data, it is suggested that dissolved iron be further investigated to determine its effect on biofouling.

The amounts of other metals including zinc, copper, cobalt, chromium, lead and magnesium in Great Lake are not significantly different to that in other lakes. Only Zinc is plotted in this analysis, as shown in Figure 4.18.

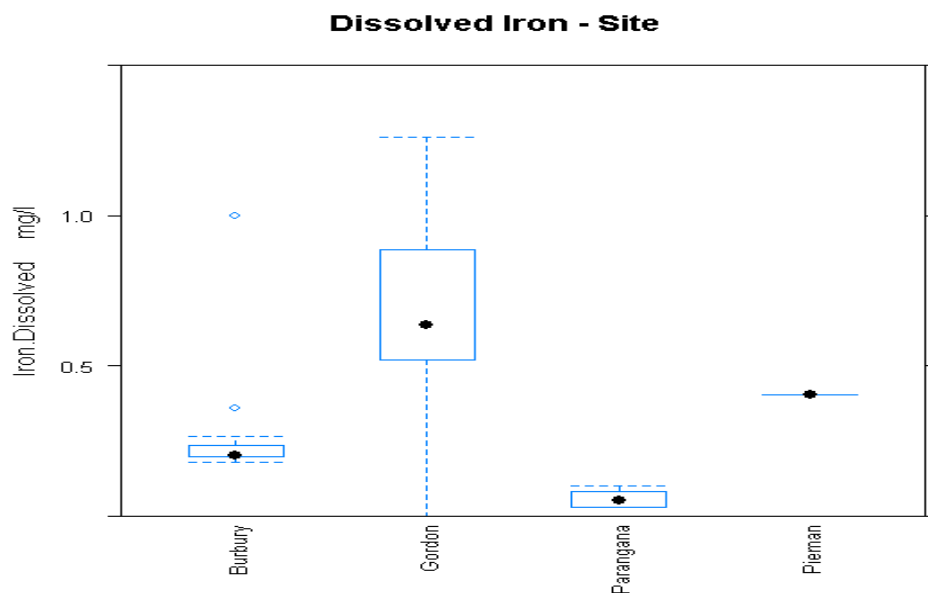


Figure 4.17 Total dissolved iron boxplots of lakes.

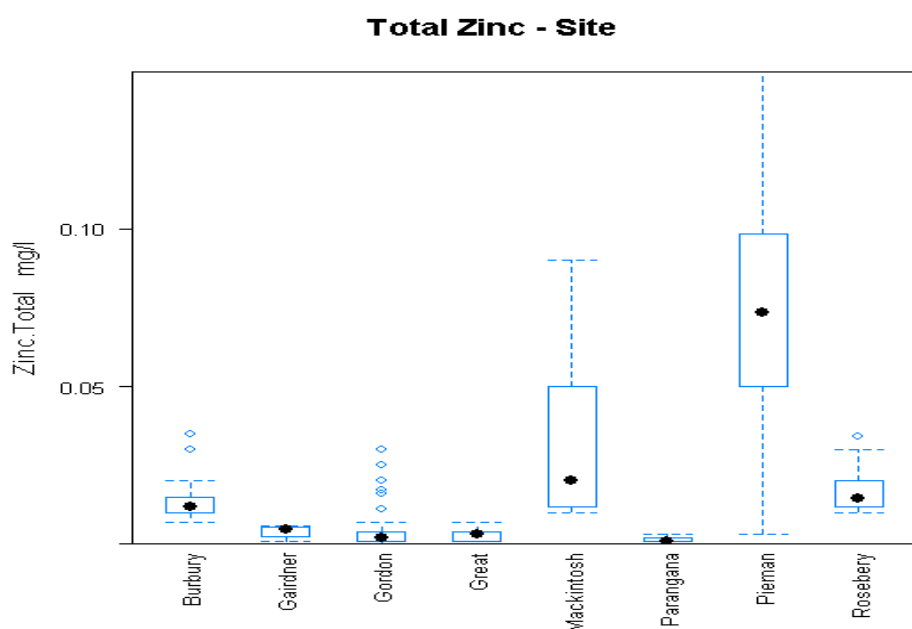


Figure 4.18 Total zinc boxplots of lakes.

The growth rate of bacteria is controlled by the concentration of nutrients in water, such as organic carbon. Organic carbon exists in a variety of types, including citrate and glucose (Cullimore et al., 1978). Pryogle et al. (1997) found that the growth of algae requires nutrients such as nitrate, nitrite, orthophosphate and ammonia.

Dissolved organic carbon (DOC) acted as a nutrition factor to increase the growth of biofouling in studies by Lambert et al. (2008; 2009). The median value of dissolved organic carbon and total kjeldahl nitrogen (the sum of organic nitrogen; ammonia and ammonium) of lakes is plotted in Figures 4.19 and 4.20. The mean values of dissolved organic carbon and total kjeldahl nitrogen are calculated in Table 4.3.

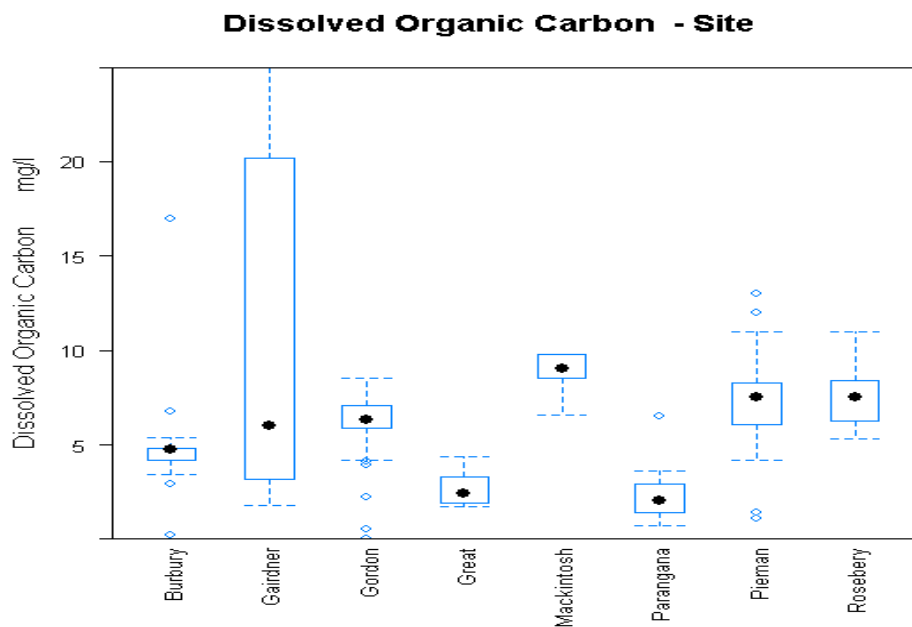


Figure 4.19 Dissolved organic carbon boxplots of lakes and canal.

It can be seen from Figures 4.19 and 4.20 that Great Lake and Lake Parangana contain less dissolved organic carbon and total kjeldahl nitrogen in the water than most lakes in the current study. In addition, the mean value of dissolved organic carbon and total kjeldahl nitrogen in Lake Parangana is also lower than Great Lake (Table 4.3). However, some water quality data such as pH value, turbidity and conductivity of Lake Parangana differ from that of Great Lake, as discussed above.

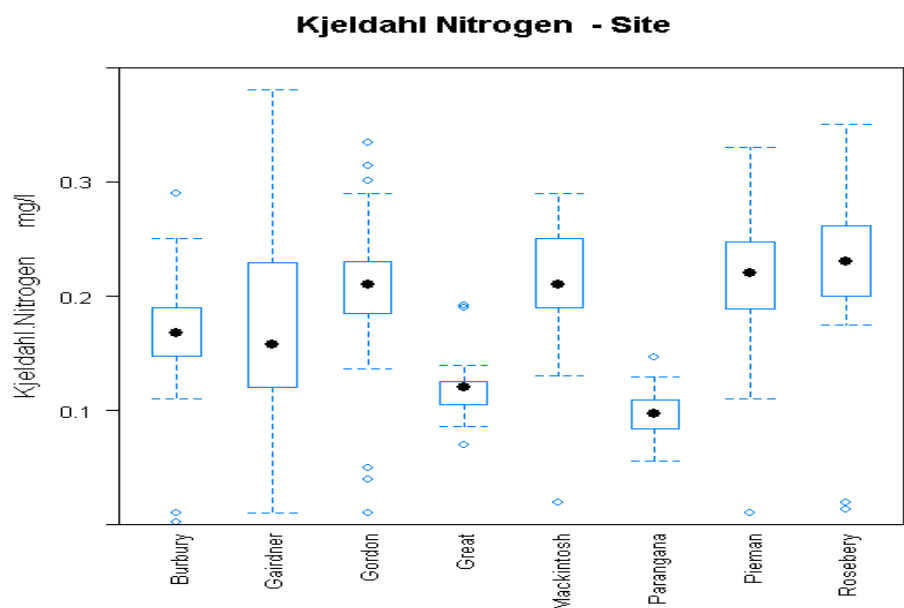


Figure 4.20 Total kjeldahl nitrogen boxplots of lakes.

Median and mean values of total nitrate as NO_3 are shown in Figure 4.21 and Table 4.3. It can be seen that both the median and mean values of total nitrate as NO_3 in Great Lake are lower than all other lakes.

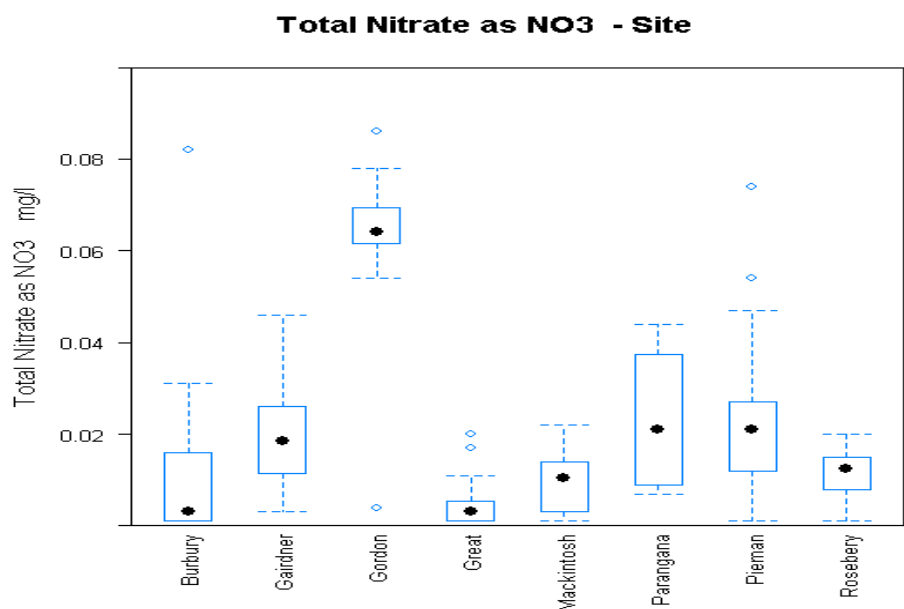


Figure 4.21 Total nitrate as NO_3 boxplots of lakes.

The amount of ammonia is also plotted with limited data (Figure 4.22). No comment can be made due to lack of ammonia data for Great Lake.

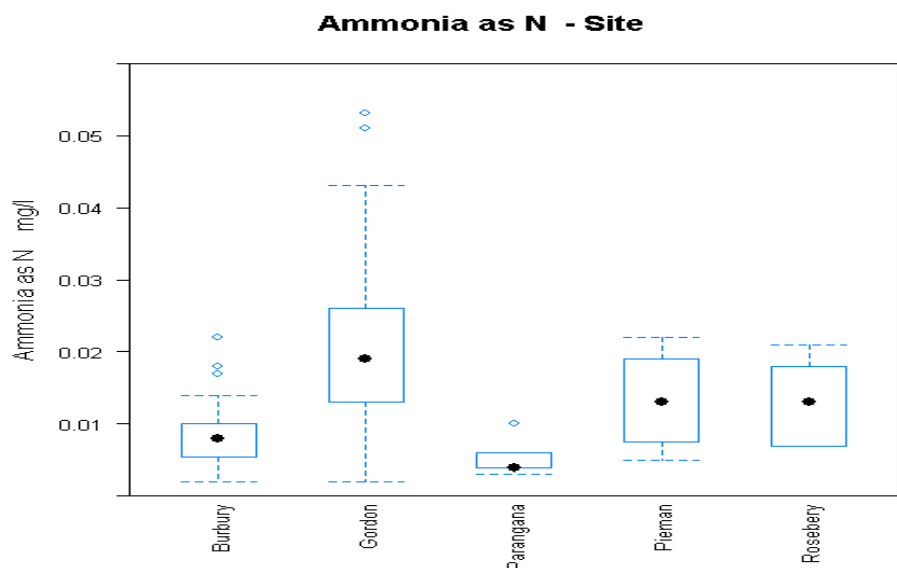


Figure 4.22 Total ammonia as N boxplots of lakes.

Median value of total sulphate is plotted in Figure 4.23. Mean value of total sulphate is calculated in Table 4.3. It can be seen that Great Lake has less sulphate than the other lakes.

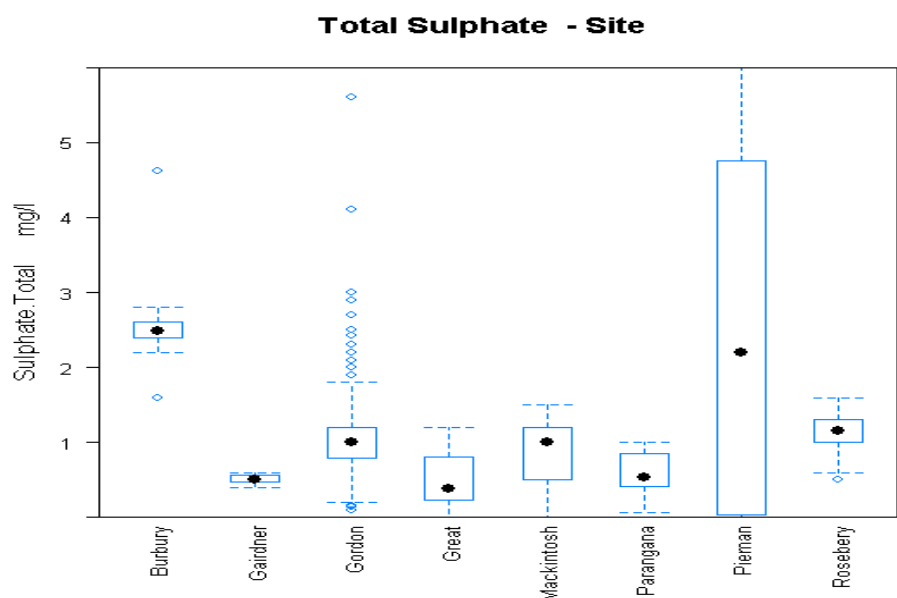


Figure 4.23 Total sulphate boxplots of lakes.

Parameters from sodium and potassium are also plotted in Figures 4.24 and 4.25. It can be seen from that sodium and potassium in Great Lake are lower than the values in other lakes.

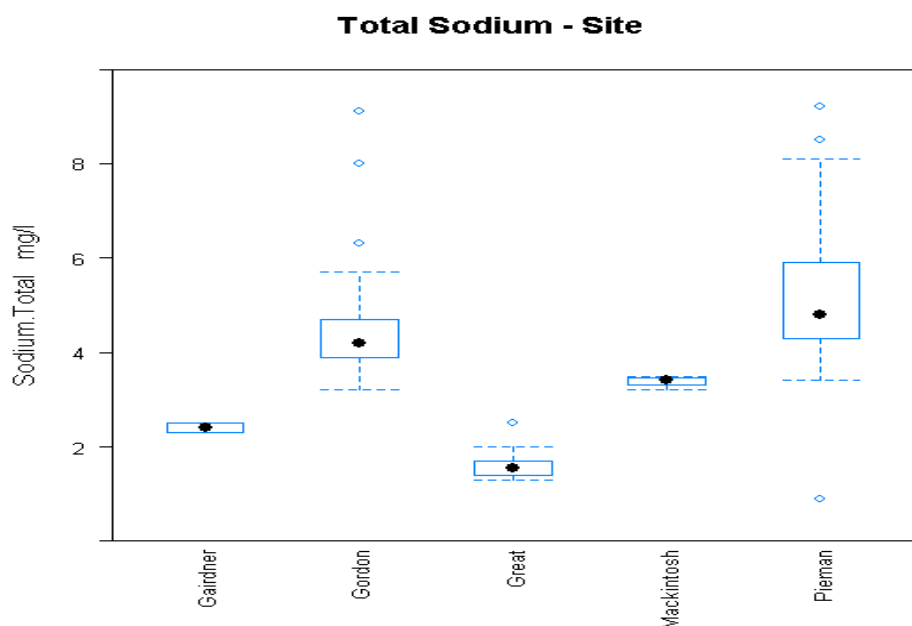


Figure 4.24 Total sodium boxplots of lakes.

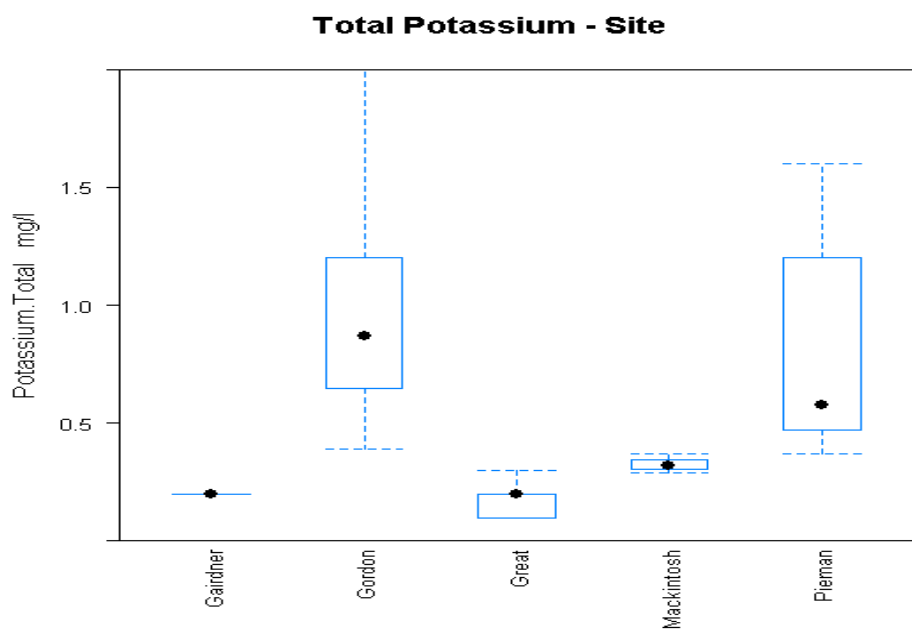


Figure 4.25 Total potassium boxplots of lakes.

4.3 Chapter Summary

The chemical composition of biofouling and the water quality parameters of lakes and canals were studied in this chapter. The relationships between the water temperature, pH values, conductivity, turbidity, nutrient concentration levels, metal content, oxygen concentration levels and organic material of water were investigated.

Professional statistics program R was used in the analysis with data being presented in xy-plots and boxplots. The following observations were drawn from the analysis, based on the available data:

1. The water temperature decreased with the depth in lakes in different seasons, similar to that reported by Tyler (1968).
2. High values of iron and manganese were found in black-brown coloured slime biofouling in cooling pipes of Wilmot Power Station. The amount of iron and manganese in power station cooling pipes was close to that found in penstocks and pipelines by previous researchers (Barton, 2007a; Tyler, 1968).
3. No biofouling problem was reported in the downstream cooling pipes of Great Lake. While there does not appear to be an immediately obvious connection to particular parameters, it may be due to the difference in the following parameters found in this water data analysis:
 - The pH value and dissolved oxygen are higher in Great Lake than in all other lakes at depths greater than 5 metres.
 - The water conductivity and turbidity are lower in Great Lake than in all other lakes at depths greater than 5 metres.
 - The amount of iron, manganese and aluminium are lower in Great Lake.
 - Lower nutrient level in Great Lake was found for the growth of bacteria and algae such as dissolved organic carbon, kjeldahl nitrogen and nitrate.

Further studies on the ecology of biofouling causing organisms are required to show which water quality parameters are likely to influence their growth. These results provide a useful reference for ongoing research in this field.

4. The surface water quality data of Lake Parangana is very similar to the Great Lake data. However, the pH and dissolved oxygen of Great Lake are higher than that of Lake Parangana; the turbidity and conductivity of Great Lake are lower than that of Lake Parangana at depths greater than 5 m.

Chapter 5 Design and Instrumentation of the Pipe Rig

This chapter describes the laboratory and site pipe rigs designed for the study of biofouling in pipes. It includes the detailed design, installation, instrumentation and calibration of the pipe rig.

5.1 Lab Pipe Rig

In order to investigate the head loss and velocity profile shape of the flow in biofouled pipes, a Lab pipe rig was designed and built, as shown in Figure 5.1. This is located in the Hydraulics laboratory in the School of Engineering at the University of Tasmania.

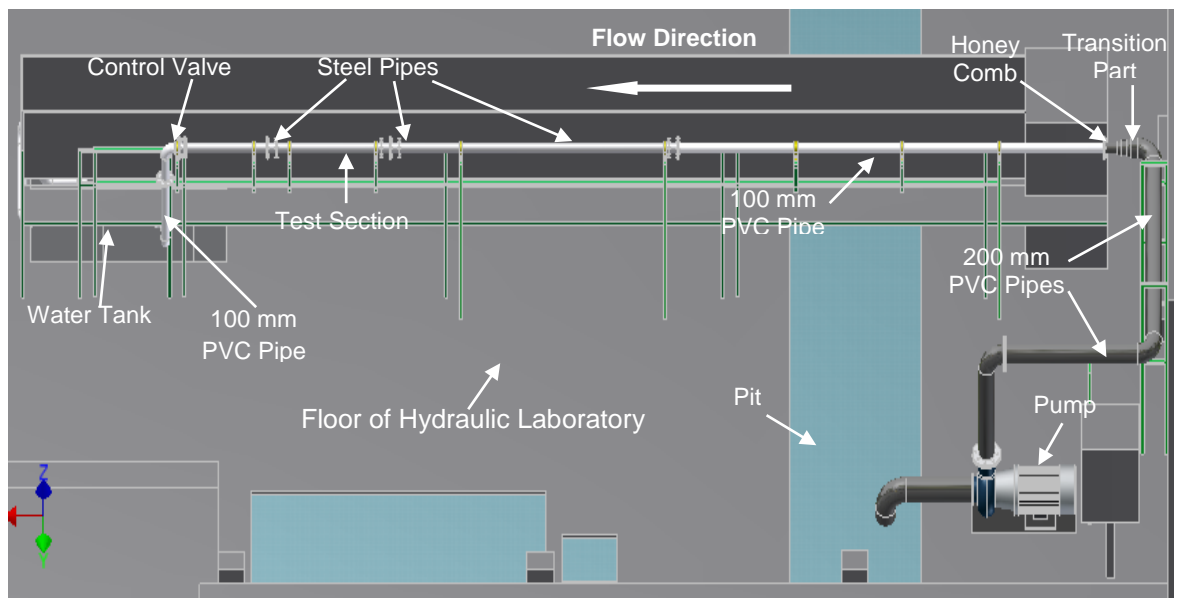


Figure 5.1 Schematic diagram of the Lab pipe rig in Hydraulic laboratory.

The Lab pipe rig is equipped with sensors to measure the velocity profile, water pressure, flow rate and water temperature. The plan and elevation views of the Lab pipe rig are shown in Figure 5.2 a) and b), and detailed dimensions are shown in Appendix C.1.

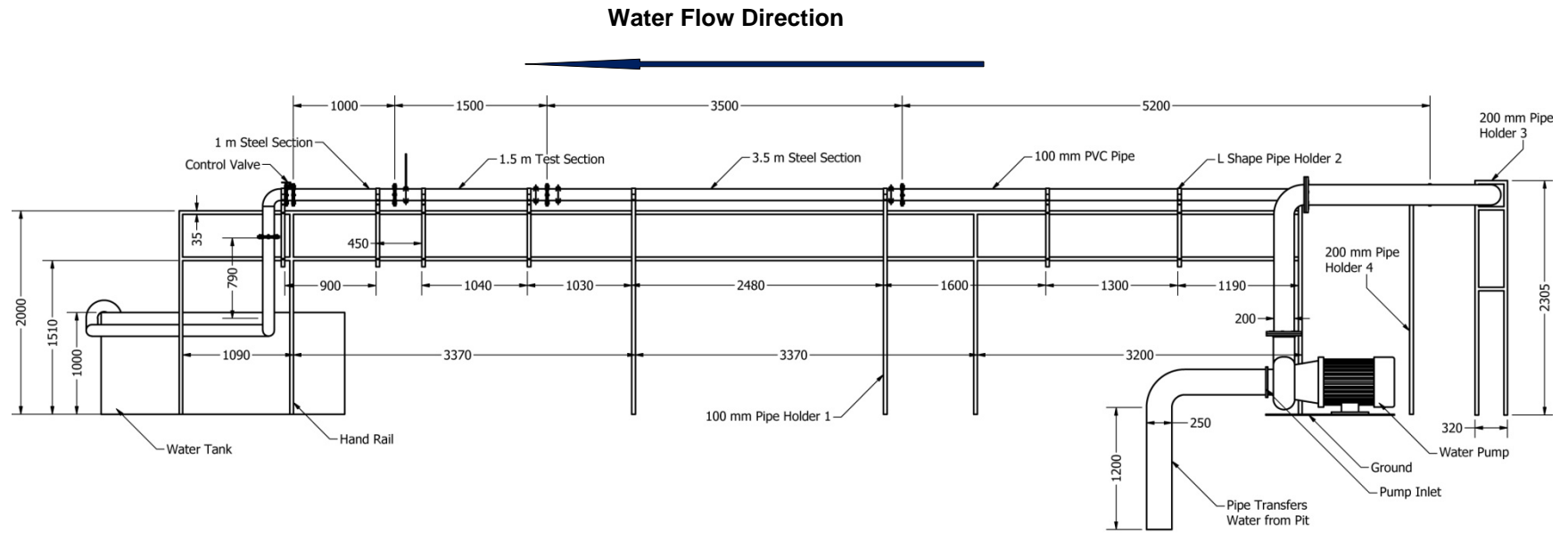


Figure 5.2 a) Elevation outline of the Lab pipe rig in laboratory (Scale 1:30).

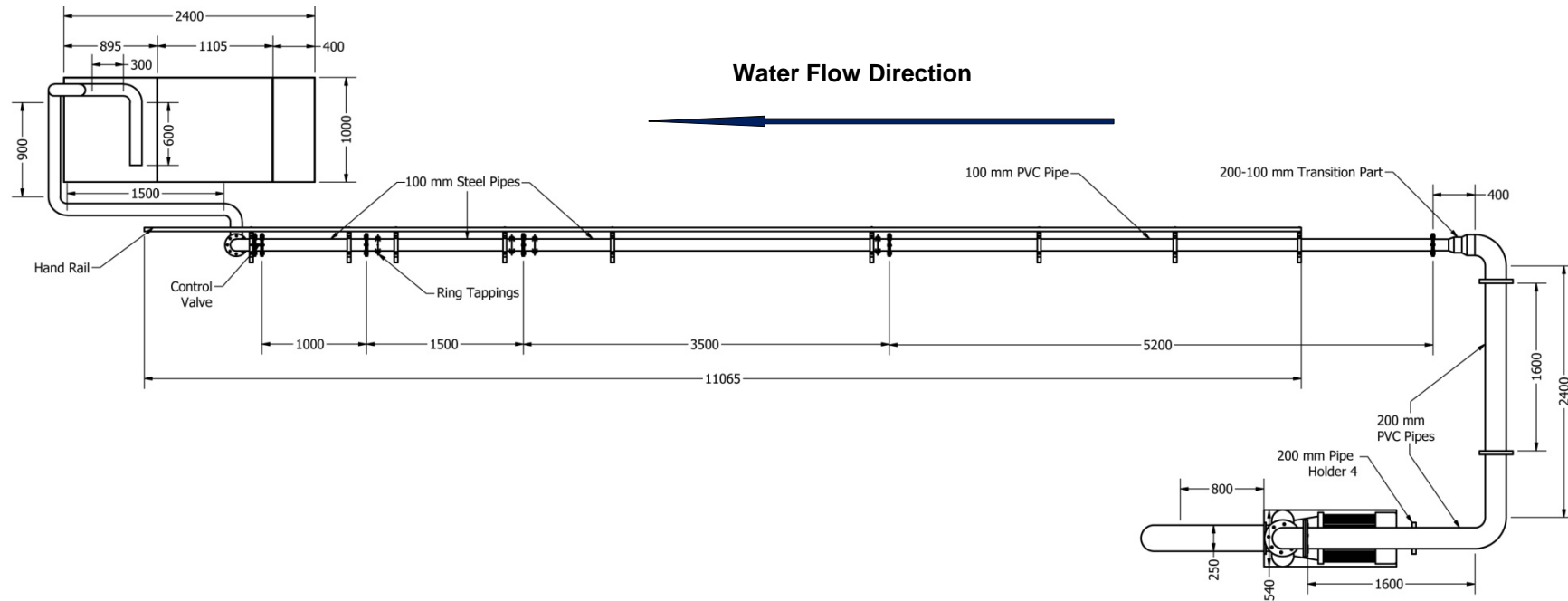


Figure 5.2 b) Plan graph of the Lab rig in laboratory (Scale 1:30).

5.1.1 Design of the Lab Pipe Rig

Dimensional analysis and the similarity method were considered in the design of the Lab pipe rig so that conditions representative of cooling water pipe flow were achieved. The maximum diameter of hydropower pipelines is over 3 m (Barton, 2007a), producing very high Reynolds numbers. Typical hydraulic conditions for Hydro Tasmania field conduits are shown in Table 5.1.

		Wilmot Penstock	Tarraleah Hilltop Pipeline	Poatina Penstock
Tested Length L (m)		331	1067	1684
Diameter D (m)		1.98	2.59	2.58
Flow rate Q(m ³ /s)	Fouled	15.41	21.18	35.38
	Clean	15.2	20.58	45.18
Mean velocity U (m/s)	Fouled	5.00	4.02	6.77
	Clean	4.94	3.91	8.64
Friction factor f	Fouled	0.0129	0.0126	0.0129
	clean	0.0099	0.0088	0.015
Wall shear stress τ_w (kg/ms ²)	Fouled	40.35	25.43	73.83
	clean	30.13	16.77	139.99
Shear velocity u_* (m/s)	Fouled	0.201	0.159	0.272
	Clean	0.174	0.130	0.374
Reynolds Number Re (x10 ⁶)	Fouled	7.6	8.0	13.4
	clean	7.5	7.7	17.1
Equivalent sand roughness k_s (mm)	Fouled	0.27	0.3	0.31
	clean	0.04	0.02	0.88
Relative Roughness (k_s/D) (x10 ⁻⁶)	Fouled	136.36	115.83	120.16
	clean	20.20	7.72	341.09

Table 5.1 Typical hydraulic conditions for Hydro Tasmania field conduits (Barton, 2007a).

To maintain exact similarity between the model pipe in the laboratory and prototype conduits on the field, three similarities need to be achieved, including geometric similarity, kinematic similarity and dynamic similarity. Geometric similarity requires the shape of the model to be the same as that of the prototype. Kinematic similarity requires the velocity at any point in the model

pipe flow to be proportional (constant scale factor) to the velocity at the corresponding point in the prototype penstock flow. Dynamic similarity requires all forces in the model pipe flow scale by a constant factor to correspond to the forces in the prototype penstock flow (force scale equivalent).

Wilmot penstock (1.98 m in diameter), which had a severe biofouling problem on the inside surface, was selected as the prototype pipe in this design. A pipe of the same shape with a diameter of 100 mm was selected as the model pipe for the geometric similarity with a scale factor of 1:20. The Buckingham Pi theorem (Cengel et al., 2006) was used to retain similarities between the pipe in the laboratory and typical cooling water pipes on site. The Buckingham Pi theorem for the current pipe rig design is introduced in Appendix C.3.

5.1.1.1 Design Calculations

Two kinds of pipes made of steel and PVC and with diameters of 100 mm and 200 mm were selected in this design. The velocity profiles (u) and the major head loss (H_f) in the biofouled test section pipe under fully developed turbulent flow were measured in the laboratory.

The total head loss (H_L) of the Lab pipe rig includes major head loss (H_f) and minor head loss (H_m). The friction factor (f) was determined for both steel and PVC pipes. The major head loss along different lengths of pipes was calculated, while minor head losses were determined for pipe sections at the location of turns, valves and contractions. All the design calculations were based on a water temperature of 10 °C. The length of pipes is shown in Table 5.2.

	PVC pipe				Steel pipe
	200mm	100mm	Honey comb	200-100 Transition	100mm
Length (m)	6	8	0.3	0.3	6.5

Table 5.2 Length of pipes of the Lab pipe rig

The total head loss (H_L), major head loss (H_f) and minor head loss (H_m) are calculated using Equations 5.1, 2.2 and 5.2 respectively. To simplify the calculation of the Lab pipe rig, a relative roughness of 0.000015 was selected for all smooth pipes with diameters of 100 and 200 mm. This value was chosen based on clean pipe results from Table 5.1. The friction factor f was found in the Moody Diagram (Moody, 1944) after the Reynolds number was calculated for the

pipes. The major and minor head losses of the Lab pipe rig were calculated and are shown in Tables 5.3 and 5.4. Minor head loss coefficients (K_l) were determined by using those suggested by Cengel et al. (2006). The total head loss was calculated in Table 5.5.

Chapter 5 –Design and Instrumentation of the Pipe Rig

Flow rate Q (m^3/s)	D (m)	Average velocity U (m/s)	Re ($\times 10^5$)	Kinematic viscosity @ 10°C (ν) $\times 10^{-6}(\text{m}^2/\text{s})$	Density ρ (kg/m^3) @ 10°C	Length (m)	Friction factor f	Wall shear stress τ_w (kg/ms^2)	Shear velocity u^* (m/s)	Predicted major head loss H_f (m)	Total predicted major head loss H_f (m)
0.015708	0.1	2.00	1.53	1.307	999.7	15	0.0165	8.25	0.091	0.505	0.512
	0.2	0.50	0.77	1.307	999.7	6	0.0190	0.59	0.024	0.007	
0.023562	0.1	3.00	2.30	1.307	999.7	15	0.0158	17.77	0.133	1.088	1.103
	0.2	0.75	1.15	1.307	999.7	6	0.0168	1.18	0.034	0.014	
0.031416	0.1	4.00	3.06	1.307	999.7	15	0.0152	30.39	0.174	1.861	1.886
	0.2	1.00	1.53	1.307	999.7	6	0.0165	2.06	0.045	0.025	
0.035343	0.1	4.50	3.44	1.307	999.7	15	0.0145	36.69	0.192	2.247	2.279
	0.2	1.13	1.72	1.307	999.7	6	0.0165	2.61	0.051	0.032	
0.047909	0.1	6.10	4.67	1.307	999.7	15	0.0135	62.77	0.251	3.844	3.901
	0.2	1.53	2.33	1.307	999.7	6	0.0158	4.59	0.068	0.056	

Table 5.3 Predicted major loss of the Lab pipe rig, given $k_s/D=0.00015$.

	90° bend (x13)	Flange union (x8)	Valve (x1)	100-200 Transition(x2) $\theta = 30^\circ$	Honey-comb (x1)	
K_i	0.3	0.08	0.2	0.02	0.6	
2g	19.6	19.6	19.6	19.6	19.6	
Mean velocity U (m/s)	Minor head loss (m)					Predicted total minor loss H_m (m)
2	0.796	0.131	0.041	0.008	0.122	1.098
3	1.791	0.294	0.092	0.018	0.276	2.470
4	3.184	0.522	0.163	0.033	0.490	4.392
4.5	4.029	0.661	0.207	0.041	0.620	5.558
6.1	7.404	1.215	0.380	0.076	1.139	10.214

Table 5.4 Predicted minor loss of the Lab pipe rig.

$$H_L = H_f + H_m \quad (\text{Equation 5.1})$$

$$H_m = K_l \frac{U^2}{2g} \quad (\text{Equation 5.2})$$

U (m/s) (in 100 mm diameter pipe)	2	3	4	4.5	6.1
Total minor loss H_m (m)	1.098	2.470	4.392	5.558	10.214
Total major loss H_f (m)	0.512	1.103	1.886	2.279	3.901
Dynamic head H_D (m)	0.204	0.459	0.816	1.033	1.898
Total head H_L (m)	2.814	5.032	8.095	9.871	17.013

Table 5.5 Major, minor and total head loss of the Lab pipe rig.

A low head high flow centrifugal pump was selected for the Lab pipe rig to propel the flow. The total head loss curve of the Lab pipe rig together with centrifugal pump performance data are shown in Figure 5.3. It can be seen that the optimised operating flow rate is around 50 L/s with a head of 17.1 m. However, due to the concern that a high flow rate might cause the biofouling inside the pipe to be flushed away, a maximum flow rate of 36 L/s was used in the experiment, corresponding to a maximum velocity of 4.5 m/s in the test section, with a diameter of 100 mm.

Three steel pipes with a nominal diameter of 100 mm were selected. The other pipes and connections in the Lab pipe rig were plastic, with a diameter of 100 mm and 200 mm. In order to achieve similar smoothness between on site penstocks (coated with coal tar enamel on the inside surface) and steel pipes, the inside of each steel pipe was painted with coating Interzone 954, which is a two component coating without antifouling properties. It is widely used for coating gates and valves at power stations in Hydro Tasmania. The steel pipes were made from galvanized iron.

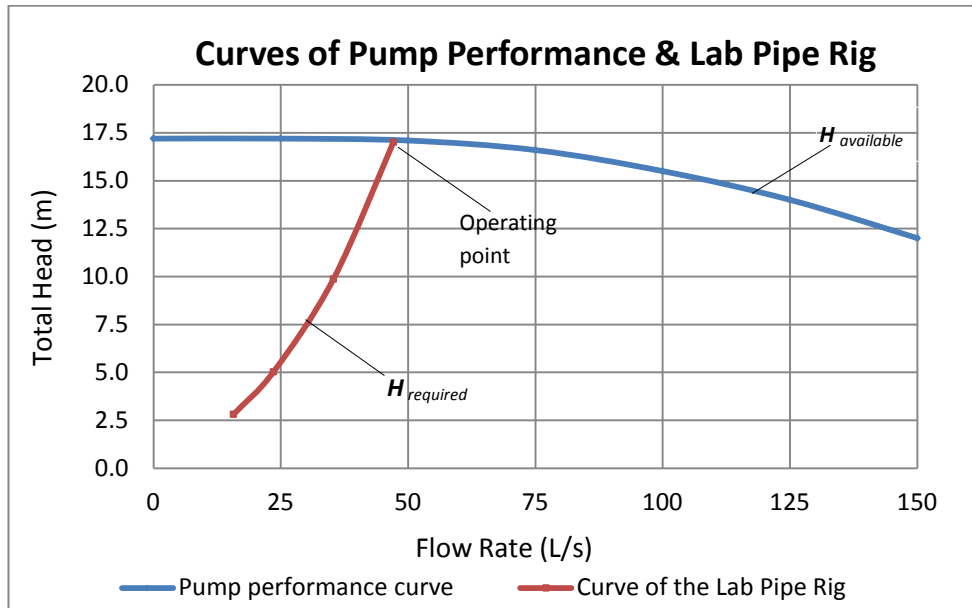


Figure 5.3 Curves of centrifugal pump performance and system head loss of the Lab pipe rig.

Equations 2.1, 2.6 and 2.5 were used to calculate the Reynolds number, the wall shear stress and shear velocity under different flow rates for both the test section and remaining sections of the Lab pipe rig. Detailed calculations of these parameters are shown in Tables 5.5 and 5.6.

Mean velocity was calculated by Equation 5.3.

$$U = \frac{Q}{A} \quad (\text{Equation 5.3})$$

5.1.1.2 Setup of the Lab Pipe Rig

The Lab pipe rig is comprised of a number of components including the pump, PVC pipes with diameters of 100mm and 200 mm, steel pipes with a diameter of 100 mm, control valves, the honeycomb, transitions and a water tank containing a V-notch weir plate.

Centrifugal pump

A 250X200-315 Southern Cross Centrifugal Pump was selected to supply water for the Lab pipe rig. The pump is classified as low head and high flow, and was manufactured by Tyco Pumping Systems, Australia. It is driven by a 6 Pole 22 KW 415V 3 phase AC motor and has the capacity to provide a maximum mean velocity of 6 m/s for the clean test section of the Lab pipe rig. The

efficiency of the pump was around 57% for a clean pipe at the operating point. For the fouled test section, the maximum mean velocity was set at around 4.5 m/s.

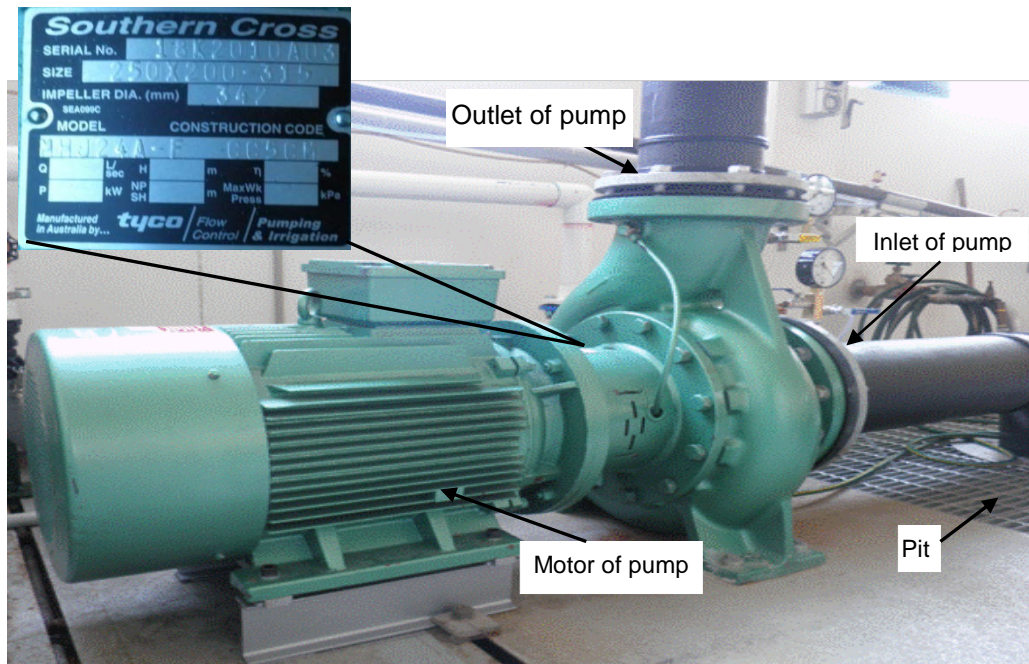


Figure 5.4 Southern Cross Centrifugal Pump type 250x200-315 in the Hydraulic laboratory.

The centrifugal pump was installed on the ground floor in the Hydraulics laboratory. The water used in the pipe rig was stored in a large pit located underneath the laboratory. When the system runs, the pump draws water from the pit through a PVC pipe with a diameter of 250 mm. The water is propelled into a black coloured PVC pipe with a diameter of 200mm. The photo of the Centrifugal pump is shown in Figure 5.4, and the pump's performance curve is shown in Appendix C.4.

PVC pipes with diameters of 200mm and 100 mm

The discharge diameter of the pump is 200 mm. A black coloured PVC pipe was used to connect the inlet of the pump (see Figure 5.4). Black coloured PVC pipes including 90 degree turns (diameter of 200 mm) were used up to the transition from 200 mm to 100 mm in diameter. The aim of this setup was to reduce the total system head loss.

A 5.2 m long PVC pipe with a diameter of 100 mm was selected after the transition from 200 mm to 100 mm diameter, to ensure a fully developed steady turbulent flow in the test section.

200 mm diameter to 100 mm diameter transition

In order to achieve the transition from the 200 mm diameter black coloured PVC pipe to the 100 mm diameter white coloured PVC pipe, a transition was used. A photo of the transition is shown in Figure 5.5 a)

Honeycomb

A plastic honeycomb (6 mm in tube diameter and 60 mm in length) was fitted inside the last segment of the transition, located before the 100 mm diameter PVC pipe. The purpose of the honeycomb block was to straighten the flow by reducing the transverse velocity component and the turbulence in the adjacent test section (Sargison et al., 2009). As recommended by Mehta et al. (1979), the length of the honeycomb section was 60 mm, which is 10 times the cell diameter.

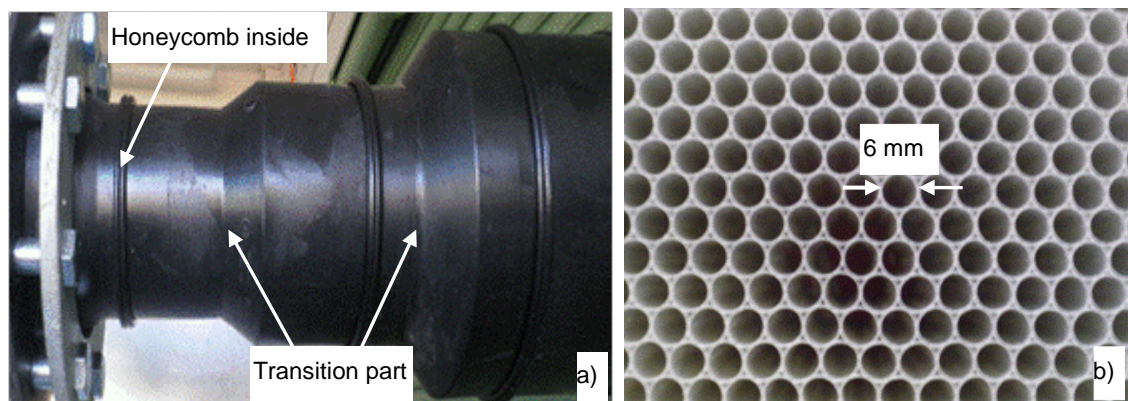


Figure 5.5 a) Diameter 200 mm -100 mm PVC transition part. b) Honeycomb.

The resistance provided by the honeycomb can improve the flow stability and reduce the fluctuation level of the fully developed turbulent flow in the pipe. However, the side effect of the honeycomb should be considered, due to the additional small scale turbulence generated by the honeycomb itself (Loehrke et al., 1976). A photo of the honeycomb is shown in Figure 5.5 b).

Steel pipes with a diameter of 100mm

The inside of the existing steel hydropower penstocks and pipelines were painted using coal tar enamel several decades ago by Hydro Tasmania. The purpose of the paint coating is to provide a smooth internal surface in the pipes, to slow down corrosion and to prevent the growth of

biofouling. Galvanized iron pipes with a diameter of 100 mm were selected to simulate penstocks and pipelines on site. For environmental reasons Hydro has started replacing the coal tar enamel coating. In this study, Interzone 954, without anti-fouling agent, was used for the coating inside the 100 mm diameter galvanized pipes.

The Lab pipe rig consists of three steel pipes with lengths of 3.5 m, 1.5 m and 1.0 m. The pipe 1.5 m in length was the test section pipe. In the upstream of the test section is the reference pipe 3.5 m long. It helps to maintain a stable fully developed turbulent flow in the test section, and also provides a reference for the measurements. The other pipe 1.0 m in length is located at the downstream of the test section to provide consistent conditions for the measurements.

Control valve

A Lug type butterfly valve was installed on the downstream end of the 1.0 m long steel pipe. The valve allows the rig to remain full to prevent the biofouling from drying out when the pump is off. A photo of the butterfly control valve is shown in Figure 5.6 a)

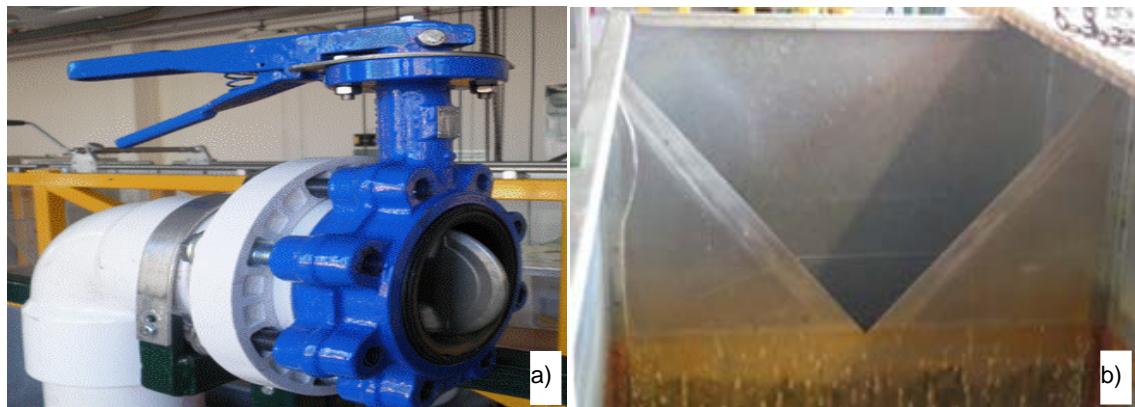


Figure 5.6 a) Lug type butterfly valve.

b) Water tank with V-notch weir inside.

Water tank and water storage pit

As part of the Lab pipe rig, an existing water storage pit located in the underground of the Hydraulics laboratory was used to store the water in the system. The pipe discharges into an existing V-notch weir to provide an alternative indication of the flow rate in the Lab pipe rig. The V-notch weir with an angle of 90° is shown in Figure 5.6 b).

5.1.2 Instrumentation of the Lab Pipe Rig

Transducers, sensors and metres were installed to measure the general water pressure, the flow rate and water level for the Lab pipe rig. The velocity profiles in the test section were calculated based on the following measurements.

5.1.2.1 Water Pressure Measurement

Validyne Engineering variable reluctance differential pressure transducers (model DP15) were used for all water pressure measurements in this study. A transducer is shown in Figure 5.7 a). Validyne DP15 is a bi-directional transducer. It is designed for fast response, making it suitable for the measurement of an unsteady flow. The diaphragm pressure range chart of the DP15 is shown in Appendix C.5. The accuracy of the DP15 is $\pm 0.5\%$ full scale (including effects of linearity, hysteresis and repeatability).

A Four-channel Validyne CD280, as shown in Figure 5.7 b) was used to amplify the input signal from the pressure transducers. The output was ± 10 Vdc full-scale.

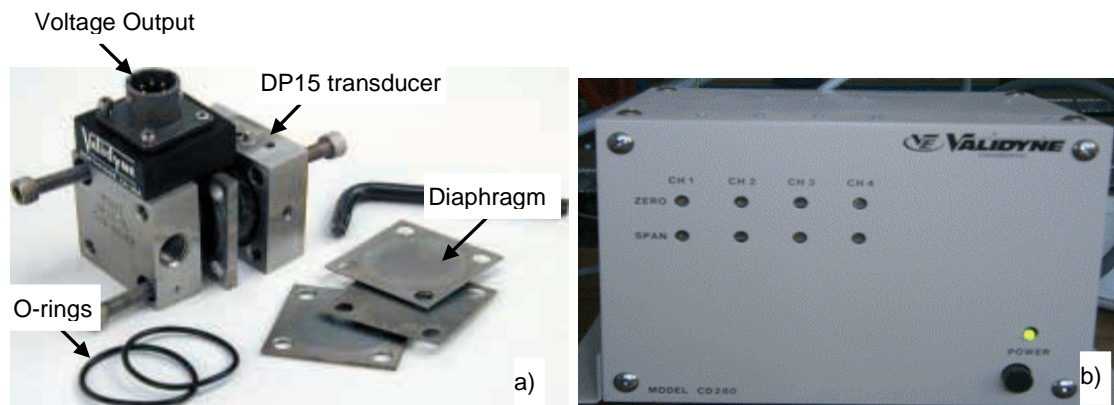


Figure 5.7 a) Validyne pressure transducers.

b) Four channel carrier demodulator.

5.1.2.2 Flow Rate Measurement

A YOKOGAWA Ultrasonic Flow metre, Model US300PM as shown in Figure 5.8 a) was selected for the mean velocity (flow rate) measurement. The measuring principle of the portable type US300PM flow metre is based on the influence of the flowing fluid to the travelling time of

sound. It calculates the speed (v) and flow (Q) of the fluid by measuring the difference in transit times of ultrasonic waves (t_{21} - t_{12}), as shown in Figure 5.8 d).

The US300PM flow metre has two clamped on transducers (Figure 5.8 c), which means no cutting of the pipe is required. In addition, since the measurement is independent of the liquid pressure or conductivity, it is suitable for measuring clean to dirty fluids in a fully filled pipe. The accuracy of the measured flow velocity is ± 0.01 m/s. The transducers were located on the 100 mm diameter section of PVC pipe upstream of the reference steel section, to avoid the complication of biofouled internal walls.

The flow rate was measured by the V-notch weir in the water tank located at the end of the Lab pipe rig, as shown in Figure 5.6 b), calculated by Equation 5.4. A mean velocity can be worked out from the calculated flow rate.

$$Q = C_{wd} \frac{8}{15} \tan\left(\frac{\theta}{2}\right) \sqrt{2g} H^{\frac{5}{2}} \quad (\text{Equation 5.4})$$

where Q is the flow rate; θ is the angle of the V-notch weir (90° in this study); H is the height from the upstream free surface to the bottom of the V-notch and C_{wd} is the weir discharge coefficient, as shown in Figure 5.8 b). C_{wd} was chosen as 0.579 in the present study according to BS3680: Part 4A (1981). H in Equation 5.4 was measured by an ultrasonic distance sensor. A TSPC-30 ultrasonic sensor was selected to measure the water height above the V-notch crest.

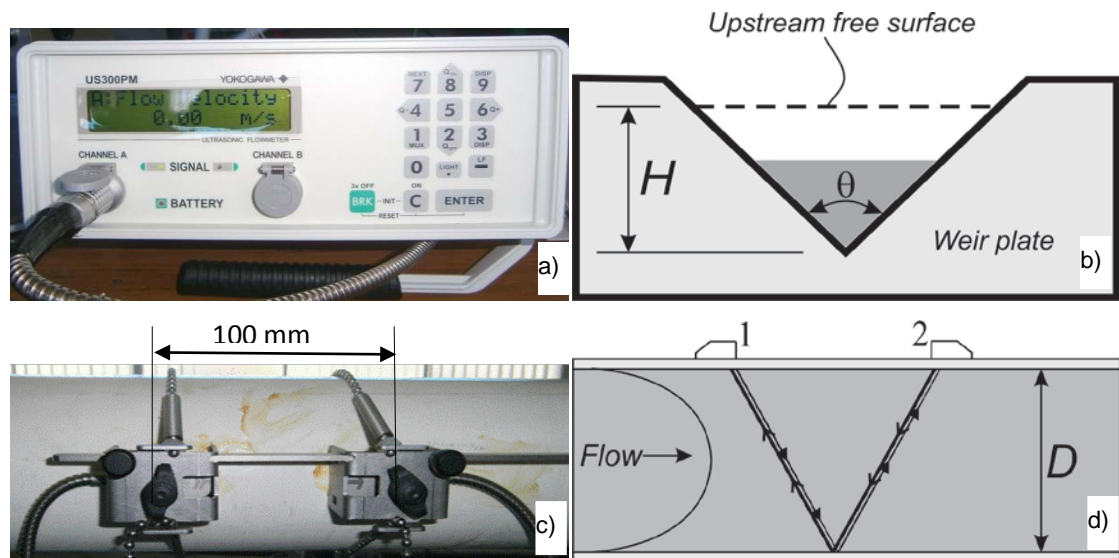


Figure 5.8 a) Portable ultrasonic flow metre US300PM. b) V-notch. The view is from downstream looking upstream. c) Two clamped-on transducers, the US300PM. d) V method of flow measurement.

5.1.2.3 Velocity Profile

A Pitot probe in conjunction with static ring tapping was selected to measure the velocity profile for the clean and fouled test section pipes. This probe was driven by an automated traverse system controlled by a National Instruments Labview program.

D (m)	Average velocity U (m/s)	Relative roughness k_s/D	Re ($\times 10^5$)	Length (m)		Friction factor f	Wall shear stress τ_w (kg/ms ²)	Shear velocity u_* (m/s)	Flow rate Q (m ³ /s)	Major head loss H_f (m)		Major head loss (kPa)		Dynamic pressure (kPa)
				Test section	Reference section					Test section	Reference section	Test section	Reference section	
0.1	2	0.00015	1.53	1.3	3.3	0.0168	8.25	0.091	0.016	0.045	0.113	0.437	1.109	1.999
0.1	3	0.00015	2.29	1.3	3.3	0.0158	17.77	0.133	0.024	0.094	0.239	0.924	2.346	4.499
0.1	4.5	0.00015	3.44	1.3	3.3	0.0145	36.69	0.192	0.035	0.195	0.494	1.909	4.845	10.122
Diaphragm number of DP15 pressure transducers:												26#	30#	32#

Table 5.6 Diaphragm selection of DP 15 pressure transducers.

5.1.3 Calibration of Instruments

Calibrations of the three DP15 pressure transducers, the YOKOGAWA flow metre and the level sensor were conducted before undertaking the velocity measurement in the pipes.

Before the calibration of the transducers, three diaphragms were selected according to the pressure drops across each pipe. The calculated pressure drops were 1.91 kPa and 4.85 kPa across the 1.5 m steel test section and 3.5 m steel reference section at a mean velocity of 4.5 m/s. The dynamic pressure for the Pitot probe velocity profiles measurement was calculated as 10.12 kPa at the mean velocity of 4.5 m/s. Hence, the diaphragms with dash numbers of 26, 30 and 32 were selected for the pressure drop of the test section, the reference section and velocity profile measurement, as shown in Table 5.6.

Calibration of pressure transducers:

The three Validyne DP15 pressure transducers were calibrated at the Hydraulics laboratory in the School of Engineering, UTAS.

A Labview program with an interface and manometer were used for the calibration of pressure transducers. Connections of the transducers, manometer and computer are shown in Figure 5.9.

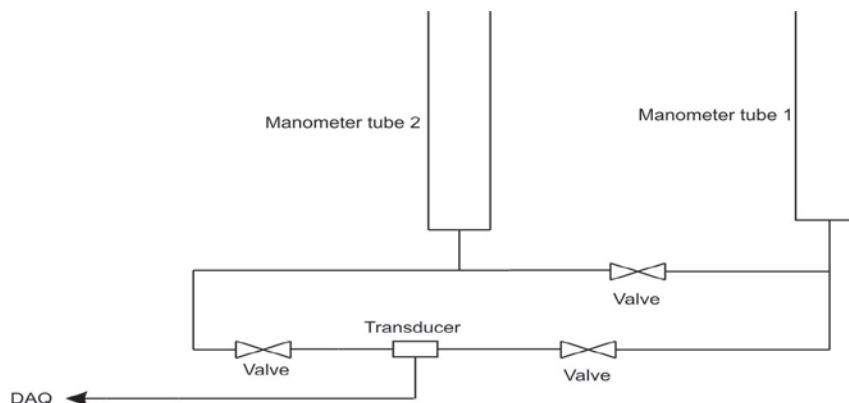


Figure 5.9 Connection of Validyne DP 15 pressure transducers, manometer and data acquisition.

Calibration of the pressure transducers was conducted by applying a known differential pressure to each transducer by pouring water into two tubes of a vertical manometer to different heights. The corresponding voltage output was collected by the DAQ system. A linear relationship between the output voltage and the pressure was obtained for each transducer, as shown in Figure 5.10 for transducers 1 and 3 (PT1 and PT3).

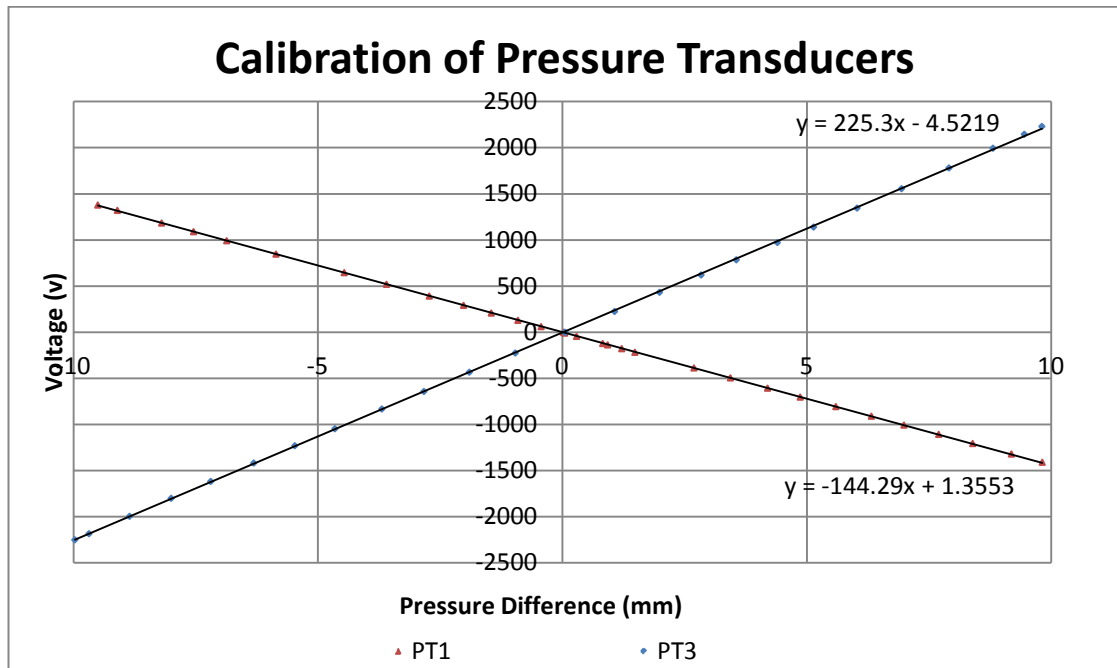


Figure 5.10 Calibration of Validyne DP 15 pressure transducers.

Calibration of mean velocity

The YOKOGAWA flow metre was set to measure the mean flow velocity. The measurement from the DAQ system was calibrated to match up with the readings from the flow metre, with the calibration result shown in Figure 5.11.

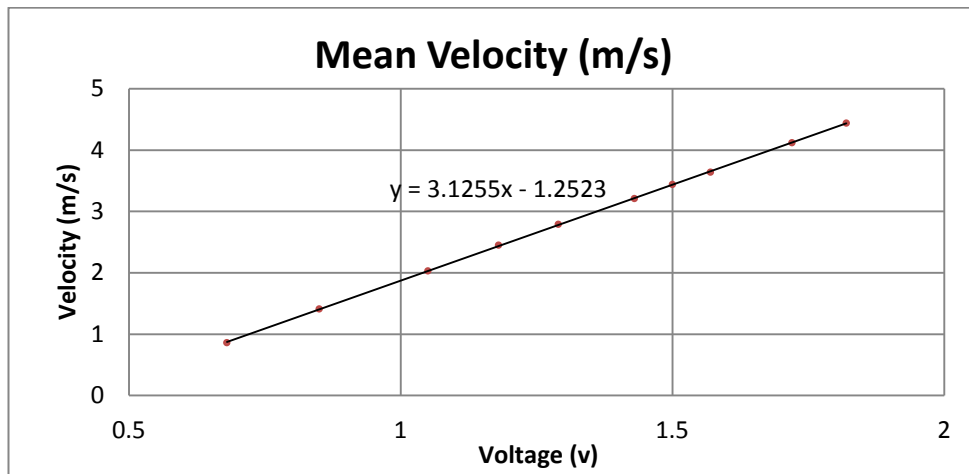


Figure 5.11 Calibration of mean velocity in Labview.

Calibration of water level sensor

A water level sensor was installed on the wall inside the water tank located at the end of the Lab pipe rig. This measured the water level and provided the value of the head above the crest (H) so that the flow rate and mean velocity in the pipe could be calculated using equation 5.4. The calibration result of the sensor is shown in Figure 5.12.

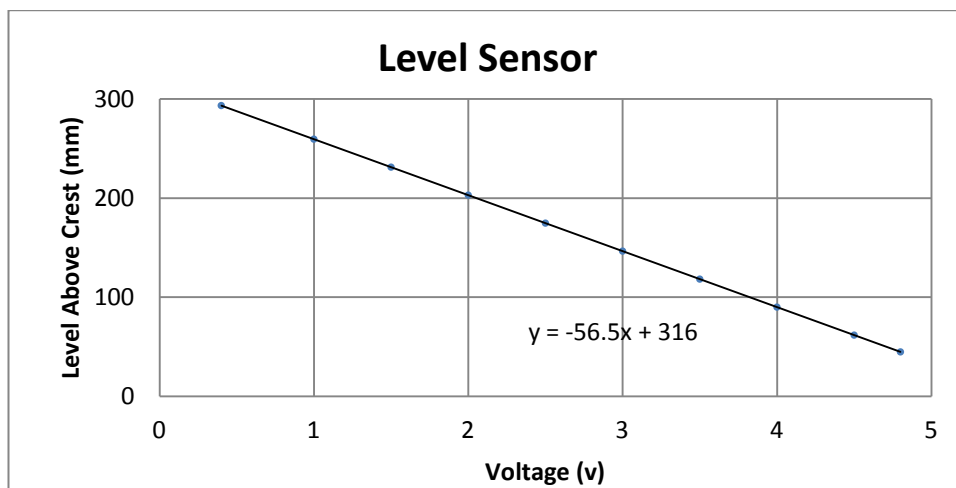


Figure 5.12 Calibration of water level in Labview.

5.2 Site Pipe Rig

A Site pipe rig was installed at Hydro Tasmania's Tarraleah Power Scheme Pond No.1 to grow flow conditioned biofilms. A pump was used to propel water from the pond through the test section pipe at a mean velocity of 1.3 m/s to allow biofouling to grow inside the pipe. A photo of the site pipe rig is shown in Figure 5.13. Details of Pond No.1 can be found in Chapter 3.

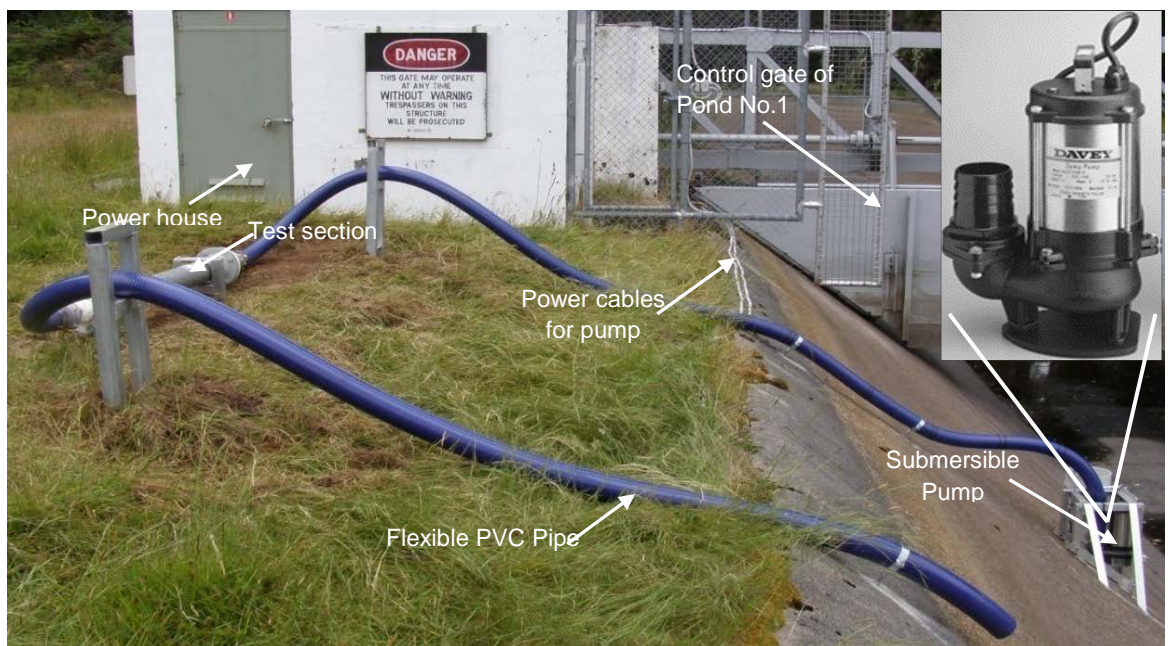


Figure 5.13 The Site pipe rig taken during the outage of Tarraleah Power Scheme.

5.2.1 Site Pipe Rig Design

The Site pipe rig is composed of a submersible pump, a steel test section pipe, flexible PVC pipes and flanges, as shown in Figure 5.13.

Submersible pump

A D150V submersible pump manufactured by Davey Water Products Pty. Ltd. was selected to propel water for the Site pipe rig. Driven by a single phase, two pole 220-240 V motor; it was installed in Pond No.1 before the control gate of Tarraleah Power Scheme in Hydro Tasmania Australia. It is shown in Figure 5.13. The performance of the D150V is shown in Appendix C.6.

Test section

The removable test section of the Site pipe rig is identical that in the Lab pipe rig. A test had been run continuously for thirteen months to allow biofouling to grow inside the pipe before the test section was transported back to the Hydraulics laboratory for measurement of head loss and velocity profile.

Flexible PVC pipes

Two flexible PVC pipes were used to connect the submersible pump and the test section and to discharge water back into Pond No.1.

Both flexible pipes were raised up higher than the test section pipe at the positions of the pipe holder 1 and pipe holder 4. With a height of 500mm, these were higher than pipe holders 2 and 3 at 300mm, as shown in Figure 5.14. The different pipe holder elevations ensured that the test section pipe was always filled with water when the pump was powered off or the water level of Pond No.1 dropped below the position of the pump.

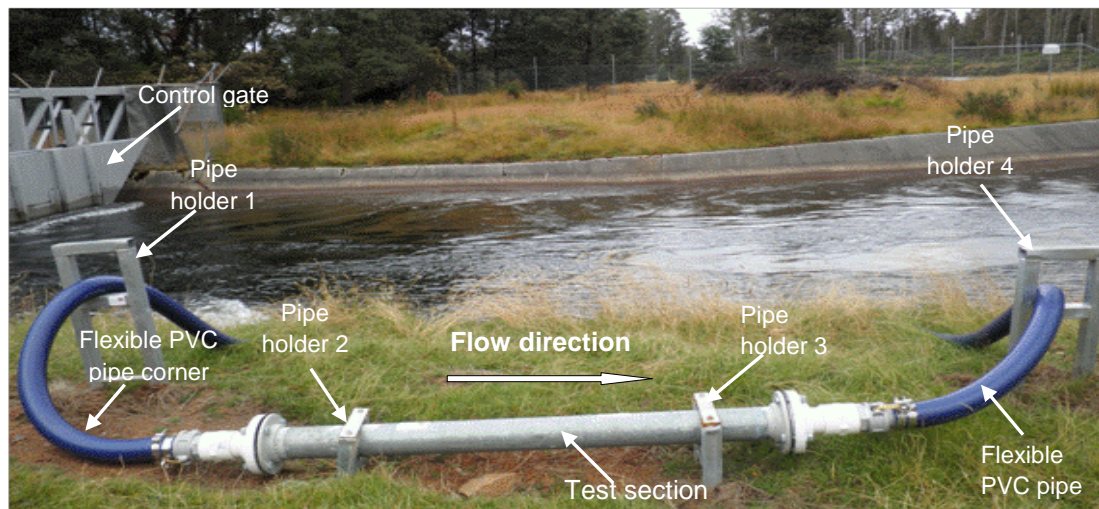


Figure 5.14 Test section of the Site pipe rig.

5.2.2 Flow Velocity of Site Pipe Rig

The submersible pump for the Site pipe rig operated at a flow rate of 620 L/min with a head of 2.2 m, as shown in Figure 5.15. The mean velocity in the test section was approximately 1.3 m/s; thus, the growth of biofouling was considered to be conditioned to a mean velocity of 1.3 m/s. Detailed calculations of the Site pipe rig are shown in Table 5.7.

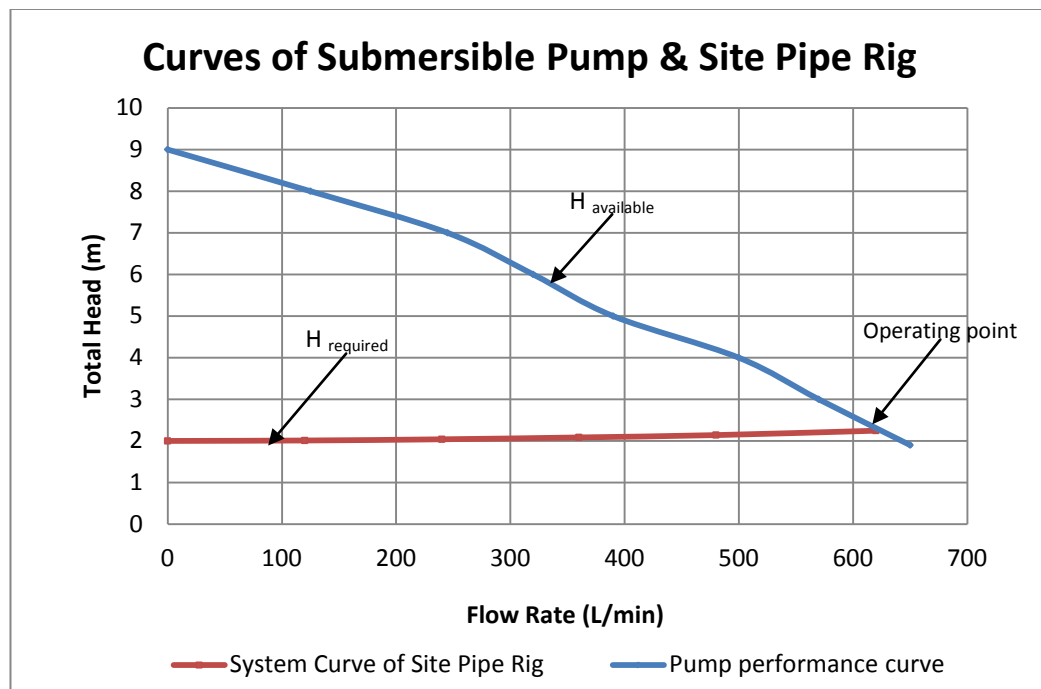


Figure 5.15 Submersible pump performance curve and system curve of the Site pipe rig.

Flow Rate (L/min)	Q (m ³ /s)	Average velocity U (m/s)	Relative roughness k_s/D	Re ($\times 10^4$)	Density ρ (kg/m ³) @ 10 ⁰ C	Kinematic viscosity @ 10 ⁰ C (ν) $\times 10^{-6}$ (m ² /s)	Length (m)	Friction factor f	Wall shear stress τ_w (kg/ms ²)	Shear velocity u_* (m/s)	Major head loss H_f (m)	Minor loss (m)	Dynamic pressure $U^2/2g$ (m)	Total Head (m)
120	0.002	0.255	0.00015	1.95	999.7	1.307	5	0.0270	0.22	0.015	0.004	0.003	0.003	2.011
240	0.004	0.509	0.00015	3.90	999.7	1.307	5	0.0220	0.71	0.027	0.015	0.012	0.013	2.040
360	0.006	0.764	0.00015	5.85	999.7	1.307	5	0.0190	1.39	0.037	0.028	0.027	0.03	2.085
480	0.008	1.019	0.00015	7.79	999.7	1.307	5	0.0153	1.98	0.045	0.040	0.049	0.053	2.142
620	0.0103	1.316	0.00015	10.07	999.7	1.307	5	0.0180	3.89	0.062	0.079	0.081	0.088	2.249

Table 5.7 Total head loss of the clean Site pipe rig at different flow rates.

5.3 Chapter Summary

A new pipe rig was designed to investigate the impact of biofouling in pipes at the School of Engineering in the University of Tasmania. This was designed for the study of velocity profiles of biofouled and clean pipes. The relationship between the Reynolds number and the friction factor of the biofouled pipe was compared to that of the clean pipe. The Reynolds numbers in this study (ranging from 9.15×10^4 to 3.92×10^5) were representative of those in many industrial pipe flows, and numbers were between those studied by previous researchers (Barton et al., 2008; Lambert et al., 2009).

The maximum mean velocity of the test section of the Lab pipe rig was designed to be 6 m/s with a flow rate of 47.9 L/s. The biofouling in the test section of the Site pipe rig was developed under a mean velocity of 1.3 m/s, and the Reynolds number (Re) for the growth of biofouling was 10×10^4 .

Chapter 6 Measurement of Velocity Profiles and Head Loss

This chapter describes the experimental measurement of the velocity profiles and head loss in biofouled and clean pipes of the Lab pipe rig. It includes detailed data analysis of friction factor and Reynolds number and the modification of the Von Karman constant k and wall constant B for a biofouled pipe. The velocity profiles of the biofouled pipe are measured and compared with those of a clean pipe and those expected for rough pipes.

6.1 Measurement of Equipment and Methods

The site pipe rig was installed at Pond No.1 on the 4th January 2011 during an outage of the Tarraleah Power Scheme, although the submersible pump was turned on in March of 2011. The test section was allowed to foul over a period of 13 months from the 22nd of March 2011 to the 27th of April 2012.

During this period, an outage occurred between the 12th and 27th of January 2012 by Hydro Tasmania. However, water remained in the test section to keep the biofouling wet during the outage due to the elevated pipe holders described in Chapter 5. The water level of Pond No.1 during the fouling period is shown in Figure 6.1.

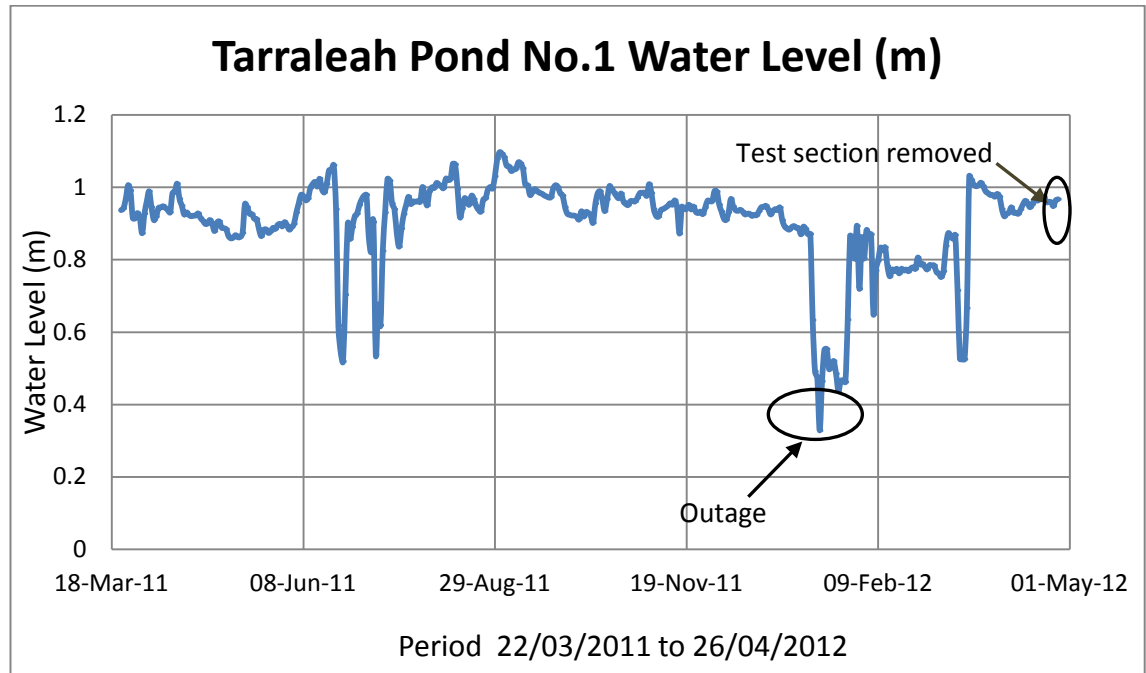


Figure 6.1 Water level of Pond No.1 during the pipe rig experiment.

A visual inspection of the biofouled test section revealed that most of the area inside the test pipe was covered by a very thin layer of dark brown, smooth slime. It was similar to the biofouling in cooling

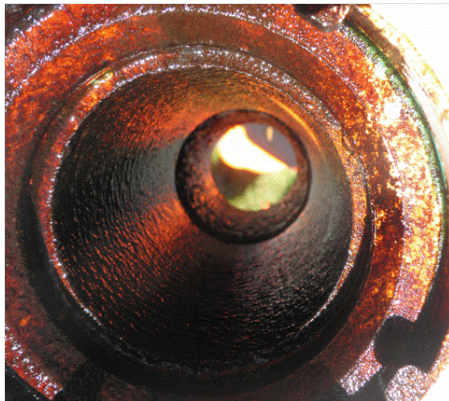


Figure 6.2 Biofouling in pipe.

pipes of the power station in Hydro Tasmania described in Chapter 4. This biofouling was thinner than that found in penstocks by Barton (2007a) and Tyler (1968). It was difficult to conduct close examination or take photos inside the pipe due to its small diameter. Figure 6.2 shows a photo of biofouling in the pipe taken from the upstream white coloured PVC connector of the test section.

After the visual inspection on site, the biofouled test section was filled with water, sealed with blank flanges and transferred back to the Hydraulics laboratory at the School of Engineering of UTAS. Static ring tapplings were built for the biofouled test section on the 27th of April 2012.

Similar procedures for measuring the boundary layer of the water tunnel (Andrewartha, 2010b) were used for the measurement of biofouled plates. The measured parameters include the head loss, the mean velocity, velocity profiles of the test section and the water temperature. Other parameters, such as the flow rate (Q), Reynolds number (Re), friction factor (f), wall shear stress (τ_w) and friction velocity (u_*) were calculated based on the above measurements.

Equations 5.3 in Chapter 5 and 2.1, 2.6 and 2.5 in Chapter 2 were used to calculate mean velocity (U), Reynolds number, wall shear stress and the friction velocity.

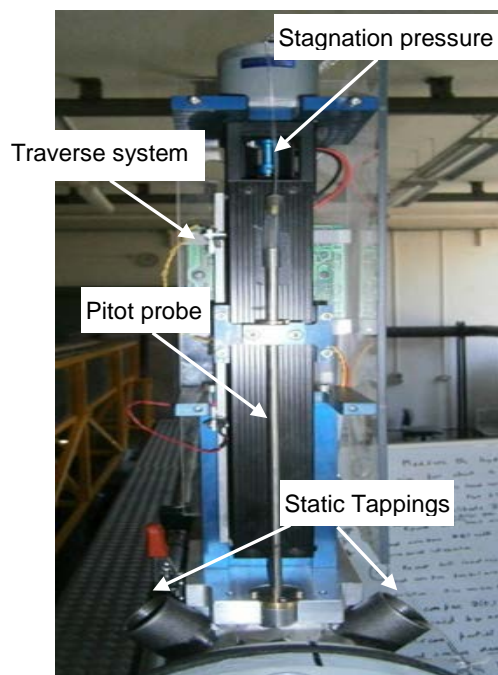


Figure 6.3 Pitot probe and static wall tapplings.

The pressure differentials (head loss H_f) across the upstream clean reference and test sections were measured using Validyne pressure transducers connected to static wall tapplings. The mean velocity of the test section was measured with the YOKOGAWA flow metre. The velocity profile was measured by the Pitot probe with static wall tapplings, as shown in Figure 6.3. Water temperatures (T) were also measured during testing.

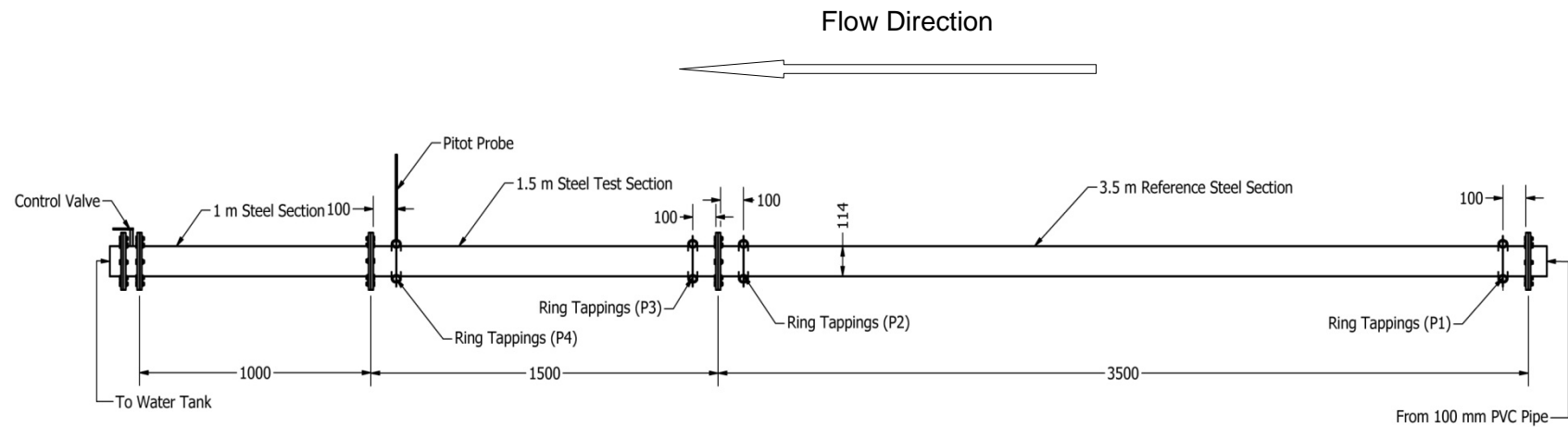


Figure 6.4 Measurement points of static wall tappings and Pitot probe.

The first set of static wall tapings was used to measure the pressure drop between point P_1 and P_2 for the steel pipe 3.5 m in length, as shown in Figure 6.4. This acted as a reference for the measurement of clean and biofouled test sections under different flow rates.

The second set of static wall tapings was used to measure the pressure drop along the 1.5 m steel test section for clean or fouled pipes. The pressure drop between points P_3 and P_4 , as shown in Figure 6.4, displayed the head loss along the test section under a certain flow rate. The friction factor of the biofouled pipe was calculated by Equation 2.7.

The static wall tapping at point P_4 and the Pitot probe were used to calculate the velocity profile (u) by Equation 2.13. The Pitot probe had a 20mm long tip with a 1mm diameter, and a 400 mm long stem with a diameter of 6.5 mm.

6.2 Head loss of Biofouled and Clean Reference Pipes

Tests were conducted for biofouled and clean reference pipes from the 30th of April to the 2nd of May 2012. The flow parameters of the biofouled test section and the reference pipe were measured under different flow rates. Reynolds numbers between 9.3×10^4 and 4.0×10^5 were obtained, corresponding to mean velocities of 1.0 m/s and 4.5 m/s respectively. When the biofouled test section was removed from the rig after testing on the 7th of May, it was found that some of the biofouling remained in the test section, as shown in Figure 6.5.



Figure 6.5 Fouled test section after testing at maximum speed.

The test section and the reference pipe were painted with the same epoxy coating using the same cleaning and painting procedures. Hence, the smoothness between the test section and the reference pipe was very similar. In this study, the smoothness of the clean test section was assumed to be the same as that of the upstream reference section pipe.

6.2.1 Flow Rate Measurement

Flow rates were calculated using Equation 5.4 for the V-notch, and the mean velocity was calculated using Equation 5.3. Results from the V-notch were higher than the velocity measured by the YOKOGAWA flow metre with an error of less than 4.5 %, as shown in Table 6.1.

Test	1	2	3	4	5	6	7	8
U_YOKOGAWA (m/s)	1.05	1.54	2.02	2.51	3.01	3.48	4.02	4.54
U_V-notch (m/s)	1.08	1.61	2.11	2.59	3.12	3.52	4.07	4.61
Difference (m/s)	0.02	0.07	0.09	0.08	0.11	0.04	0.05	0.07
Percentage (%)	2.05	4.42	4.49	3.09	3.77	1.29	1.17	1.64

Table 6.1 Mean velocity was measured by YOKOGAWA and V-notch.

6.2.2 Head Loss Measurement

Head loss across the biofouled test section and the clean reference section were measured by static wall tapings, as shown in Figure 6.4. The head losses and friction factors between the two pipes were compared, displayed in Table 6.2.

It can be seen from Table 6.2 that the head loss ratio of the biofouled test section to the clean reference section was at least 1.25 per metre of pipe length. The maximum difference of the head loss between the two pipes occurred at a mean velocity of 1.77 m/s, where the head loss of the biofouled test section was 1.69 times that of the clean reference section. The head loss is far higher than previously measured results for fouled pipes (Barton et al., 2008). Barton et al. (2008) found a 25% improvement in head loss over the biofouled pipe conditions after the cleaning of the pipe.

U (m/s)	Re	Head loss (mm)		Friction factor f		Head loss per metre (mm/m)		Head loss difference per metre (Fouled/Clean)
		Fouled (1.5 m)	Clean (3.5 m)	Fouled (1.5 m)	Clean (3.5 m)	Fouled (1.5 m)	Clean (3.5 m)	
1.05	93247	22	41	0.0301	0.0210	16.75	12.39	1.35
1.27	112142	32	57	0.0305	0.0211	24.53	17.23	1.42
1.51	133751	45	78	0.0305	0.0206	34.94	23.60	1.48
1.77	156681	67	100	0.0327	0.0193	51.29	30.28	1.69
2.02	178708	78	126	0.0293	0.0187	59.83	38.26	1.56
2.27	200624	95	156	0.0284	0.0184	73.13	47.36	1.54
2.51	221550	112	188	0.0275	0.0181	86.45	56.92	1.52
2.75	242969	127	223	0.0259	0.0179	97.78	67.44	1.45
3.01	266264	143	264	0.0243	0.0176	110.00	79.85	1.38
3.25	287623	163	305	0.0237	0.0175	125.30	92.51	1.35
3.49	308769	182	349	0.0230	0.0174	140.12	105.90	1.32
3.74	330405	205	399	0.0225	0.0173	157.32	120.79	1.30
3.99	352478	226	451	0.0219	0.0172	173.69	136.73	1.27
4.27	377156	254	515	0.0215	0.0172	195.39	156.10	1.25
4.52	399583	282	574	0.0213	0.0170	217.23	173.85	1.25

Table 6.2 Head loss of pipes under different flow rates.

6.2.3 Moody Diagram

Reynolds numbers in Table 6.2 are plotted against the friction factors for the biofouled test section and the reference section in the Moody diagram as shown in Figure 6.6.

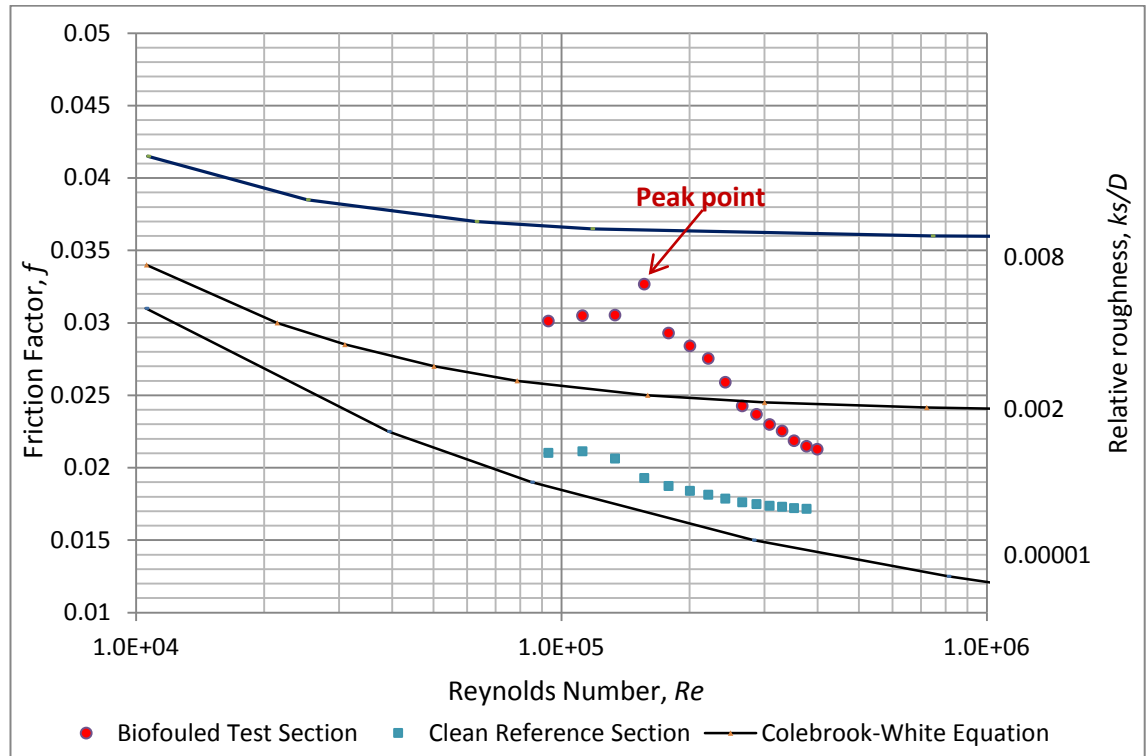


Figure 6.6 Colebrook-White curves with observed data of fouled test section and reference pipe.

It was found that the relationship between the Reynolds number and the friction factor of the fouled pipe does not follow the widely used Colebrook-White equation (Equation 2.3) from Moody (1944).

For the biofouled test section, it was found that the Darcy-Weisbach friction factor increased with the increase of the Reynolds number, reaching the peak point at the mean velocity of 1.77 m/s ($f = 0.033$ and $Re = 1.56 \times 10^5$, as shown in Table 6.2). The friction factor started to decrease with the increase of the Reynolds number when the mean velocity was higher than 1.77 m/s. The rate of decrease was higher than that of a typical rough pipe curve (Colebrook-White equation) as shown in Figure 6.6.

The sequence of tests was from low to high velocity, and it is likely that at a velocity of 1.77 m/s, the biofilm started to detach and the pipe wall became smoother. This hypothesis is supported by comparing photographs of the biofouling in the pipe pre- and post-testing. Figure 6.5 shows that a significant amount of biofouling was sheared off during testing compared to the pre-testing photo in Figure 6.2. The increase in friction factor with Reynolds number before the

biofouling started detaching may be due to the visco-elastic character of the biofilm and the motion of the biofilm under flow conditions.

For the clean reference section, the friction factor decreased with an increase in the Reynolds number as expected, as shown in Figure 6.6.

This different relationship between friction factor and Reynolds number for biofouled pipes was observed by Barton (2008) and Lambert (2009). Barton (2008) found that the friction factor increased with an increase of the Reynolds number in both the Wilmot penstock and the Tarraleah No.1 Hilltop pipeline. Lambert (2009) also showed that the friction factor initially increased with an increasing Reynolds number. For Lambert's cases 1 and 2, the friction factor reached a peak value and then decreased with further increases in Reynolds number. This was attributed to detachment of the biofilm (Lambert, 2009). No such detachment was reported for cases 3 and 4, which saw no reduction in f with increasing Re .

The results are plotted in Figure 6.7 together with those studied by Barton (2008) and Lambert (2009). It can be seen from Figure 6.7 that the Reynolds numbers in this study are between those reported by Barton (2008) and Lambert (2009), and extend the body of research to cover Reynolds numbers found in many industrial pipe flows. The biofouled pipe data in the present study followed a similar trend, with an initial increase in friction factor (f) with Reynolds number (Re), followed by a reduction in the friction factor, likely due to the fouling detachment.

6.2.4 Roughness Height of Biofilms in Biofouled Pipe

A variable roughness height of biofilms (k_s) at different velocities was reported by Barton et al. (2008) in the penstocks and pipelines of Hydro Tasmania. Similar findings were derived by Andrewartha (2010b) on biofouled plates and Lambert et al. (2009) in pipes. The variable roughness height versus the flow rate or velocity reported by Barton et al. (2008) and by Andrewartha (2010b) are summarised in Tables 6.3 and 6.4 respectively.

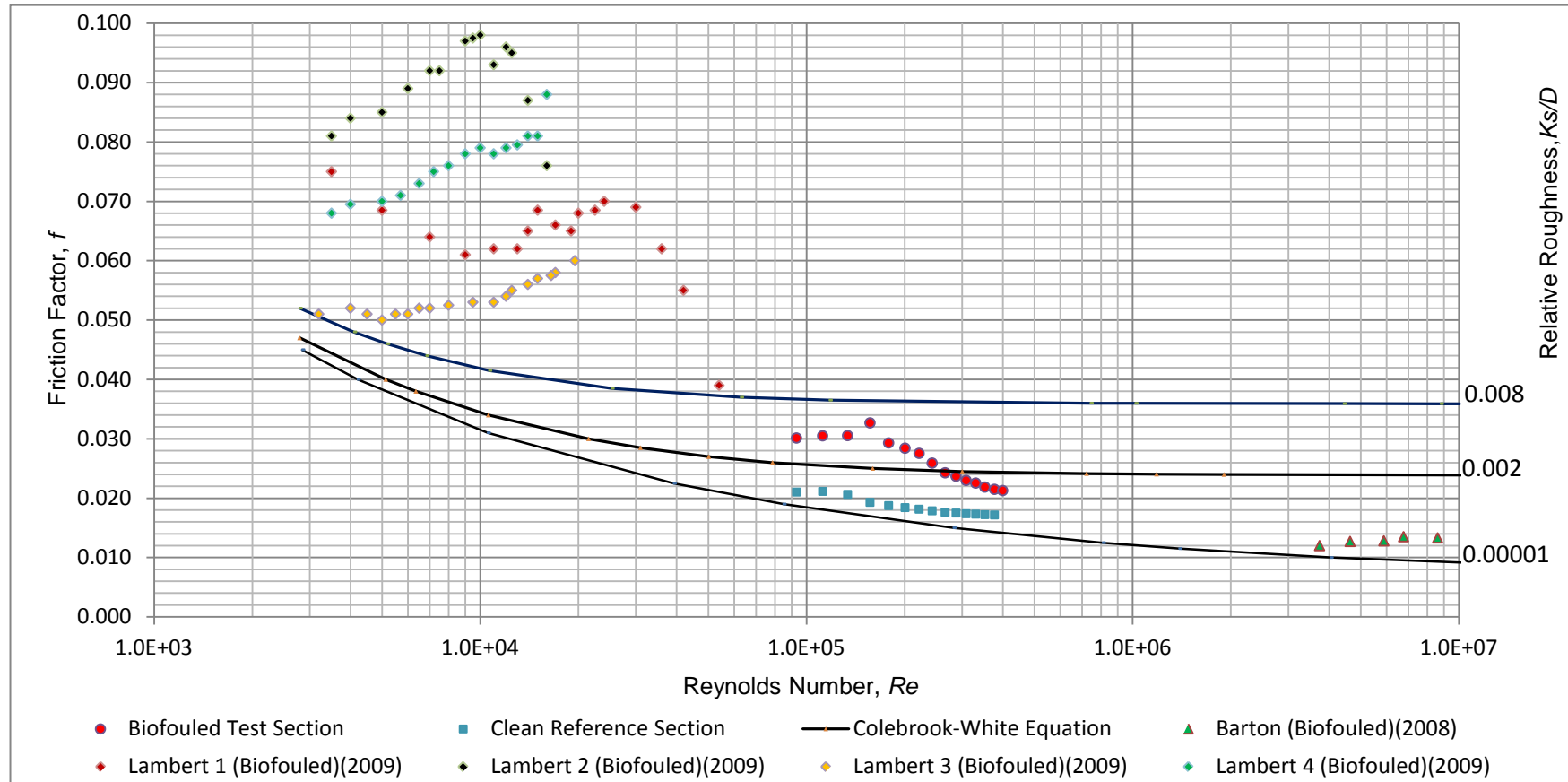


Figure 6.7 Comparison of results from this study and previous researchers (Barton et al., 2008; Lambert et al., 2009).

Poatina			Tarraleah			Wilmot		
Flow rate (m ³ /s)	k_s (mm)	Re (X10 ⁶)	Flow rate (m ³ /s)	k_s (mm)	Re (X10 ⁶)	Flow rate (m ³ /s)	k_s (mm)	Re (X10 ⁶)
23.0	0.43	7.83	10.10	0.22	3.50	12.49	0.24	7.19
24.4	0.30	8.29	14.23	0.29	4.93	13.49	0.29	7.77
25.9	0.25	8.80	16.36	0.29	5.78	14.44	0.22	8.53
27.6	0.28	9.46	18.60	0.36	6.57	15.41	0.33	8.88
28.1	0.69	9.71	21.18	0.24	7.48			
35.4	0.49	12.2						

Table 6.3 Equivalent sand grain roughness of penstocks of Barton et al. (2008) (Bacterial biofilm).

Plates	K_s (mm) at the location of $X= 850$ mm			
	1.00 m/s	1.25 m/s	1.75 m/s	2.00 m/s
RP1 F1	5.18	4.61	5.37	5.53
SP1 F2	0.76	0.89	0.81	0.78
RP1 F4	3.31	3.14	3.47	3.47
RP2 F5	1.84	2.66	3.61	2.59

Table 6.4 Equivalent sand grain roughness of plates of Andrewartha (2010b) (Algal biofilm).

The velocity profiles were measured at the downstream end of the test section, as shown in Figure 6.4. The Reynolds number and the friction factors were calculated using Equations 2.1 and 2.7 respectively after the mean velocity and the head loss across the biofouled test section were measured.

The wall shear stress, the shear velocity and the equivalent sand grain roughness were calculated using Equations 2.6, 2.5 and 6.1 respectively after the Reynolds number and friction factor were calculated, as shown in Table 6.2. The results of the biofouled test section are listed in Table 6.5. It can be seen that the wall shear stress and the shear velocity decrease with a decrease in the mean velocity.

$$k_s = 3.7D(\exp^{-\left(\frac{1.3254}{f}\right)^{0.5}} - \frac{2.51}{\text{Re}\sqrt{f}})$$

(Equation 6.1)

The equivalent sand grain roughness of the biofouled test section was not constant over the range of Reynolds numbers tested. Its value depended on the mean velocity. It increased with an increase of the mean velocity, peaking at 0.6 mm at a mean velocity of 1.77 m/s before starting to decrease. The variation in the roughness height of the biofilms may be due to the fact

that biofilms are flexible and have less rigidity than rough pipes. In addition, the lower k_s values may be caused by fouling being washed off at higher velocities. Therefore the roughness was not uniform under different flow conditions. Roughness (k_s) values at low mean velocities were comparable to Barton's results for Poatina penstocks. At higher mean velocities, k_s values were closer to those of Tarraleah and Wilmot penstocks (Barton et al., 2008).

U (m/s)	Re	k_s (mm)		k_s/D		Wall shear stress τ_w (kg/ms ²)	Wall Shear velocity u_* (m/s)
		Fouled	Clean	Fouled	Clean	Fouled	Fouled
1.05	93247	0.4240	0.0540	0.00416	0.00053	4.186	0.065
1.27	112142	0.4559	0.0690	0.00447	0.00068	6.129	0.078
1.51	133751	0.4671	0.0657	0.00458	0.00064	8.730	0.093
1.77	156681	0.6013	0.0436	0.00590	0.00043	12.817	0.113
2.02	178708	0.4122	0.0384	0.00404	0.00038	14.951	0.122
2.27	200624	0.3714	0.0366	0.00364	0.00036	18.273	0.135
2.51	221550	0.3331	0.0353	0.00327	0.00035	21.602	0.147
2.75	242969	0.2645	0.0337	0.00259	0.00033	24.432	0.156
3.01	266264	0.2045	0.0322	0.00200	0.00032	27.487	0.166
3.25	287623	0.1864	0.0323	0.00183	0.00032	31.310	0.177
3.49	308769	0.1653	0.0323	0.00162	0.00032	35.014	0.187
3.74	330405	0.1530	0.0328	0.00150	0.00032	39.312	0.198
3.99	352478	0.1348	0.0328	0.00132	0.00032	43.401	0.208
4.27	377156	0.1257	0.0335	0.00123	0.00033	48.824	0.221
4.52	399583	0.1213	0.0327	0.00119	0.00032	54.280	0.233

Table 6.5 Equivalent sand grain roughness, relative roughness, wall shear stress and wall shear velocity of biofouled test section.

6.3 Velocity Profiles of the Biofouled Pipe

During the test, the position of the Pitot probe was controlled by a linear actuator through a Labview program. The frequency of the data acquisition was 1 kHz with a measuring time of 20 seconds at each measuring point; i.e., around 20,000 data were acquired at each measurement point within the 20 seconds. The test was repeated three times at each flow velocity, and the average of data derived from the three tests was used to calculate the velocity profile.

The water temperature was measured by a temperature sensor located at the end of the rig. The average temperature under different flow rates was 15.5 °C during the testing.

6.3.1 Velocity Profiles of Biofouled Pipe

The theoretical biofouled pipe velocity profiles corresponding to the equivalent sand roughness in Table 6.5 were calculated using Equation 6.2.

$$\frac{u}{u_*} = \frac{1}{\kappa} \ln \frac{y}{k_s} + B \quad (\text{Equation 6.2})$$

where k_s is the variable equivalent sand grain roughness in Table 6.5 and $B=8.48$ for artificial rough pipes given by Nikuradse (1933).

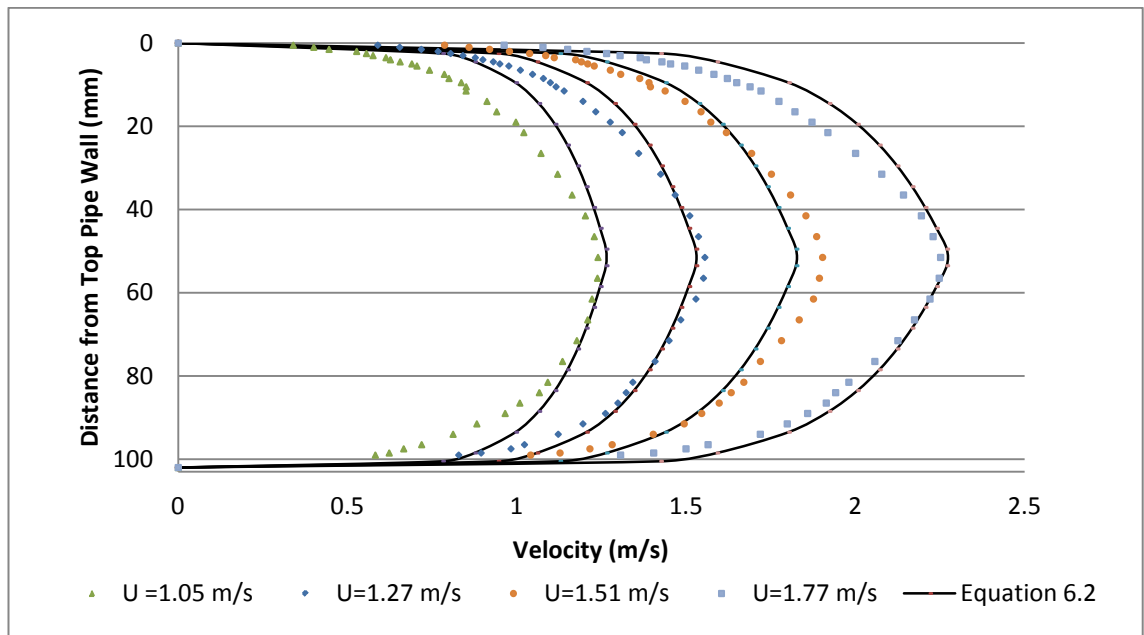


Figure 6.8 Measured and theoretical velocity profiles of biofouled test section at mean velocity of 1.05, 1.27, 1.51 and 1.77 m/s (corresponding to $Re = 93247, 112142, 133751$ and 156681), using k_s values from Table 6.5.

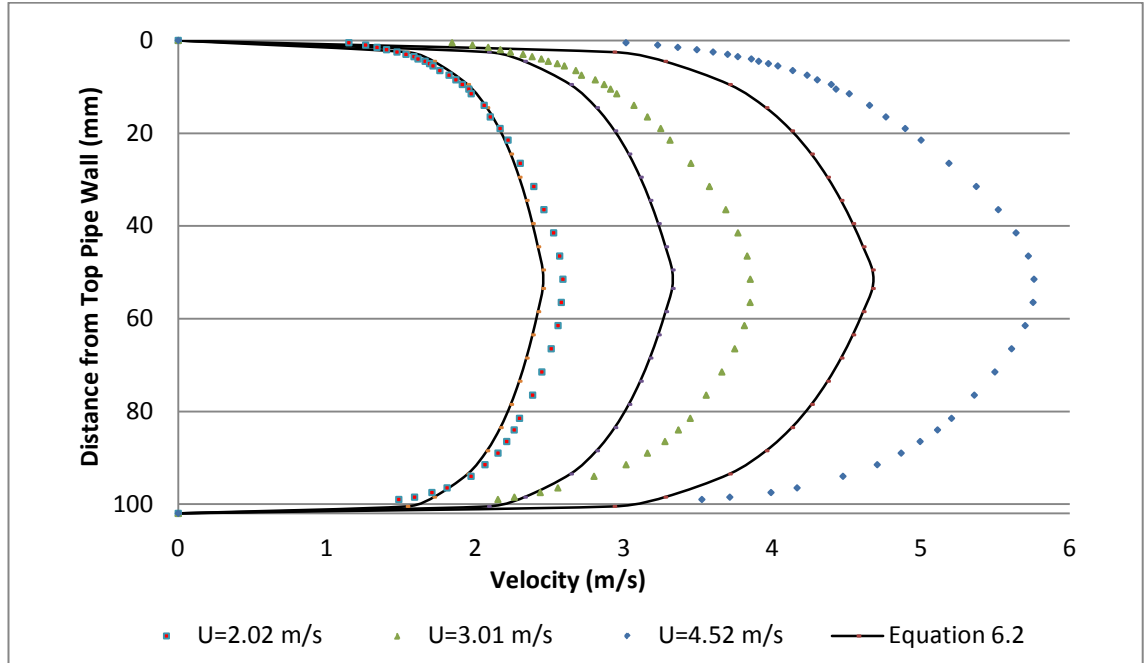


Figure 6.9 Measured and theoretical velocity profiles of biofouled test section at mean velocities of 2.02, 3.01 and 4.52 m/s (corresponding to $Re = 178708$, 266264 and 399583), using k_s values from Table 6.5.

The measured velocity profiles were plotted in Figures 6.8 and 6.9 together with the theoretical velocity profiles. It can be seen from Figure 6.8 that good agreement between the measured and theoretical velocities was achieved at the velocities of 1.27 and 1.77 m/s. At other velocities, the measured velocities were either lower or higher than the theoretical velocities along the centre line of the pipe. Therefore the theoretical velocity profiles of the typical rough pipe cannot be applied directly to biofouled pipes. The Von Karman constant κ (0.4) and the constant B (8.48) of the typical rough pipe in Equation 6.2 were not suitable for the biofouled pipe due to the variation in roughness height of the biofilms. Modification to these constants is required in order to match the theoretical velocities to the measured ones for the biofouled pipe.

Lambert et al. (2009) assumed a fixed roughness height of 1.725 mm and used a linear regression method to determine the Von Karman constant (κ) and constant B in 6.2 for a biofouled pipe with a diameter of 50 mm. The results are shown in Table 6.6.

Bulk velocity of profile (m/s)	κ	B
1.15	0.3569	12.25
0.89	0.3106	8.85
0.22	0.2821	9.60

Table 6.6 Modified values of κ and B obtained by Lambert et al. (2009).

To simplify the data analysis of the biofouled pipe with variable roughness heights, an average roughness height of 0.487 mm was assumed by using values in Table 6.5 at the velocities of 1.05, 1.27, 1.51 and 1.77 m/s, as all biofouling was still being attached at these velocities.

The same linear regression method was used in this study to determine κ and B constants as follows:

$$\text{let } y = \frac{u}{u_*} \quad \text{and} \quad x = \ln \frac{y}{k_s}$$

$$\text{then Equation 6.2 became: } y = mx + n$$

$$\text{where } m = \frac{1}{\kappa} \quad \text{and} \quad n = B$$

Through linear regression, the best fit slope (m) and y-intercept (n) were determined for each profile. The values of κ and B found for each flow are listed in Table 6.7.

It can be seen from Table 6.7 that the values of the Von Karman constant (κ) for biofouled pipes are lower than the widely accepted value of 0.4. It was found that the Von Karman constant κ increased with an increase in mean velocity, peaking when the velocity reached 1.77 m/s, then starting to decrease with increasing mean velocity due to part of the biofouling detaching and being washed away. It was also found that the constant B increased with increased mean velocity.

The modified theoretical velocity profiles were calculated using Equation 6.2 and the modified Von Karman constant κ and constant B listed in Table 6.7. The modified theoretical velocity profiles and the measured velocity profiles are plotted in Figures 6.10 and 6.11 for different mean velocities.

U (m/s)	Re	k	B
1.05	93247	0.2908	3.09
1.27	112142	0.3284	5.47
1.51	133751	0.3373	6.44
1.77	156681	0.3613	6.91
2.02	178708	0.3447	7.53
2.27	200624	0.3415	7.71
2.51	221550	0.3361	7.88
2.75	242969	0.3333	8.29
3.01	266264	0.3300	8.89
3.25	287623	0.3308	9.24
3.49	308769	0.3321	9.67
3.74	330405	0.3344	10.09
3.99	352478	0.3350	10.26
4.27	377156	0.3360	10.57
4.52	399583	0.3600	11.56

Table 6.7 Values of k and B for measured velocities at $k_s=0.487$ mm.

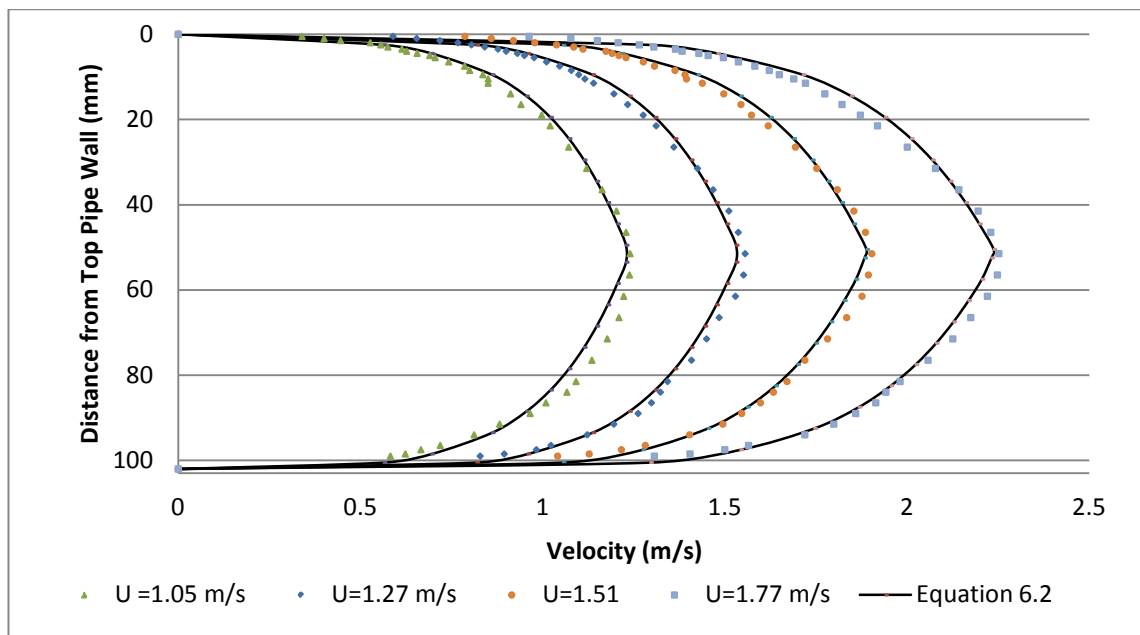


Figure 6.10 Measured and theoretical velocity profiles using k and B in Table 6.7 for velocities 1.05, 1.27, 1.51 and 1.77 m/s (corresponding to $Re = 93247, 112142, 133751$ and 156681).

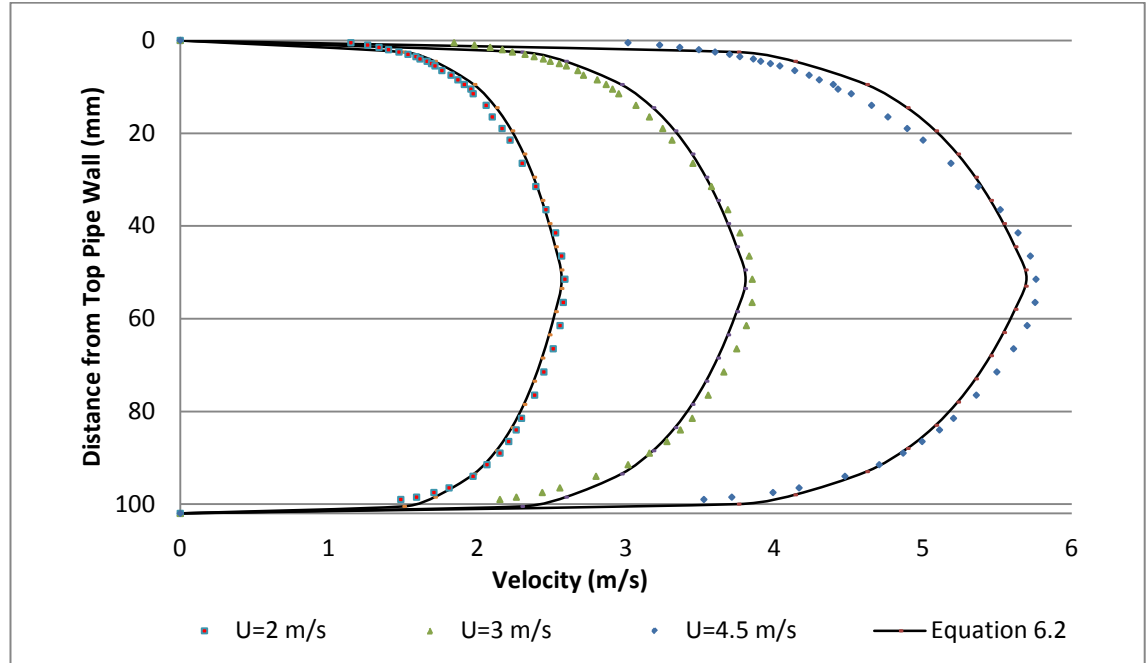


Figure 6.11 Measured and theoretical velocity profiles using κ and B in Table 6.7 for velocities 2.02, 3.01 and 4.52 m/s (corresponding to $Re = 178708$, 266264 and 399583).

It can be seen from Figures 6.10 and 6.11 that the modified theoretical velocity profiles using the linear regression method are well matched with the measured profiles.

6.3.2 Non-Dimensional Analysis

The velocity profiles were presented in non-dimensional form using the average velocity U and maximum velocity U_{max} in the biofouled test section. The velocity profiles at the mean velocities of 1.51, 1.77, 3.01 and 4.52 m/s are plotted in Figure 6.12 as $\frac{y}{D}$ versus $\frac{u}{U}$. It can be seen from Figures 6.12 that points consistently match up.

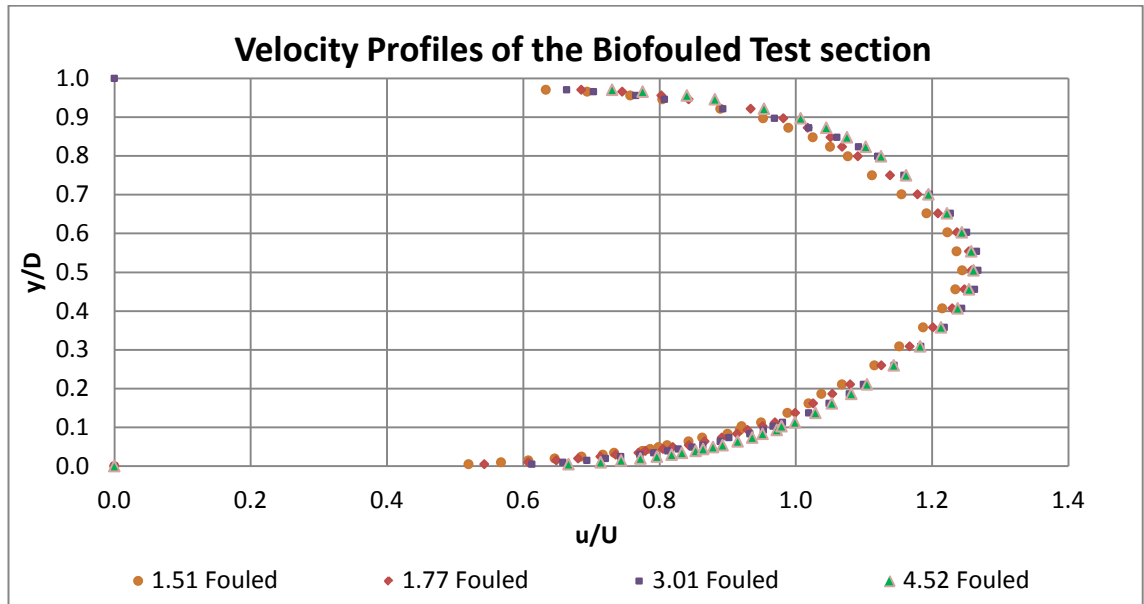


Figure 6.12 Velocity profiles of biofouled test section (u/U , non-dimensional analysis. Corresponding to $Re = 133751, 156681, 266264$ and 399583).

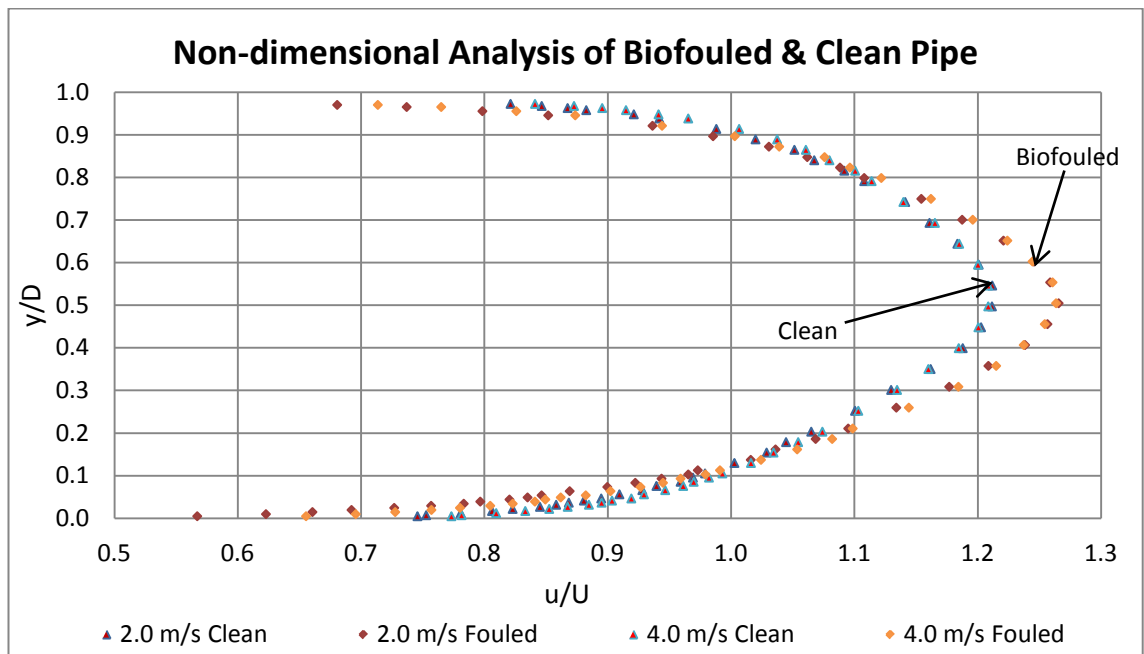


Figure 6.13 Velocity profiles of biofouled and clean pipes (non-dimensional analysis. Corresponding to $Re = 178708$ and 352478).

The non-dimensional velocity profiles of the biofouled test section and clean test section at mean velocities of 2.0 and 4.0 m/s are plotted as $\frac{y}{D}$ versus $\frac{u}{U}$ and $\frac{y}{D}$ versus $\frac{u}{U_{\max}}$ in

Figures 6.13 and 6.14 respectively. It can be seen in Figure 6.13 that the shape of the non-dimensional velocity profiles of the biofouled section differs from that of the clean pipe; i.e., the velocity is higher at the centreline and lower near the pipe wall in the biofouled test section than in the clean pipe. This difference in the shape of non-dimensional velocity profiles between the fouled and clean sections is consistent for different mean velocities.

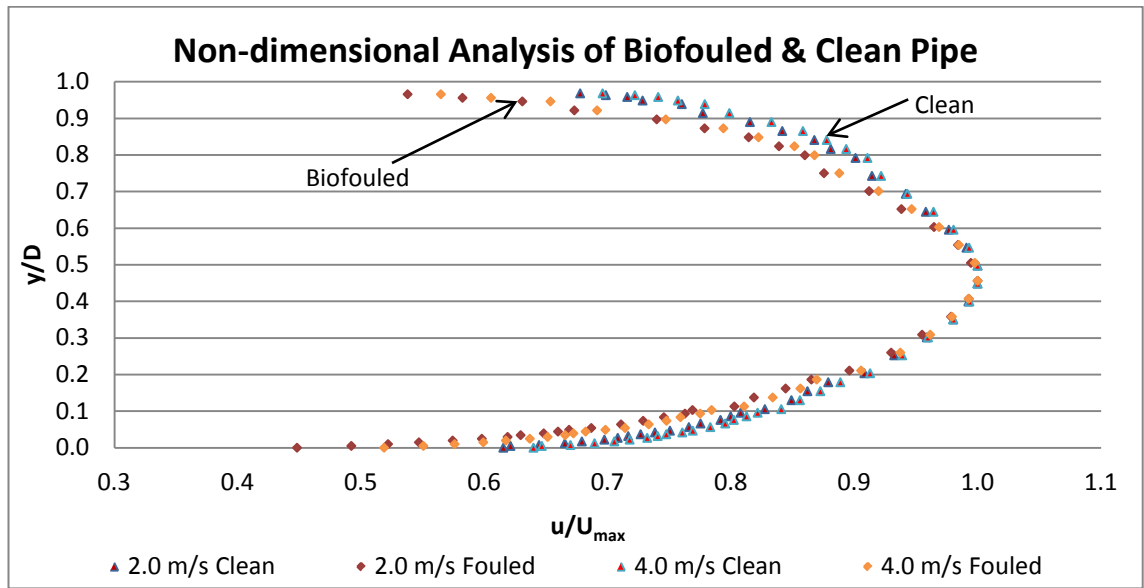


Figure 6.14 Velocity profiles of biofouled and clean pipes (non-dimensional analysis. Corresponding to $Re = 178708$ and 352478).

6.3.3 Modification of the Colebrook-White Equation

The modified Colebrook-White equation of Lambert et al. (2009) (Equation 2.9), was used to compare the measured data with the modified relationship of the Reynolds number and friction factor of the biofouled pipe.

$$\frac{1}{\sqrt{f}} = -\frac{1}{\sqrt{8\kappa}} \ln\left(\frac{k_s}{0.85D} + \frac{2.51}{Re\sqrt{f}}\right) \quad (\text{Equation 2.9})$$

The κ values calculated in Table 6.7 were expressed as a function of the Reynolds number. Linear regression was used to fit κ to the Reynolds number in Equation 2.9. The modified Colebrook-White equation (Equation 2.9) and the traditional Colebrook-White equation (Equation 2.3) curves were plotted in Figure 6.14, together with the measured data of the biofouled test section.

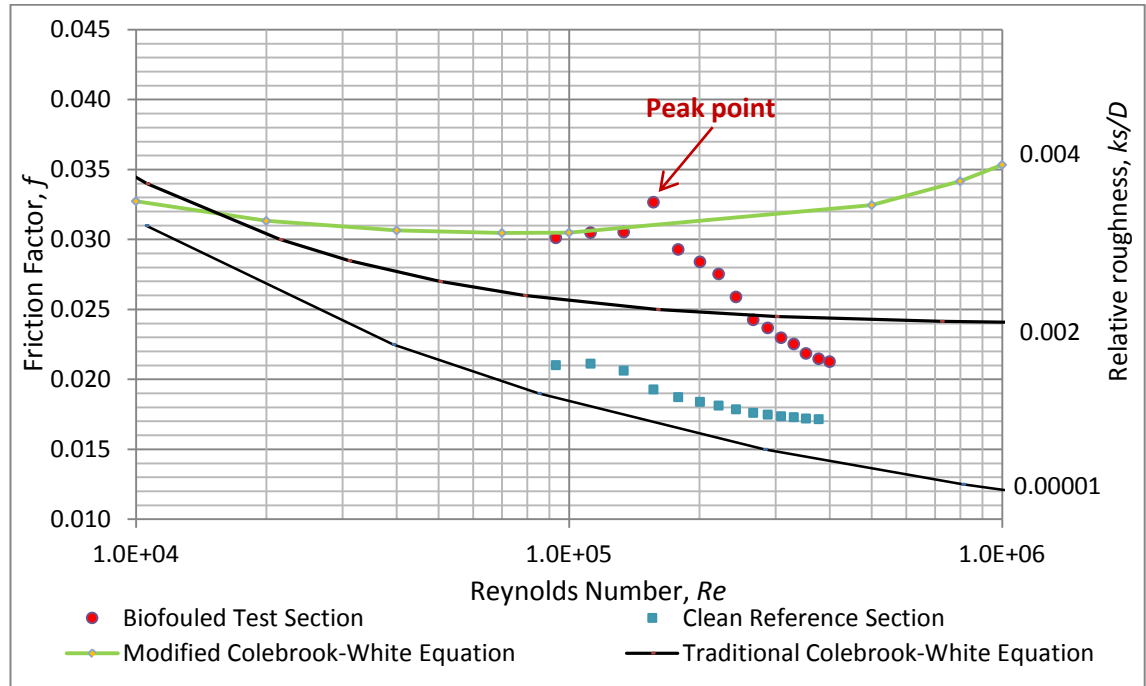


Figure 6.15 Modified Colebrook-White curve.

It can be seen from Figure 6.14 that the modified Colebrook-White curve matches the limited measured biofouling at low Reynolds number (Re) except for the peak point at the mean velocity of 1.77 m/s. Future studies are recommended to confirm this relationship. The modified Colebrook-White curve of Lambert et al. (2009) is quite useful for the biofouled pipe flow in this study.

6.4 Chapter Summary

Reynolds numbers between 9.15×10^4 and 3.92×10^5 were studied for the biofouled test section. Velocity profiles and head loss of the biofouled test section were measured, as was the head loss of the reference steel pipe located in the upstream of the test section.

The following conclusions on the impact of biofouling in pipes were drawn based on the measurements in this study:

- Biofouling in pipes results in significant head loss. This loss increased with the increase of Reynolds numbers until the mean velocity reached 1.77 m/s.
- The head loss ratio of the biofouled test section to the clean reference section was at least 1.25 per metre pipe length. The maximum ratio was up to 1.69 at the mean velocity of 1.77 m/s.
- The relationship between Reynolds number Re and friction factor f of the biofouled pipe does not agree with the Colebrook-White equation for turbulent flow in rough pipes.
- The equivalent roughness height of the biofouled pipe was not constant, as for an artificial rough pipe. This changed with the Reynolds number.
- The expected velocity profile of artificial rough pipe did not match the velocity distribution of the biofouled pipe.
- Modification of the Von Karman constant and constant B was found by linear regression. The Von Karman constant in the biofouled pipe was lower than 0.4 and the constant B increased with the increase of Reynolds numbers.
- The velocity profiles expected for rough pipe flows with modified constants agreed well with the measured profiles.
- The velocity profiles of the fouled test section under different flow rates were consistently matched up when non-dimensional analysis was conducted. The shape of the velocity profiles in the biofouled pipe differed from that of the clean pipe under the non-dimensional analysis.
- The measured data of the biofouled pipe fit well with the modified Colebrook-White equation suggested by Lambert et al. (2009). Further studies are recommended at different Re to confirm the modified Colebrook-White equation.

Chapter 7 Conclusions and Recommendations

This study conducted a range of experiments relating fresh water biofouling to flow in hydraulic conduits, aiming to investigate the effect of substratum colour and ambient light on fresh water biofouling and the impact of biofouling in pipes. It involved a field study, data analysis of water in lakes and the measurement of flow in biofouled pipes.

7.1 Effect of Substratum Colour and Ambient Light Conditions on Biofouling

The field study, reported in Chapter 3, demonstrated the effect of substratum colour and ambient light on the growth of biofouling in a Tasmanian hydropower canal.

The effect of colour on marine biofouling has been investigated over the last few decades (Dahlem et al., 1984; Shine et al., 2010; Su et al., 2007), and the effect of colour on fresh water biofouling was investigated in a slow flow river by Swain et al. (2006). It was found that acrylic plates with a white colour background had less fouling than those with a black background.

Two site trials under different flow conditions at different locations were conducted. Water temperature, total light and UV light were measured for slow flow (1 m/s) under full sunlight conditions. Water temperature and total light were also measured for fast (2 m/s) flow under partial sunlight conditions. Biofouling samples grown on different substratum colours were weighed in wet and dry conditions.

The following conclusions on the substratum colour and ambient light effects on fresh water biofouling were drawn, based on the measurements in this study:

- Black substrates attracted earlier settlement and faster growth rates of biofouling than grey or white substrates. The amount of biofouling increased progressively from the colours white, lightbox grey, blue grey to black at the settlement stage of biofouling. However, the effect of colour on the growth of biofouling became less significant as biofouling became fully developed, which supports the findings of Swain et al. (2006).

- Plates located at Pond No.1 received earlier and higher total light than those at Transition 4, since Transition 4 is partly shaded by trees and plates were located in deeper water at Transition 4.
- The amount of biofouling increased with depth under slow flow (1 m/s) and full sunlight conditions (Pond No.1), as demonstrated by the bottom panels (0.3 m under the water) attracted more fouling than top panels (0.15 m under the water). It was also found that the light intensity was higher at shallower depths, as the top plate received higher light intensity and longer total light than the bottom plate. This strongly supports findings by Andrewartha (2010b) and Barton (2007a) that shaded surfaces are better collectors of biofouling organisms than well illuminated substrates.
- The top plates received more UV (UVA+UVB) light than the bottom plates, and the top plates attracted less biofouling than the bottom plates under slow flow and full sunlight conditions (Pond No.1). This finding agrees with that reported by previous researchers Hung et al. (2005), Dobretsov et al. (2010), Li et al. (2005) and Perkins (2010a) regarding the impact of UV light on biofouling.
- In contrast, the amount of biofouling decreased with an increase in water depth under fast flow (2 m/s) and partially shaded conditions (Transition 4), as the bottom panels had less biofouling. The top plate received higher intensity and longer total light than the bottom plate. This may be due to the light intensity being too low for the growth of biofouling on the bottom plate. More tests are needed to further investigate this hypothesis.

7.2 Biofouling and Water Quality in Tasmanian Hydropower Schemes

Chapter 4 discussed the variability of water quality parameters in Tasmanian Hydropower Storages. The parameters of water temperature, pH value, conductivity, turbidity, nutrient concentration levels, metal content, oxygen concentration levels and organic material of water were studied.

Water data from eight Tasmanian lakes were extracted from TimeStudio database by Entura (former Hydro Tasmania Consulting). These included Great Lake, Lake Burbury, Lake Gairdner, Lake Gordon, Lake Mackintosh, Lake Parangana, Lake Pieman and Lake Rosebery.

The statistics program 'R' was used in this analysis. The XY plot and boxplot methods were selected to analyse water parameters. The following observations and conclusions were drawn from the analysis based on the available data:

1. The water temperature in lakes decreases with depth. This result is similar to that reported by Tyler (1968) for Lake St. Clair and Lake King William.
2. High values of iron and manganese were found in black brown coloured slime biofouling in cooling pipes of Wilmot Power Station. The amount of iron and manganese in power station cooling pipes was close to that of penstocks and pipelines found by previous researchers (Barton, 2007a; Tyler, 1968). The source water of conduits with reported fouling problems had higher levels of manganese and iron than source water for a system with no reported fouling problems.
3. No biofouling problem was reported in the downstream cooling pipes of Great Lake. There does not appear to be an immediately obvious connection to particular parameters, but this may be due to differences found in the following parameters in this analysis:
 - The pH value and dissolved oxygen are higher in Great Lake than in all other lakes at depths greater than 5 metres.
 - The water conductivity and turbidity are lower in Great Lake than in all other lakes at depths greater than 5 metres.
 - The amounts of iron, manganese and aluminium are lower in Great Lake. Tyler (1968) also reported that Great Lake water contained low iron and manganese.
 - A lower nutrient level in Great Lake was found for the growth of bacteria and algae such as dissolved organic carbon, kjeldahl nitrogen and nitrate.

The effect of the above parameters on biofouling will depend on the nature of the organisms responsible for fouling. This is likely to vary between sites and as local conditions change. While no definitive connection can be made between water quality and biofouling, this analysis makes

a useful contribution in presenting how water varies in Tasmanian Hydropower Storages. Further research on the biological process of biofouling is required.

4. The surface water quality data of Lake Parangana (reported fouling problem) is very similar to Great Lake data (no reported biofouling problem). However, the pH and dissolved oxygen of Great Lake are higher than that of Lake Parangana; the turbidity and conductivity of Great Lake are lower than that of Lake Parangana at depths greater than 5 m.

7.3 The Impact of Biofouling in Pipes

The impact of biofouling in pipes was discussed in Chapters 5 and 6. A purpose built pipe rig was designed and constructed to investigate the impact of biofouling in pipes.

7.3.1 New Pipe Rig Design and Calibration

Dimensional analysis and the similarity method were reviewed in the design of the Lab pipe rig. Head loss and velocity profiles were measured by using a smooth pipe with internally coated epoxy Interzone 954. The measurements showed that flow conditions matched the design values and displayed expected flow velocity distributions in the test section.

A new pipe rig with removable test section was built in the Hydraulics laboratory at the School of Engineering of the University of Tasmania. The removable test section was placed in a purpose built site test rig installed in a hydroelectric power station canal.

It was found that the purpose built pipe rig is a reliable instrument to measure the skin friction of biofouled pipes. From these measurements, a hydraulic roughness could be obtained for comparison with that of unfouled rough pipes.

7.3.2 Biofouling of the Test Section

The Reynolds numbers in this study, ranging from 9.15×10^4 to 3.92×10^5 , represent many industrial pipe flows. These numbers lie between those studied by previous researchers (Barton et al., 2008; Lambert et al., 2009). The pressure drop across the test section and the reference

steel clean pipe under different flow rates was measured with pressure transducers during testing. Velocity profiles were also measured by a Pitot probe at the downstream of the test section.

The following conclusions on the impact of biofouling in pipes were drawn, based on the measurements in this study:

- Biofouling in pipes results in significant head loss. This loss increased with the increase of Reynolds numbers until the mean velocity reached 1.77 m/s. The head loss ratio of the biofouled test section to the clean reference section was at least 1.25 per metre pipe length. The maximum ratio was up to 1.69 at the mean velocity of 1.77 m/s.
- The relationship between Reynolds number Re and friction factor f of the biofouled pipe does not agree with the Colebrook-White equation and Moody Diagram. The equivalent roughness height of the biofouled pipe was not constant, as for a typical rough pipe, changing with Reynolds number. These findings support those by Lambert et al. (2009) for lower Reynolds numbers and Barton et al. (2008) for higher Reynolds numbers.
- The theoretical velocity profile for an artificial rough pipe did not match the velocity distribution of the biofouled pipe. Modification of the Von Karman constant and constant B was conducted using the linear regression method. It was found that the Von Karman constant in the biofouled pipe was lower than the widely accepted value of 0.4. This was also reported by Lambert et al. (2009). The modified Von Karman constant κ increased with an increase in the mean velocity and peaked when velocity reached 1.77 m/s, starting to decrease with increasing mean velocity due to part of the biofouling detaching and being washed away. It was also found that the constant B increased with an increase of Reynolds numbers. The theoretical velocity profiles modified by the linear regression method were well matched with the measured profiles.
- The velocity profiles of the biofouled test section under different flow rates collapsed well when non-dimensional analysis was conducted. The shape of the velocity profiles in the biofouled pipe differed from that of the clean pipe under the non-dimensional analysis.

- The measured Reynolds numbers and friction factors of the biofouled pipe were well matched to the modified values based on the Colebrook-White equation of Lambert et al. (2009) in the Moody diagram.

7.4 Recommendations

The following recommendations are made for future studies.

7.4.1 Effect of Substratum Colour and Ambient Light conditions on Biofouling

It is suggested that another UV be purchased to measure UV light on the top and bottom plates simultaneously. Synchronised results measured by dual channels of the PMA2100 will be more accurate regarding the impact of UV light on the growth of biofouling on the top and bottom plates.

7.4.2 Biofouling and Water Quality in Tasmanian Hydropower Schemes

Further studies of the ecology of biofouling causing organisms are required to definitively link particular water properties to biofouling behaviour.

As mentioned in section 4.2.2.2 of Chapter 4, iron and manganese are likely to be the key factors affecting the growth of biofouling. However, only water data at depths less than 5 metres were available for analysis in this study. It is recommended that iron and manganese data be obtained at the intake level of lakes for further investigation.

The impact of aluminium has also been identified as potentially important to fouling growth, and more data is needed from different depths.

7.4.3 The Impact of Biofouling in Pipes

Further studies are required to investigate the possibility of using faster flows to detach biofilms as this study showed that they begin to detach at a particular Reynolds number.

More extensive data of biofouling in pipes are required to further verify the friction-flow relationship and the effect of scaling of equivalent roughness height in biofouled pipes.

The Reynolds numbers used in the laboratory experiments ranged from 93247 to 399583, and that used during the biofouling growth was 100700. It is recommended that in future experiments, biofilms should be grown at the highest Re at which they will be tested.

References

- Allen, J. J., Shockling, M. A., Kunkel, G. J., & Smits, A. J. (2007). Turbulent flow in smooth and rough pipes. *Philosophical Transactions of the Royal Society, Vol. 365*, pp. 699-714.
- Andrewartha, J., Perkins, K., Sargison, J., Osborn, J., Walker, G., Henderson, A., & Hallegraeff, G. (2010). Drag force and surface roughness measurements on freshwater biofouled surfaces. *Biofouling, 26*(4), 487-496.
- Andrewartha, J. M. (2010b). The Effect of Freshwater Biofilms on Turbulent Boundary Layers and the Implications for Hydropower Canals *PhD Thesis, School of Engineering, University of Tasmania*.
- Andrewartha, J. M., & Perkins, K. J. (2009). *Test Plates Trials - An Investigation of Biofilm Growth on Various Substrates Based on Upgrade Options for Hydroelectric Canals*.
- Andrewartha, J. M., Sargison, J. E., & Perkins, K. J. (2007). *The Effect of Gomphonema and Filamentous Algae Streamers on Hydroelectric Canal Capacity and Turbulent Boundary Layer Structure*. Paper presented at the 16th Australasian Fluid Mechanics Conference.
- Barton, A. F. (2003). Wilmot Power Station Penstock Cleaning and Power Conduit Headloss Estimation. *Report for Hydro Tasmania, 1-32*.
- Barton, A. F. (2004). Poatina Power Scheme Penstock Cleaning and Headloss Estimation. *Report for Hydro Tasmania, 1-32*.
- Barton, A. F. (2005). Tarraleah Power Station Hilltop No.1 Pipeline Cleaning and Headloss Estimation. *Report for Hydro Tasmania, 1-48*.
- Barton, A. F. (2007a). Friction, roughness and boundary layer characteristics of freshwater biofilms in hydraulic conduits *PhD Thesis, School of Engineering, University of Tasmania*.
- Barton, A. F., & Sargison, J. E. (2004). *Tarraleah Canal Paint Trials*. Hobart: University of Tasmania.
- Barton, A. F., Sargison, J. E., Brandner, P., & Walker, G. J. (2007b). *A Force Balance to Measure the Total Drag of Biofilms on Test Plates*. Paper presented at the 16th Australasian Fluid Mechanics Conference.
- Barton, A. F., Sargison, J. E., Osborn, J. E., Perkins, K., & Hallegraeff, G. (2010). Characterizing the roughness of freshwater biofilms using a photogrammetric methodology. *Biofouling, 26*(4), 439 – 448.
- Barton, A. F., Wallis, M. R., Sargison, J. E., Buia, A., & Walker, G. J. (2008). Hydraulic roughness of biofouled pipes, biofilm character, and measured improvements from cleaning. *Journal of Hydraulic Engineering, 134*(6), 852-857.
- Bott, T. R. (2009). Biofouling control in cooling water. *International J. Chemical Engineering, ID 619873, 4*.
- Bott, T. R., & Pinheiro, M. M. V. P. S. (1977). Biological Fouling: Velocity and Temperature Effects. *Canadian Journal of Chemical Engineering, 55*, 473-474.
- Bott, T. R., & Miller, P. C. (1983). Mechanisms of biofilm formation on aluminium tubes. *J.Chem. Tech. Biotechnol, 33B*, 177 - 184.
- Braun, W. J., & Murdoch, D. J. (2007). *A First Course in Statistical Programming with R* (1st ed.). Cambridge, UK: Cambridge University Press.

- Brett, T. M. (1980). Head-loss Measurement on Hydroelectric Conduits. *Journal of the Hydraulics Division*, 106(1), 173-190.
- Brito, D., Nataf, H. C., Cardin, P., Aubert, J., & Masson, J. P. (2001). Ultrasonic Doppler velocimetry in liquid gallium *Experiments in Fluids*, 31, 653-663.
- Broekman, S., Pohlmann, O., Beardwood, E. S., & de Meulenaer, E. C. (2010). Ultrasonic treatment for microbiological control of water systems. *Ultrasonics Sonochemistry*, 17(6), 1041-1048.
- BS3680. (1981). Part 4A. *Methods of measurement of liquid flow in open channels. Weirs and flumes. Method using thin-plate weirs.*
- Callow, M. E. (1993). A Review of Fouling in Freshwater. *Biofouling*, 7, 313-327.
- Callow, M. E., & Callow, J. A. (2000). Substratum location and zoospore behaviour in the fouling alga *Enteromorpha*. *Biofouling*, 15(1-3), 49-56.
- Candries, M., & Atlar, M. (2005). Experimental Investigation of the Turbulent Boundary Layer of Surfaces Coated With Marine Antifoulings. *Journal of Fluids Engineering*, Vol. 127, 219-232.
- Candries, M., Atlar, M., & Anderson, C. D. (2000b). *Considering the use of alternative antifoulings: the advantages of foul-release systems*. Paper presented at the Conference Proceedings ENSUS 2000.
- Cengel, Y. A., & Cimbala, J. M. (2006). *Fluid Mechanics Fundamentals and Applications* (1st ed.). New York: McGraw-Hill Companies Inc.
- Characklis, W. G. (1973). Attached Microbial Growths - II. Frictional Resistance due to Microbial Slimes. *Water Research*, 7.
- Characklis, W. G. (1981). Fouling Biofilm Development: A Process Analysis. *Biotechnology and Bioengineering*, 23(9), 1923-1960.
- Cloete, T. E., Westaard, D., & Vuuren, S. J. (2003). Dynamic response of biofilm to pipe surface and fluid velocity. *Water Sci Technol*. 2003;47(5):57-9., 47(5), 57-59.
- Colebrook, C. F. (1939). Turbulent Flow in Pipes, with Particular Reference to the Transition Between the Smooth and Rough Pipe Laws. *Journal of Civil Engineers*, 11, 133-157.
- Coletti, F., Ishiyama, E. M., Paterson, W. R., Wilson, D. I., & Macchietto, S. (2010). Impact of Deposit Aging and Surface Roughness on Thermal Fouling: Distributed Model. *American Institute of Chemical Engineers*, 56(12).
- Colman, R. (2005). *Penstock cleaning -likely benefits at Hydro Tasmania station* (No. DMS-63214). Hydro Tasmania, Hobart.
- ColourChart. (1996). The Standards Association of Australia. AS 2700--1996.
- Crawley, M. J. (2007). *The R Book*: John Wiley & Sons Ltd.
- Cullimore, D. R., & E., M. A. (1978). The Identification, Cultivation and Control of Iron Bacteria in Ground Water. *Aquatic Microbiology*, Editors Skinner & Shewan Academic Press 1978, 32.
- Dahlem, C., Moran, P., & Grant, T. (1984). Larval settlement of marine sessile invertebrates on surfaces of different colour and position. *Ocean Science and Engineering*, 9, 225-236.
- Dalgaard, P. (2002). *Introductory Statistics with R*: Springer-Verlag New York, Inc.
- Den Toonder, J. M. J., & Nieuwstadt, F. T. M. (1997). Reynolds number effects in a turbulent pipe flow for low to moderate Re. *Physics of Fluids*, 9(11), 3398-3409.

References

- Dobretsov, S. V., Gosselin, L., & Qian, P. Y. (2010). Effects of solar PAR and UV radiation on tropical biofouling communities. *Marine Ecology Progress Series*, 402 31–43.
- Dobretsov, S. V., Qian, P. Y., & Wahl, M. (2005). Effect of solar ultraviolet radiation on the formation of shallow, early successional biofouling communities in Hong Kong. *Marine Ecology Progress Series*, 290, 55-65.
- Flemming, H. C. (2002). Biofouling in water systems - cases, causes and countermeasures. *Applied Microbiol Biotechnol*, 59, 629-640.
- Flemming, H. C., Neu, T. R., & Wozniak, D. J. (2007). The EPS Matrix: The "House of Biofilm Cells". *Bacteriology*, 7945-7947.
- Forward, P. (1994). *Control of iron biofouling in submersible pumps in the Woolpunda Salt Interception Scheme in South Australia*.
- Ghiorse, W. C. (1984). Biology of Iron-and Manganese-Depositing Bacteria. *Microbiology*, 38, 515-550.
- Guenther, J., Carl, C., & Sunde, L. M. (2009). The effects of colour and copper on the settlement of the hydroid *Ectopleura larynx* on quaculture nets in Norway. *Aquaculture* 292 (2009) 252–255.
- Hallam, N. B., West, J. R., Forster, C. F., & Simms, J. (2001). The potential for biofilm growth in water distribution systems. *Water Research*, 35(17), 4063-4071.
- Hodson, S. L., Burke, C. M., & Bissett, A. P. (2000). Biofouling of fish-cage netting: the efficacy of a silicone coating and the effect of netting colour. *Aquaculture*, 184, 277-290.
- Hung, O. S., Gosselinb, L. A., Thiyagarajan, V., Wu, R. S. S., & Qian, P. Y. (2005). Do effects of ultraviolet radiation on microbial films have indirect effects on larval attachment of the barnacle *Balanus amphitrite*? *Experimental Marine Biology and Ecology*, 323, 16-26.
- Huovinen, P. S., Penttila, H., & Soimasuo, M. R. (2003). Spectral attenuation of solar ultraviolet radiation in humic lakes in Central Finland. *Chemosphere*, 51, 205-214.
- Hurtubise, R. D., & Havel, J. E. (1998). The effects of ultraviolet-B radiation on freshwater invertebrates: Experiments with a solar simulator. *Limnol. Oceanogr. by the American Society of Limnology and Oceanography, Inc.*, 43(6), 1082-1088.
- International Hydropower Association. (2012). Hydropower: the largest source of renewable energy from <http://www.hydropower.org/>
- Kruger, M. (2009). Cooling Water Design Standard. *Hydro Tasmania*, 34.
- Lakretz, A., Ronb, E. Z., & Mamane, H. (2010). Biofouling control in water by various UVC wavelengths and doses. *Biofouling*, 26(3), 257-267.
- Lambert, M. F., Brooks, J., Kildea, M., Geantham, T., & McFarlane, B. (2008). *Understanding the Impact of Biofilm Growth on Pipe Roughness*. Paper presented at the World Environmental and Water Resources Congress 2008: Ahupua'A.
- Lambert, M. F., Edwards, R. W. J., Howie, S. J., Gilio, B. B. D., & Quinn, S. P. (2009). The Impact of Biofilm Development on Pipe Roughness and Velocity Profile *Proceedings of World Environmental and Water Resources Congress 2009 - World Environmental and Water Resources Congress 2009: Great Rivers*.
- Lauchlan, C., Forty, J., & May, R. (2007). Discussion: Flow resistance of wastewater pumping mains. *Proceedings of the ICE - Water Management* 160(1), 51 –57.

- LeChevallier, M. W. (1991). *Biocides and the current status of biofouling control in water systems*. New York: Springer.
- Lee, H. J., Han, D., Lee, S. H., Yoo, J. W., Baek, S. H., & Lee, E. K. (1998). On-line monitoring and quantitative analysis of biofouling in low-velocity cooling water system. *Korean J. Chem. Eng.*, 15(1), 71-77.
- Lehtola, M. J., Nissinenb, T. K., Miettinen, I. T., & Marti, P. J. (2004). Removal of soft deposits from the distribution system improves the drinking water quality. *Water Research*, 38(3), 601-610.
- Li, B., & Loganb, B. E. (2005). The impact of ultraviolet light on bacterial adhesion to glass and metal oxide-coated surface. *Colloids and Surfaces B: Biointerfaces* 41, 153–161.
- Loehrke, R. J., & Nagib, H. M. (1976). Control of Free-Stream Turbulence by means of Honeycombs - A Balance Between Suppression and Generation. *ASME Journal of Fluids Engineering*, 98, 342-355.
- McFie, H. (1973). Biological, Chemical and Related Engineering Problems in Large Storage Lakes of Tasmania. In W. C. Ackermann, White, G.F. and Worthington, E.B. (Ed.), *Man-Made Lakes: Their Problems and Environmental Effects* (Vol. 17, 56-62). Washington, D.C.: American Geophysical Union.
- McFie, H. (1976). *Power Storage Lakes: Biological Depositions and Energy Losses in Tasmania*. Paper presented at the 47th ANZAAS Congress, Hobart.
- McKeon, B. J., Li, J., Jiang, W., Morrison, J. F., & Smits, A. J. (2003). Pitot probe corrections in fully developed turbulent pipe flow. *Measurement Science and Technology*, 14(8), 1449-1458.
- Mehta, R. D., & Bradshaw, P. (1979). Design Rules for Small Low Speed Wind Tunnels. *The Aeronautical Journal of the Royal Aeronautical Society*, 443-449.
- Melo, L. F., & Bott, T. R. (1997). Biofouling in Water System. *Experimental Thermal and Fluid Science*, 14, 375-381.
- Minkus, A. J. (1954). Deterioration of the Hydraulic Capacity of Pipelines. *Transactions of New England Water Works Association*, LXVIII, 1-10.
- Moody, L. F. (1944). Friction Factors for Pipe Flow. *Transactions of the A.S.M.E.*, 671-684.
- Munshi, H. A., Saeed, M. O., Green, T. N., Al-Hamza, A. A., Farooque, M. A., & Ismail, A. R. A. (2005). *Impacts of UV irradiation on controlling biofouling problems in NF-SWRO desalination process*. Paper presented at the International Desalination Association (IDA) World Congress Conference.
- Nikuradse, J. (1933). Laws of Flow in Rough Pipes. *NACA TM 1292,1950*.
- Pabich, W. J., Valiela, I., & Hemond, H. F. (2001). Relationship between DOC concentration and vadose zone thickness and depth below water table in groundwater of Cape Cod, U.S.A. *Biogeochemistry* 55, 247-268.
- Panchal, C. B., Takahashi, P. K., & Avery, W. (1995). *Biofouling control using ultrasonic and ultraviolet treatments*. Paper presented at the Conference: Fouling mitigation of industrial heat exchangers.
- Pelletier, É., Bonnet, C., & Lemarchand, K. (2009). Biofouling Growth in Cold Estuarine Waters and Evaluation of Some Chitosan and Copper Anti-Fouling Paints. *International Journal of Molecular Sciences*, 10, 3209-3223.

- Perkins, K. J. (2010a). Taxonomy, Ecophysiology and Mitigation of Fouling Diatoms in a Hydro Electric Canal at Tarraleah (Tasmania) *PhD Thesis, School of Plant Science, University of Tasmania*.
- Perkins, K. J., Andrewartha, J. M., McMinn, A., Cook, S. S., & Hallegraeff, G. M. (2010b). Succession and physiological health of freshwater microalgal fouling in a Tasmanian hydropower canal. *Biofouling*, 26(6), 637-644.
- Picologlou, B. F., Zilver, N., & Charaklis, W. G. (1980). Biofilm growth and hydraulic performance. *ASCE J. Hydraulics Division*, HY5, 733-747.
- Pinheiro, M. M., Melo, L. F., Bott, T. R., Pinheiro, J. D., & Leita, L. (1988). Surface Phenomena and Hydrodynamic Effects on the Deposition of *Pseudomonas fluorescens*. *The Canadian Journal of Chemical Engineering*, 66, 63-67.
- Pollard, A. L., & House, H. E. (1959). An Unusual Deposit in a Hydraulic Tunnel. *Journal of the Power Division Proceedings of the A.S.C.E*, 163-171.
- Polzin, D. (2010). Biofouling Audit. *Hydro Tasmania*.
- Prendergast, G. S., Zurn, C. M., Bers, A. V., Head, R. M., Hansson, L. J., & Thomason, J. C. (2009). The relative magnitude of the effects of biological and physical settlement cues for cypris larvae of the acorn barnacle, *Semibalanus balanoides* L. *Biofouling*, 25(1), 35-44.
- Pryogle, P. A., Rinehart, B. N., & Ghio, E. J. (1997). Control of Nuisance Algae Growth in Hydropower Distribution Systems. *Waterpower '97*, 69-75.
- Pujo, M., & Bott, T. R. (1991). Effects of Fluid Velocities and Reynolds Numbers on Biofilm Development in water systems. *Experimental Heat Transfer, Fluid Mechanics and Thermodynamics*, 1358-1362.
- Sargison, J. E., Barton, A. F., Walker, G. J., & Brandner, P. (2009). Design and calibration of a water tunnel for skin friction research. *Australian Journal of Mechanical Engineering*, 7(2), 111-124.
- Satheesh, S., & Wesley, S. G. (2010). Influence of substratum colour on the recruitment of macrofouling communities. *Journal of the Marine Biological Association of the United Kingdom*, 90(5), 941-946.
- Sato, Y., Mori, M., Takeda, Y., Hishida, K., & Maeda, M. (2002). *Signal Processing for Advanced Correlation Ultrasonic Velocity Profiler*. Paper presented at the Third International Symposium on Ultrasonic Doppler Methods for Fluid Mechanics and Fluid Engineering EPFL.
- Schultz, M. P. (2004). Frictional Resistance of Antifouling Coating Systems. *Journal of Fluids Engineering*, Vol. 126, 1039-1047.
- Schultz, M. P., & Swain, G. W. (1999). The Effect of Biofilms on Turbulent Boundary Layers. *Journal of Fluids Engineering*, Vol. 121, 44-51.
- Schultz, M. P., Swain, G. W. (2000). The Influence of Biofilms on Skin Friction Drag. *Biofouling*, Vol 15(1-3), 129-139.
- Schwartz, T., & Hoffmann, S., Obst U. (2003). Formation of natural biofilms during chlorine dioxide and u.v. disinfection in a public drinking water distribution system. *Journal of Applied Microbiology* 95, 591-601.
- Shine, R., Brischoux, F., & Pile, A. J. (2010). A seasnake's colour affects its susceptibility to algal fouling. *The Royal Society*, doi: 10.1098/rspb.2010.0255, 1-7.

- Sommaruga, R., & Psenner, R. (1997). Ultraviolet Radiation in a High Mountain Lake of the Austrian Alps: Air and Underwater Measurement. *Photochemistry and photobiology*, 65(6), 957-963.
- Sommerfeld, E. O. (1999). *Iron Bacteria and Organic Carbons: What They Mean to Iron and Manganese Removal*. Paper presented at the AWWWOA Operator's Seminar.
- Stuetz, R. M., & McLaughlan, R. G. (2004). Impact of localised dissolved iron concentrations on the biofouling of environmental wells. *Water Science and Technology*, 49, 107-113.
- Su, Z., Huang, L., Yan, Y., & Li, H. (2007). The effect of different substrates on pearl oyster *Pinctada martensii* (Dunker) larvae settlement. *Aquaculture*, 271, 377-383.
- Swain, G., Herpe, S., Ralston, E., & Tribou, M. (2006). Short-term testing of antifouling surfaces: the importance of colour. *Biofouling*, 22(6), 452-429.
- Takeda, Y. (1995). Velocity profile measurement by ultrasonic doppler method *Experimental Thermal and Fluid Science*, 10(4), 444-453.
- Teng, F., Guan, Y. T., & Zhu, W. P. (2008). Effect of biofilm on cast iron pipe corrosion in drinking water distribution system: Corrosion scales characterization and microbial community structure Investigation. *Corrosion Science*, 50(10), 2816-2823.
- Terry, I. (2007). *Tungatinah Power Station Conservation Management Plan*. Hobart: Austral Archaeology Pty Ltd, 1-114.
- Tyler, P. A. (1968). Microbiological deposition of manganese in freshwater distribution systems. *University of Tasmania, PhD Thesis Hobart*.
- Verran, J., Lees, G. C., & Shakespeare, A. P. (1991). The effect of surface roughness on the adhesion of *Candida albicans* to acrylic. *Biofouling*, 3(3), 183-191.
- Vieira, M. J., & Melo, L. F. (1995). Effect of Clay Particles on The Behaviour of Biofilms Formed by *Pseudomonas Fluorescens*. *War. Sci. Tech.*, 32(8), 45-52.
- Vieira, M. J., Melo, L. F., & Pinheiro, M. M. (1993). Biofilm Formation: Hydrodynamic Effects on Internal Diffusion and Structure. *Biofouling*, 7, 67-80.
- Volk, C. J., & LeChevallier, M. W. (1999). Impacts of the Reduction of Nutrient Levels on Bacterial Water Quality in Distribution Systems. *Applied and Environmental Microbiology*, 65(11), 4957-4966.
- Yule, A. B., & Walker, G. (1984). The temporary adhesion of barnacle cyprids: effects of some differing surface characteristics *Journal of the Marine Biological Association of the United Kingdom*, 64, 429-439.
- Zagarola, M. V., & Smits, A. J. (1997). Scaling of the Mean Velocity Profile for Turbulent Pipe Flow. *Physical Review Letters From The American Physical Society*, VOLUME 78, pp. 239-242.
- Zidouh, H. (2009). Velocity Profiles and Wall Shear Stress in Turbulent. Transient Pipe Flow. *International Journal of Dynamics of Fluids*, 5(1), 61-83.

Appendices

A Water Level and Water Temperature Data for Chapter 3

A.1 Water Level of Pond No.1 and Transition 4

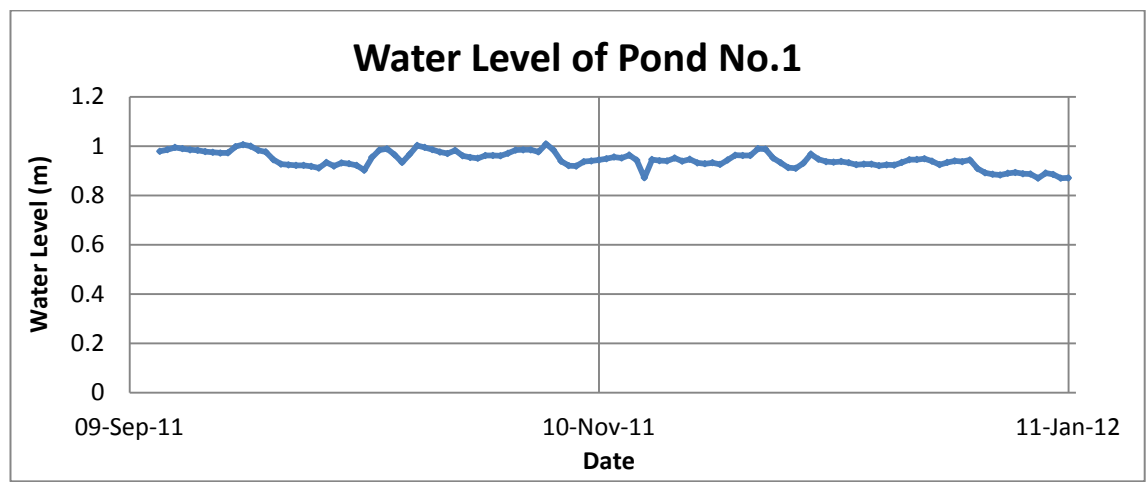


Figure A.1 Water level of Pond No.1.

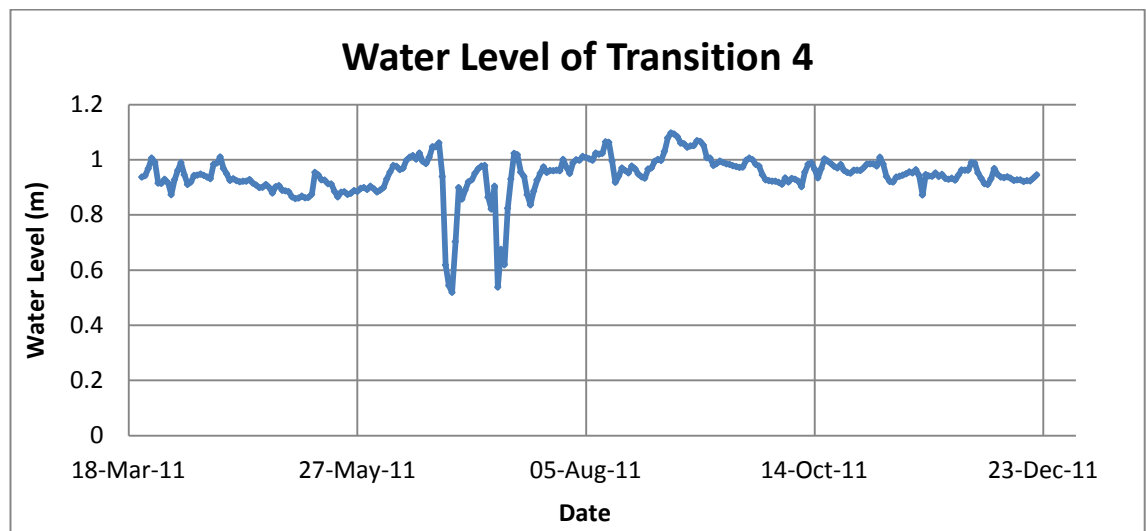


Figure A.2 Water level of Transition 4.

A.2 Water Temperature of Pond No.1 and Transition 4

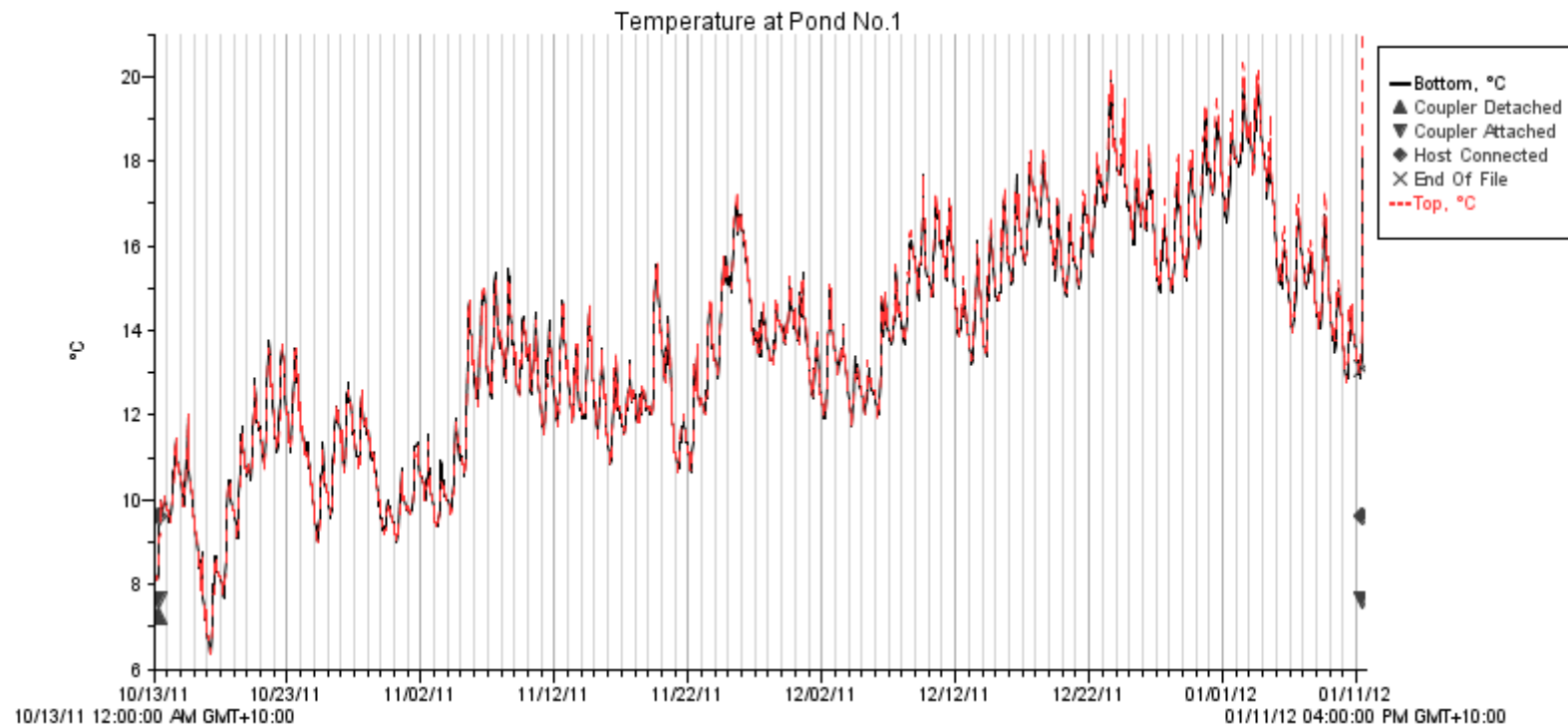


Figure A.3 Water temperature of Pond No.1.

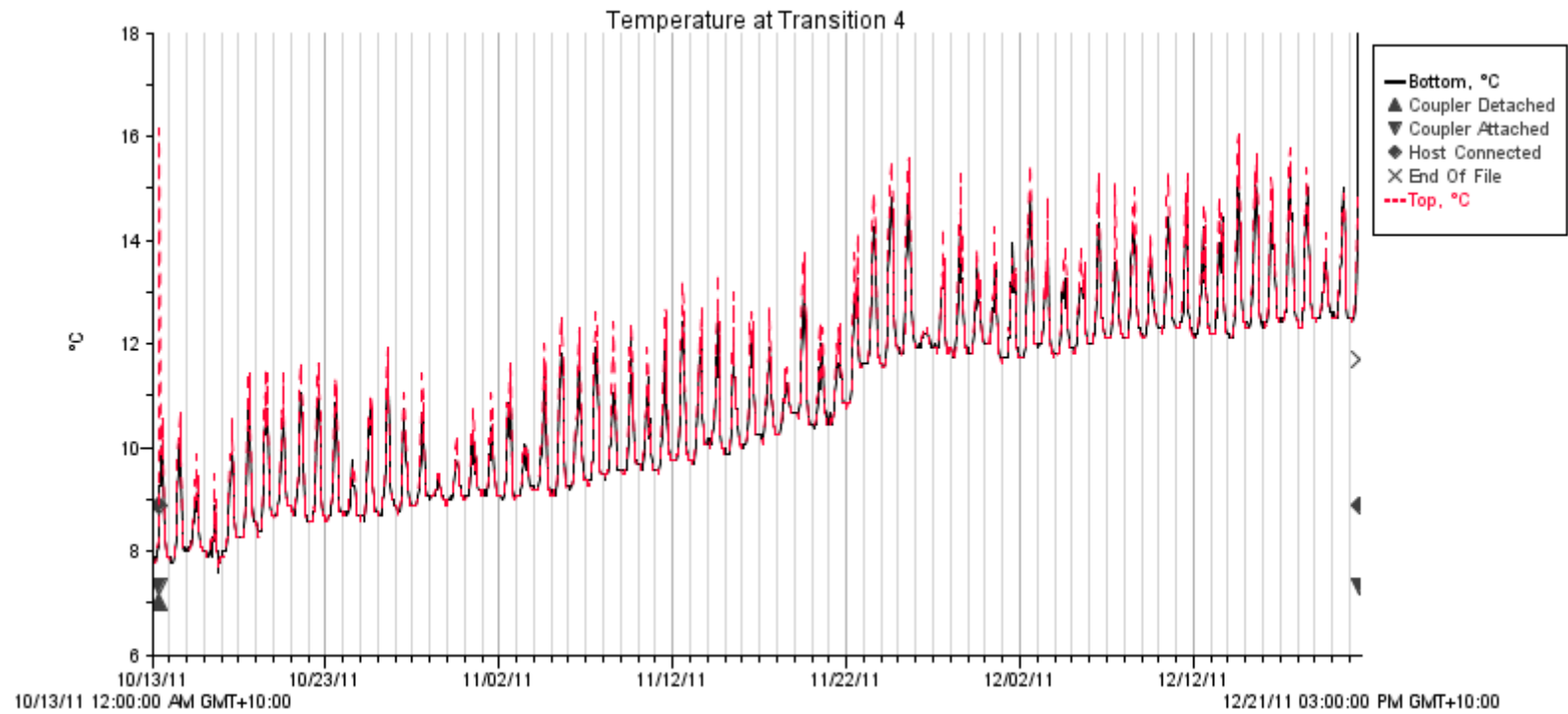


Figure A.4 Water temperature of Transition 4.

B Biofouling Data and R Program for Chapter 4

B.1 Biofouling Chemical Analysis

	Wilmot cooling pipe (4/8/2010)		Fisher cooling pipe (16/7/2010)	Poatina Penstock (6/6/2010)	Wilmot Penstock (3/2003) (Barton, 2007a)	Poatina Penstock (8/2004) (Barton, 2007a)		Tarraleah Pipeline (9/2004) (Barton, 2007a)
	Dried	Wet				Tunnel	IP4	
Al (mg/kg)	24200	19300	52000	21500	NA	18100	30600	54400
As (mg/kg)	265	73	8	16	NA	14	11	28
Ca (mg/kg)	7400	5220	7890	16300	NA	9350	13400	10200
Cd (mg/kg)	63	1	8	7	65	4	6	14
Co (mg/kg)	1190	199	475	125	831	145	185	280
Cr (mg/kg)	25	53	70	19	29	159	61	110
Cu (mg/kg)	177	199	706	331	140	131	200	91
Fe (mg/kg)	153000	134000	42900	23300	169000	15700	22600	32400
K (mg/kg)	708	967	377	798	NA	44	728	742
Mg (mg/kg)	1900	2400	1110	27800	NA	16400	3490	2410
Mn (mg/kg)	180000	21800	250000	182000	230000	97500	145000	208000
Na (mg/kg)	208	275	163	274	NA	200	305	303
Ni (mg/kg)	406	84	232	496	417	642	654	338
Pb (mg/kg)	230	185	91	38	228	40	37	56
Phosphorous (mg/kg)	601	821	797	642	NA	383	610	958
S (mg/kg)	1070	1560	2660	4700	NA	3990	4090	2260
Zn (mg/kg)	2830	218	1780	619	2600	414	577	664
Total (mg/kg)	374273	187355	361267	278965	NA	163216	222554	313254

Table B.1 Chemical analysis of biofouling in Hydro Tasmania conduits.

148

```

txt <- sub("^SampleDepth$", "Depth", txt)
txt <- sub("^DateAndTime$", "Date", txt)
txt
}
## Read one Lake_Name.csv file
lake.csv <- function(file) {
  ## Read csv file
  d <- read.csv(paste("Lake_", file, ".csv", sep = ""))
  ## Standardize names
  colnames(d) <- fix.colnames(colnames(d))
  ## Add site name, trim dates and replace parameter code with parameter name
  d$Date <- as.Date(strptime(fix.date(d$Date), "%d/%m/%Y %H:%M"))
  if(!is.integer(d$Parameter))
    d$Parameter <- as.integer(round(100*d$Parameter))
  d$Site <- rep(file, nrow(d))
  d <- d[,c("Site", "Date", "Depth", "Parameter", "Value")]
  d <- d[order(d$Parameter, d$Date, d$Depth),]
  d$Parameter <- codes$name[match(d$Parameter, codes$code)]
  d
}
## Read all data and merge
lakes <- c("Rosebery", "Pieman", "Parangana", "Mackintosh", "Great", "Gordon", "Burbury", "Gairdner")
d <- NULL
for(l in lakes) {
  d <- rbind(lake.csv(l), d)
}
rownames(d) <- NULL
## Add in rough seasons
season <- c("Sum", "Aut", "Win", "Spr")
d$Season <- factor(season[((as.POSIXlt(d$Date)$mon+1)%%12)%%3+1], labels=season)
d$Year <- as.POSIXlt(d$Date)$year+1900
d$Epoch <- factor(ifelse(d$Year >= 1990, "Post 90", "Pre 90"))
## These are all the parameters we have.
unique(d$Parameter)
#####
## Example plots
library(lattice)

```

```
## xyplot
## pch - sets plot symbol
## alpha - sets transparency
## ylim - sets the range of the y axis (need to set this because there are some huge outliers).
## subset - condition that describes the subset of the data to plot
## xlab, ylab - the x and y axis labels
## main - main plot label
## Plot Water Temperature against Depth separately for each Site, coloured by Season.
xyplot(Value~Depth | Site, group=Season,
        data=d,subset=Parameter=="Water.Temperature",
        ylim=c(0,25),
        pch=20,alpha=0.1,
        ylab="Water Temperature Degree C",
        xlab="Depth (m)",
        main="Water Temperature - Depth")
## Plot temperatures in Depth > 5m
bwplot(Value~Site,
        data=d,subset=Parameter=="Water.Temperature" & Depth > 5,
        ylim=c(0,20),
        ylab="Water Temperature Degree C",
        main="Water Temperature - Site Depth > 5 m",
        ## Rotate x axis labels
        scales=list(x=list(rot=90)))
## Make tables of mean, min, max, 5th, 50th and 95th percentiles
## Function to construct the summary
table.summary <- function(x) {
  c("mean"=mean(x,na.rm=T),
    "min"=min(x,na.rm=T),
    "max"=max(x,na.rm=T),
    quantile(x,prob=c(0.05,0.25,0.5,0.75,0.95),na.rm=T))
}
## with(data,expression) - evaluate expression using data
## split(x,g) - divide x into groups defined by g
## sapply(l,f) - apply function f to each element of list g
## t - transpose
## Basically, using the water temp data, group the temperatures by
## site and compute the summary for each. Transpose results so each
## row is a site.
```

```

with(d[d$Parameter=="Water.Temperature",],
  t(sapply(split(Value,Site),table.summary)))
#####
##Plot pH Value against Depth for each Site
xyplot(Value~Depth | Site,
  data=d,subset=Parameter=="pH.field",
  ylim=c(4,9),
  pch=20,alpha=0.5,
  ylab="Field pH ",
  xlab="Depth (m)",
  main="Field pH - Depth")
## Boxplot of PH by Site in Depth> 5m
bwplot(Value~Site,
  data=d,subset=Parameter=="pH.field" & Depth > 5,
  ylim=c(4,8),
  ylab="Field pH ",
  main="Field pH - Site Depth > 5 m",
  ## Rotate x axis labels
  scales=list(x=list(rot=90)))
## Make tables of mean, min, max, 5th, 25th,50th 75th and 95th percentiles
with(d[d$Parameter=="pH.field",],
  t(sapply(split(Value,Site),table.summary)))
#####
## Plot Turbidity against Date separately for each Site
xyplot(Value~Depth | Site,
  data=d,subset=Parameter=="Turbidity",
  ylim=c(0,80),
  pch=20,alpha=0.5,
  ylab="Turbidity NTU",
  xlab="Depth (m)",
  main="Turbidity - Depth")
## Boxplots of Turbidity by Site
bwplot(Value~Site,
  data=d,subset=Parameter=="Turbidity" & Depth > 5,
  ylim=c(-0.1,20),
  ylab="Turbidity NTU",
  main="Turbidity - Site Depth > 5 m",
  ## Rotate x axis labels

```



```

scales=list(x=list(rot=90)))
## Make tables of mean, min, max, 5th, 25th,50th 75th and 95th percentiles
## Turbidity only
with(d[d$Parameter=="Turbidity",],
  t(sapply(split(Value,Site),table.summary)))
#####
## Plot Conductivity against Date separately for each Site
xyplot(Value~Depth | Site,
  data=d,subset=Parameter=="Conductivity.TRef",
  ylim=c(0,100),
  pch=20,alpha=0.5,
  ylab="Conductivity us/cm",
  xlab="Depth (m)",
  main="Conductivity - Depth")
## Boxplots of Conductivity by Site
bwplot(Value~Site,
  data=d,subset=Parameter=="Conductivity.TRef" & Depth > 5,
  ylim=c(10,70),
  ylab="Conductivity us/cm",
  main="Conductivity - Site Depth > 5 m",
  ## Rotate x axis labels
  scales=list(x=list(rot=90)))
## Make tables of mean, min, max, 5th, 50th and 95th percentiles
with(d[d$Parameter=="Conductivity.TRef",],
  t(sapply(split(Value,Site),table.summary)))
#####
## Plot Iron against Date separately for each Site
xyplot(Value~Date | Site,
  data=d,subset=Parameter=="Iron.Total.NonFilt",
  ylim=c(0,2),
  pch=20,alpha=0.5,
  ylab="Total Iron mg/l",
  xlab="Time",
  main="Total Iron - Time")
## Boxplots of Iron by Site
bwplot(Value~Site,
  data=d,subset=Parameter=="Iron.Total.NonFilt",
  ylim=c(0,1.2),

```

```

ylab="Iron.Total  mg/l",
main="Total Iron - Site",
  ## Rotate x axis labels
scales=list(x=list(rot=90)))
## Make tables of mean, min, max, 5th, 50th and 95th percentiles
with(d[d$Parameter=="Iron.Total.NonFilt" & d$Value <2,],
  t(sapply(split(Value,Site),table.summary)))
#####
## Boxplots of dissolved Iron by Site
bwplot(Value~Site,
  data=d,subset=Parameter=="Iron.Dissolved.Fi",
  ylim=c(0,1.5),
  ylab="Iron.Dissolved  mg/l",
  main="Dissolved Iron - Site",
  ## Rotate x axis labels
  scales=list(x=list(rot=90)))
#####
## Plot Manganese against Date separately for each Site
xyplot(Value~Date | Site,
  data=d,subset=Parameter=="Manganese.Total.No",
  ylim=c(0,0.5),
  pch=20,alpha=0.5,
  ylab="Total Manganese  mg/l",
  xlab="Time",
  main="Total Manganese - Time")
## Boxplots of Manganese by Site
bwplot(Value~Site,
  data=d,subset=Parameter=="Manganese.Total.No",
  ylim=c(0,0.15),
  ylab="Manganese.Total  mg/l",
  main="Total Manganese - Site",
  ## Rotate x axis labels
  scales=list(x=list(rot=90)))
with(d[d$Parameter=="Manganese.Total.No" & d$Value <2,],
  t(sapply(split(Value,Site),table.summary)))
#####
## Boxplots of Zinc by Site
bwplot(Value~Site,

```

```

data=d,subset=Parameter=="Zinc.Total.NonFilt",
ylim=c(0,0.15),
ylab="Zinc.Total  mg/l",
main="Total Zinc - Site",
  ## Rotate x axis labels
scales=list(x=list(rot=90))
#####
## Boxplots of Aluminium by Site
bwplot(Value~Site,
  data=d,subset=Parameter=="Aluminium.Total.No",
  ylim=c(0,0.6),
  ylab="Aluminium.Total  mg/l",
  main="Total Aluminium - Site",
  ## Rotate x axis labels
  scales=list(x=list(rot=90)))
with(d[d$Parameter=="Aluminium.Total.No" & d$Value <1,],
  t(sapply(split(Value,Site),table.summary)))
#####
## Boxplots of Dissolved Oxygen by Site
bwplot(Value~Site,
  data=d,subset=Parameter=="Dissolved.Oxygen.DO" & Depth > 15,
  ylim=c(-0.5,120),
  ylab="Dissolved Oxygen  mg/l",
  main="Dissolved Oxygen - Site  Depth >15 m",
  ## Rotate x axis labels
  scales=list(x=list(rot=90)))
## Value in Depth >=15 m only
with(d[d$Parameter=="Dissolved.Oxygen.DO" & d$Depth >= 15,],
  t(sapply(split(Value,Site),table.summary)))
#####
## Plot Dissolved Organic Carbon.Dis  against site
bwplot(Value~Site,
  data=d,subset=Parameter=="Organic.Carbon.Dis",
  ylim=c(0,25),
  ylab="Dissolved Organic Carbon  mg/l",
  main="Dissolved Organic Carbon - Site",
  ## Rotate x axis labels
  scales=list(x=list(rot=90)))

```

```

with(d[d$Parameter=="Organic.Carbon.Dis" & d$Value <35,],
  t(sapply(split(Value,Site),table.summary)))
#####
## Boxplots of Sodium by Site
bwplot(Value~Site,
  data=d,subset=Parameter=="Sodium.Total.as.Na",
  ylim=c(0,10),
  ylab="Sodium.Total  mg/l",
  main="Total Sodium - Site",
  ## Rotate x axis labels
  scales=list(x=list(rot=90)))
with(d[d$Parameter=="Sodium.Total.as.Na" & d$Value <8,],
  t(sapply(split(Value,Site),table.summary)))
#####
## Plot Sulphate.Total against Date separately for each Site
bwplot(Value~Site,
  data=d,subset=Parameter=="Sulphate.Total.as",
  ylim=c(0,6),
  ylab="Sulphate.Total  mg/l",
  main="Total Sulphate - Site",
  ## Rotate x axis labels
  scales=list(x=list(rot=90)))
with(d[d$Parameter=="Sulphate.Total.as" & d$Value <10,],
  t(sapply(split(Value,Site),table.summary)))
#####
## Boxplots of Potassium by Site
bwplot(Value~Site,
  data=d,subset=Parameter=="Potassium.Total.a",
  ylim=c(0,2),
  ylab="Potassium.Total  mg/l",
  main="Total Potassium - Site",
  ## Rotate x axis labels
  scales=list(x=list(rot=90)))
with(d[d$Parameter=="Potassium.Total.a" & d$Value <10,],
  t(sapply(split(Value,Site),table.summary)))
#####
## Plot Phosphorus against Date separately for each Site
bwplot(Value~Site,

```

```

data=d,subset=Parameter=="Phosphorus.as.P.To",
ylim=c(0,0.015),
ylab="Phosphorus    mg/l",
main="Phosphorus - Site",
    ## Rotate x axis labels
scales=list(x=list(rot=90)))
#####
## Plot Kjeldahl.Nitrogen against Date separately for each Site
bwplot(Value~Site,
    data=d,subset=Parameter=="Kjeldahl.Nitrogen.T",
    ylim=c(0,0.4),
    ylab="Kjeldahl.Nitrogen    mg/l",
    main="Kjeldahl Nitrogen - Site",
        ## Rotate x axis labels
scales=list(x=list(rot=90)))
with(d[d$Parameter=="Kjeldahl.Nitrogen.T" & d$Value <1,],
    t(sapply(split(Value,Site),table.summary)))
#####
## Plot Nitrate.as.NO3 against Date separately for each Site
bwplot(Value~Site,
    data=d,subset=Parameter=="Nitrate.as.NO3.Tot",
    ylim=c(0,0.1),
    ylab="Total Nitrate as NO3    mg/l",
    main="Total Nitrate as NO3 - Site",
        ## Rotate x axis labels
scales=list(x=list(rot=90)))
with(d[d$Parameter=="Nitrate.as.NO3.Tot" & d$Value <0.1,],
    t(sapply(split(Value,Site),table.summary)))
#####
## Plot Ammonia.as.N against Date separately for each Site
bwplot(Value~Site,
    data=d,subset=Parameter=="Ammonia.as.N",
    ylim=c(0,0.06),
    ylab="Ammonia as N    mg/l",
    main="Ammonia as N - Site",
        ## Rotate x axis labels
scales=list(x=list(rot=90)))

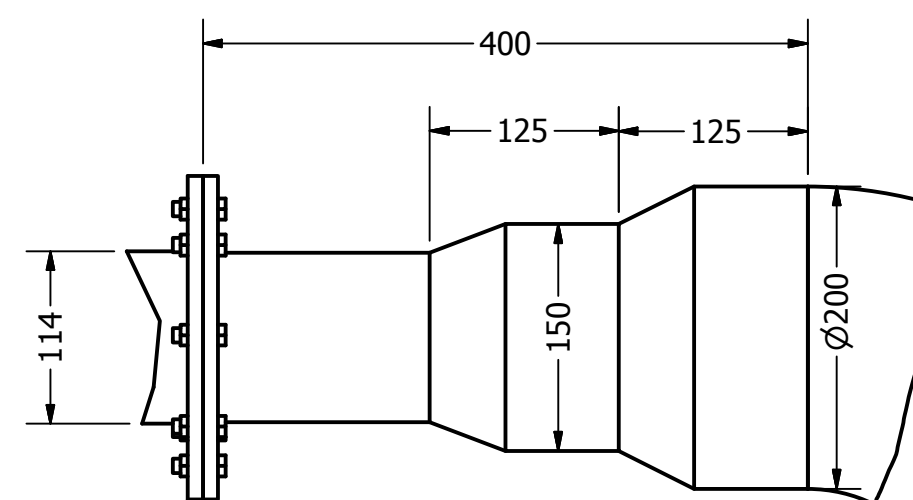
```

C Design of the New Pipe Rig

C.1 Dimension of the Lab Pipe Rig



Technical drawing of a 200 mm PVC pipe system. The drawing shows a horizontal section of the pipe with a transition part labeled "200-100 mm Transition Part" and a vertical section labeled "200 mm PVC Pipes". The horizontal section has a length of 5200 mm. The vertical section has a height of 2400 mm, with a 1600 mm segment from the horizontal section to the top. The horizontal section is supported by a "200 mm Pipe Holder 4" with a width of 800 mm. The vertical section is supported by a "200 mm Pipe Holder 4" with a width of 1600 mm. The transition part has a diameter of 400 mm. The vertical section has a diameter of 250 mm. The horizontal section has a diameter of 200 mm. The vertical section has a diameter of 200 mm. The transition part is labeled "A".



The drawing consists of two parts: a side view on the left and a cross-section A-A on the right.

Side View: Shows a horizontal cross-section of a ring. A vertical dashed line indicates the center. Two circular features, representing tapping holes, are shown on the vertical centerline. Arrows labeled 'A' point to the left from the top and bottom of the ring.

Section A-A: A circular cross-section of the ring. The outer diameter is labeled $\varnothing 102$. The inner diameter is labeled R95. The thickness of the ring is labeled 40. The section is divided into eight segments by radial lines.

Labels:

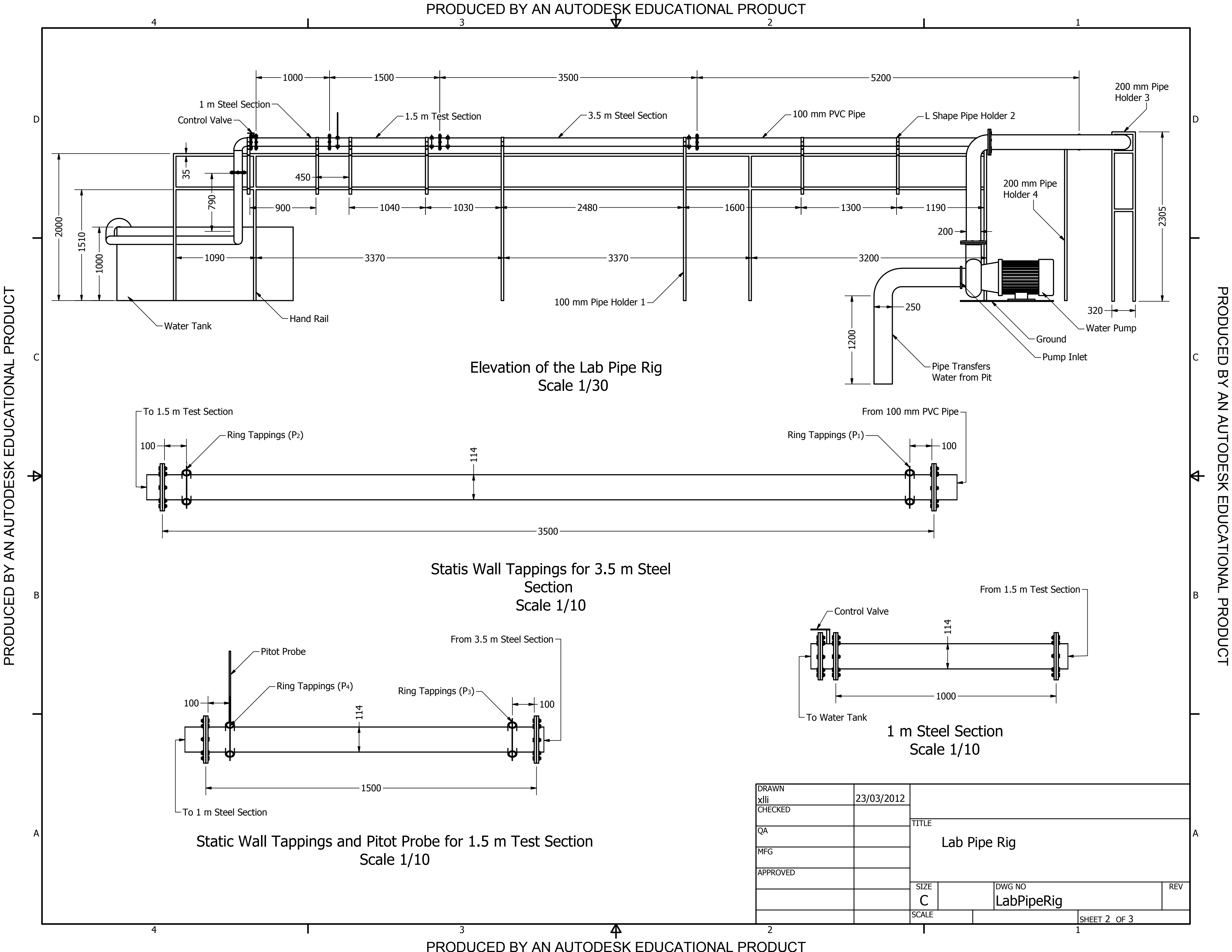
- A
- R95
- $\varnothing 102$
- 40
- 40
- A

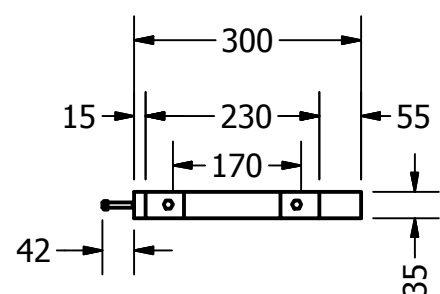
Static Ring Tapping Detail B
Scale 1 / 5

Section A-A
Scale 1 / 5

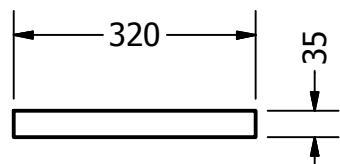
Side Elevation of the Lab Pipe Rig 1/30

PRODUCED BY AN AUTODESK EDUCATIONAL PRODUCT

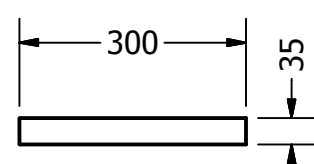




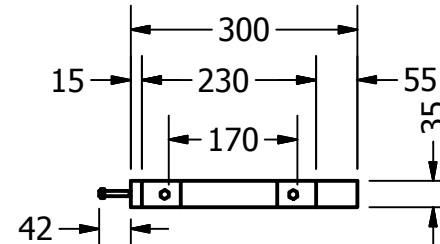
View A-A
Scale 1/10



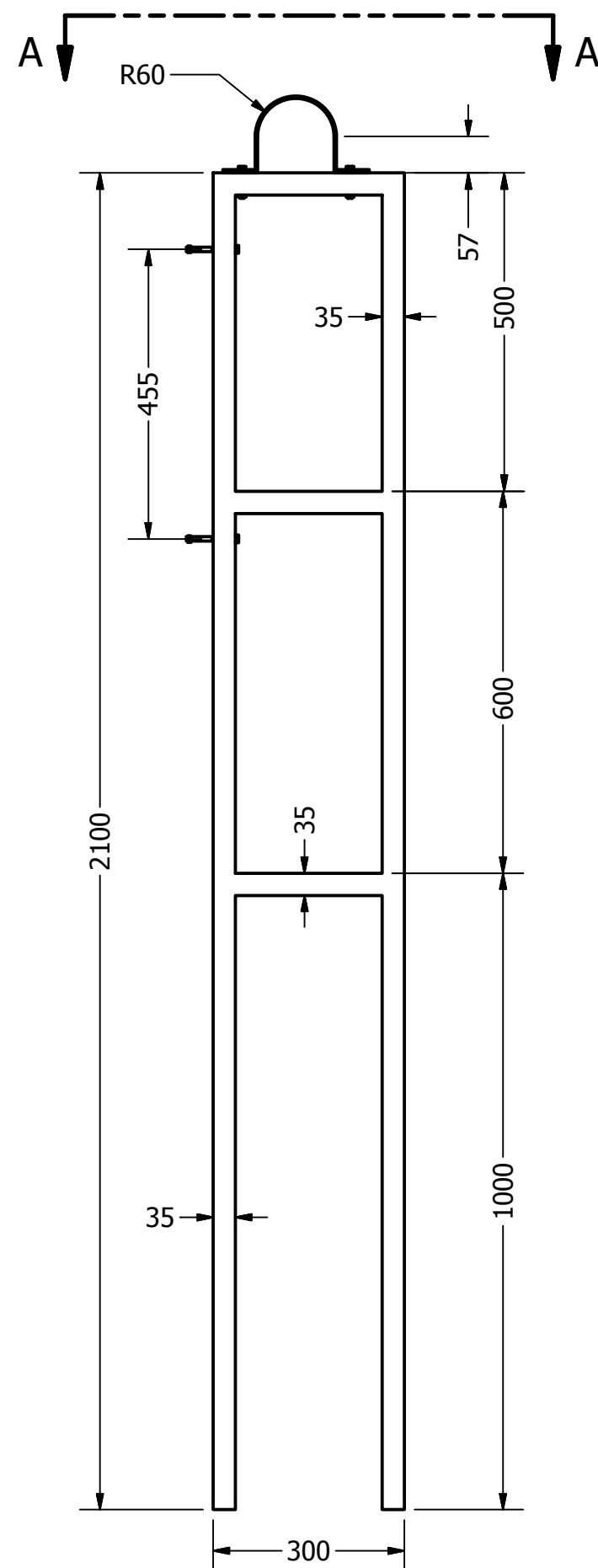
View C-C
Scale 1/10



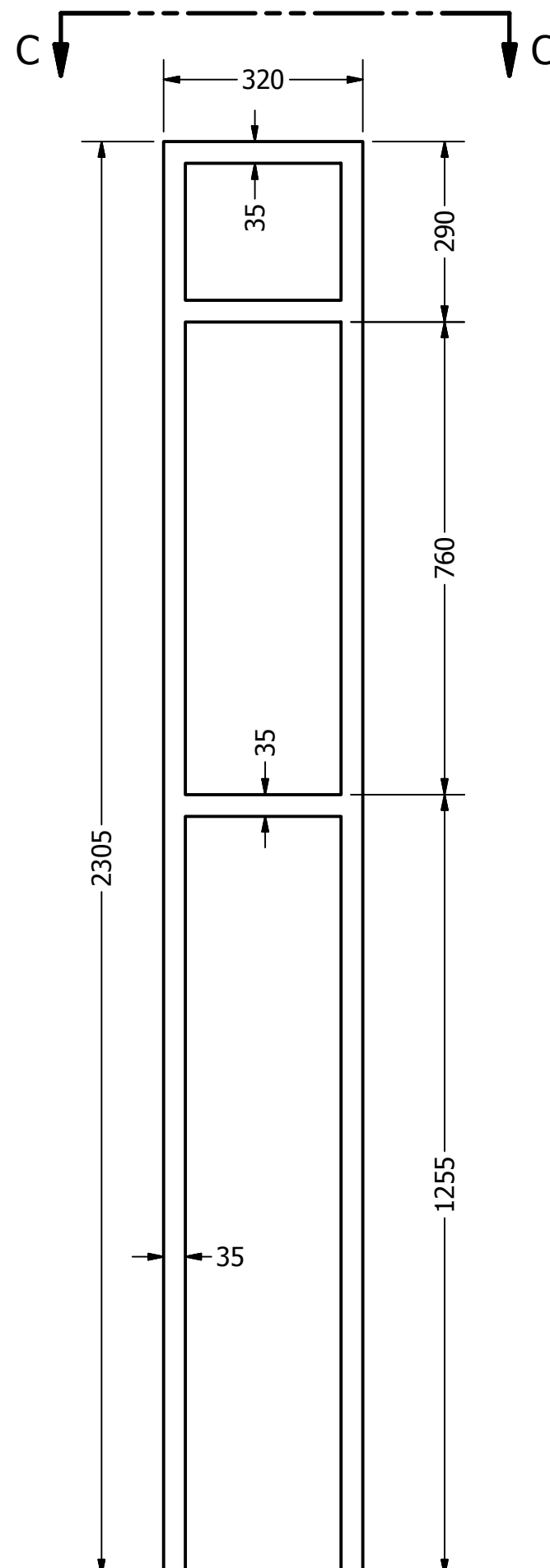
View D-D
Scale 1/10



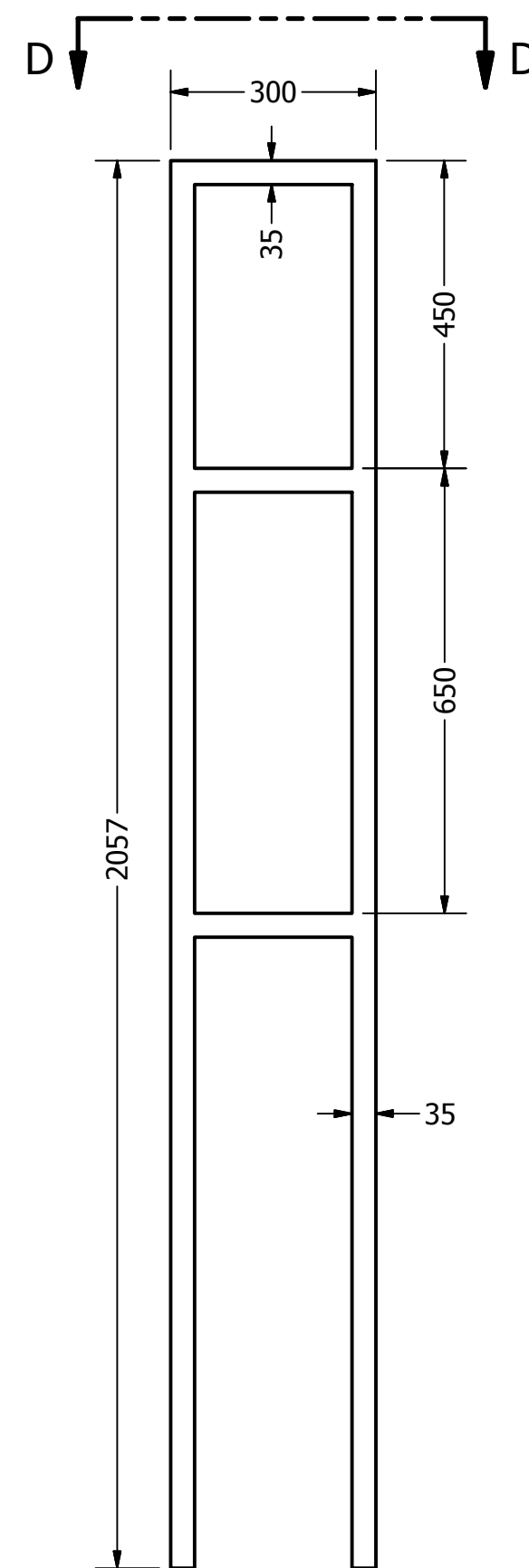
View B-B
Scale 1/10



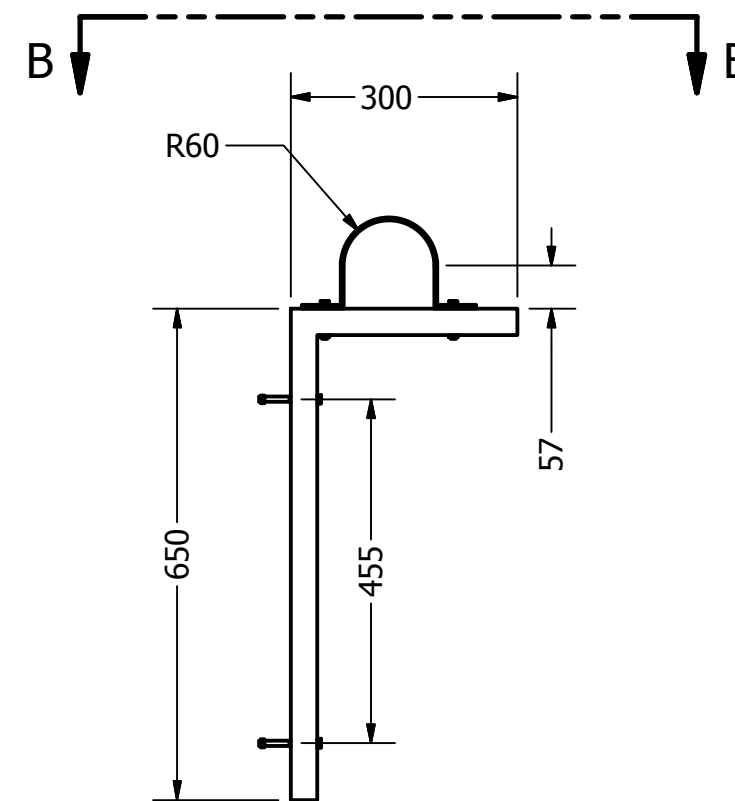
100 mm Pipe Holder 1
Scale 1/10



200 mm Pipe Holder 3
Scale 1/10



200 mm Pipe Holder 4
Scale 1/10



L-Shape 100 mm Pipe
Holder 2
Scale 1/10

DRAWN xlli	23/03/2012	TITLE Holders of the Lab Pipe Rig		
CHECKED				
QA				
MFG				
APPROVED		SIZE C	DWG NO LabPipeRig	REV
		SCALE	SHEET 3 OF 3	

C.2 Data of Penstock on Site

The range of friction factor, Reynolds number, relative roughness, wall shear stress and shear velocity are summarized, as shown in Table C.1.

D (m)	Friction factor f		Reynolds Number Re ($\times 10^6$)		Relative Roughness (k_s/D) ($\times 10^{-6}$)		Hydraulic roughness k_s (mm)		Wall shear stress τ_w (kg/ms ²)		Shear velocity u_* (m/s)	
	Fouled	clean	Fouled	clean	Fouled	clean	Fouled	clean	Fouled	clean	Fouled	Clean
1.98 - 3.05	0.0126 - 0.0164	0.0088 - 0.0150	7.5772 - 13.350	7.4740 - 17.0542	115.83 - 422.95	7.72 - 341.09	0.27 - 1.29	0.02 - 0.88	25.432 - 73.829	16.770 - 139.993	0.159 - 0.272	0.130 - 0.374

Table C.1 Data of penstocks and pipeline on site (Barton, 2007a).

C.3 Buckingham Pi Theorem

As mentioned in Chapter 5, the Buckingham Pi theorem (Cengel et al., 2006) was used to maintain similarities between pipes in a laboratory and typical cooling water pipes on site. The water flow in the clean Lab pipe rig was fully developed turbulent flow. This study aims to investigate the Reynolds number between 9.15×10^4 and 3.92×10^5 . In a fully developed turbulent water flow pipe, the wall shear stress (τ_w) is a function of other parameters, such as the diameter of the pipe (D), average velocity of the flow in the pipe (U), water density (ρ), water viscosity (μ) and the average roughness height along the pipe inside the wall (k_s). Buckingham Pi theorem was used to find the non-dimensional relationship between wall shear stress and other parameters.

The following step-by-step method of repeating variables was employed to find the relationship between wall shear stress and other parameters.

Step 1 There are 6 variables in this problem; $n=6$, listed as a function form below:

$$\tau_w = f(D, U, \rho, \mu, k_s)$$

Step 2 The primary dimensions of each parameter are listed.

τ_w	D	k_s	U	ρ	μ
$\{m^1 L^{-1} t^{-2}\}$	$\{L^1\}$	$\{L^1\}$	$\{L^1 t^{-1}\}$	$\{m^1 L^{-3}\}$	$\{m^1 L^{-1} t^{-1}\}$

Step 3 As the guess in Step1, the number of primary dimensions j , represented in this problem is set as 3, m, L and t.

$$j = 3$$

The expected number of Π 's is $i = n - j = 6 - 3 = 3$ if the value of j is correct.

Step 4 Three repeating parameters were chosen due to $j = 3$, with the best choice found to be D , U and ρ . Certain guidelines were followed by choosing the above parameters, shown in Table 7-3 of Cengel et al. (2006).

Step 5 The dependent Π is generated:

$$\Pi_1 = \tau_w D^{a_1} U^{b_1} \rho^{c_1} \longrightarrow \{\Pi_1\} = \{(m^1 L^{-1} t^{-2})(L^1)(L^1 t^{-1})(m^1 L^{-3})\}$$

from which $a_1=0, b_1=-2$ and $c_1=-1$, and dependent Π is

$$\Pi_1 = \frac{\tau_w}{\rho U^2}$$

It was found that the most similar to the Π_1 in the established non-dimensional parameters of Table 7-5 by Cengel et al.(2006) is the Darcy friction factor. The modified Π_1 is expressed below:

$$\Pi_{1,modified} = \frac{8\tau_w}{\rho U^2} = \text{Darcy friction factor} = f$$

Similar to Π_1 , the two dependents were also generated as follows:

$$\Pi_2 = \mu D^{a_2} U^{b_2} \rho^{c_2} \quad \Pi_2 = \frac{\rho U D}{\mu} = \text{Reynolds number} = Re$$

$$\Pi_3 = \epsilon D^{a_3} U^{b_3} \rho^{c_3} \quad \Pi_3 = \frac{k_s}{D} = \text{Relative roughness}$$

Step 6 The final function relationship was written as:

$$f = \frac{8\tau_w}{\rho U^2} = f(Re, \frac{k_s}{D})$$

C.4 Southern Cross Centrifugal Pump Performance in Lab

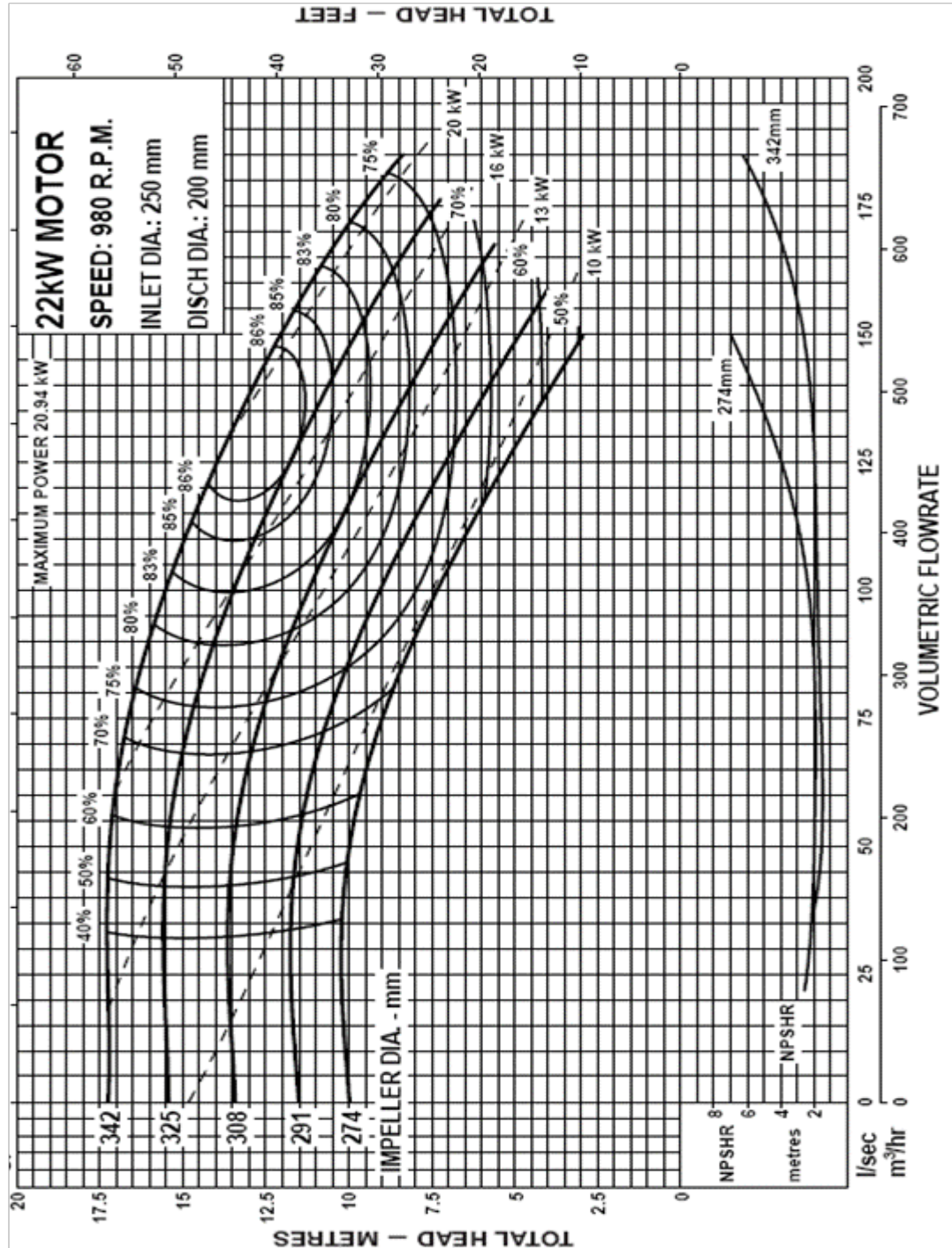


Figure C.1 Pump performance curve of Lab pipe rig.

C.5 Validyne DP15 Pressure Range Chart

PRESSURE RANGE CHART						
Range Dash No.	PSI	IN HG.	IN H ₂ O	KPA	TORR	CM H ₂ O
	.08	.16	2.22	.55	4.14	5.60
20	.125	.25	3.5	.86	6.5	8.80
22	.20	.41	5.5	1.40	10.3	14.0
24	.32	.65	8.9	2.2	16.5	22.5
26	.50	1.02	14.0	3.5	25.8	35.0
28	.80	1.6	22.2	5.5	41.4	56.0
30	1.25	2.5	35.0	8.6	65.0	88.0
32	2.0	4.1	55.0	14.0	103	140
34	3.2	6.5	90	22.0	165	225
36	5.0	10.2	140	35.0	258	350
38	8.0	16.0	222	55.0	414	560
40	12.5	25.0	350	86.0	650	880
42	20	41.0	550	140	1030	1400
44	32	65.0	890	220	1650	2250
46	50	102	1400	350	2580	3500
48	80	160	2220	550	4140	5600
50	125	250	3500	860	6500	8800
52	200	410	5500	1400	10300	14000
54	320	650	8900	2200	16500	22500
56	500	1020	14000	3500	25800	35000
58	800	1600	22200	5500	41400	56000
60	1250	2500	35000	8600	65000	88000
62	2000	4100	55000	14000	103000	140000
64	3200	6500	89000	22000	165000	225000

Table C.2 Range chart of pressure transducers.

C.6 Performance of the Submersible Pump of the Rig on Site

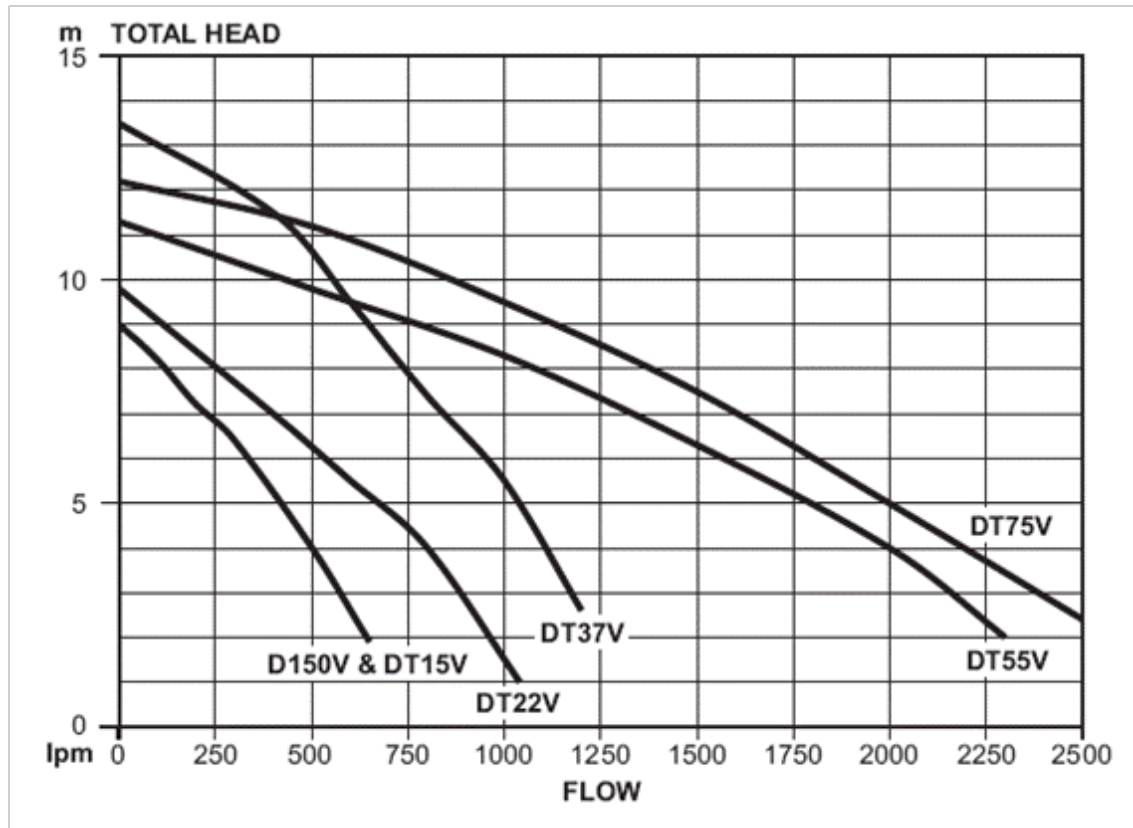


Figure C.2 Pump performance of Site pipe rig.